Western Michigan University
College of Engineering and Applied Sciences

Development and Validation of a Sensor-Based Health Monitoring Model for the Parkview Bridge Deck

By

Osama Abudayyeh, Ph. D., P.E., Principal Investigator
Professor of Civil and Construction Engineering and Associate Dean
College of Engineering and Applied Sciences
Western Michigan University
Kalamazoo, MI 49008-5314

Haluk Aktan, Ph. D., P.E., Co-Principal Investigator
Professor and Chair of Civil and Construction Engineering

Ikhlas Abdel-Qader, Ph. D., P.E., Co-Principal Investigator
Professor of Electrical and Computer Engineering

Upul Attanayake, Ph. D., P.E., Co-Principal Investigator
Assistant Professor of Civil and Construction Engineering

Sponsored by Michigan Department of Transportation

Final Report

January 31, 2012

Technical Report Documentation Page

1. Report No. RC - 3786	2. Government Accession No.	3. MDOT Project Manager Steve Kahl, P.E.
4. Title and Subtitle **Development and Validation of a Sensor-Based Health Monitoring Model for the Parkview Bridge Deck**		5. Report Date **January 31, 2012**
7. Author(s) **Dr. Osama Abudayyeh, P.E., Dr. Haluk Aktan, P.E., Dr. Ikhlas Abdel-Qader, P.E., and Dr. Upul Attanayake, P.E.,**		6. Performing Organization Code **WMU**
9. Performing Organization Name and Address **Western Michigan University 1903 W. Michigan Ave, Kalamazoo, MI**		8. Performing Org Report No.
12. Sponsoring Agency Name and Address **Michigan Department of Transportation Construction and Technology Division PO Box 30049, Lansing MI 48909**		10. Work Unit No.
		11. Contract Number : 109028
		11(a). Authorization Number: 2009-0433/Z1
15. Supplementary Notes		13. Type of Report and Period Covered **Final Report, 2010-2012**
		14. Sponsoring Agency Code

16. Abstract

Accelerated bridge construction (ABC) using full-depth precast deck panels is an innovative technique that brings all the benefits listed under ABC to full fruition. However, this technique needs to be evaluated and the performance of the bridge needs to be monitored. Sensor networks, also known as health monitoring systems, can aid in the determination of the true reliability and performance of a structure by developing models that predict structure behavior and component interaction. The continuous monitoring of bridge deck health can provide certain stress signatures at the onset of deterioration. The signatures are vital to identify type of distress and to initiate corrective measures immediately; as a result, bridge service life increases and eliminates costly repairs This project focused on the continuous monitoring and evaluation of the structural behavior of the Parkview Bridge full-depth deck panels under loads using the sensor network installed. Special attention was placed on the durability performance of the connections between precast components. However, after careful evaluation of the designs and construction process, it was identified that the transverse joints between deck panels are the weakest links, in terms of durability, in the system.

        Analysis of sensor data and load test data showed that the live load effect on the bridge is negligible. The dominant load is the thermal. Using three years of data from the sensors, stress envelopes were developed. These envelopes serve as the basis for identifying the onset of bridge deterioration. A detailed finite element model was developed, and the model was first calibrated using load test data. However, due to the dominance of thermal loads, it was required to calibrate the model using stresses developed in the structural system due to thermal loads. This was a great challenge due to a lack of sensors along depth of the bridge superstructure cross-section. A few models were identified that are capable of representing the thermal gradient profile from 12 p.m. to 6 p.m. in a summer day. The FE model was calibrated using sensor data and the thermal gradient profile of the specific duration. Construction process simulation with the calibrated model shows that all the joints between the panels are in compression, as expected at the design. Stress signatures were developed simulating the debonding of a transverse joint between panels. The signatures show a distinct pattern than what is observed from a bridge without distress. Hence, the onset of deterioration can be identified from the sensor data to make necessary maintenance decisions. The proposed signatures are applicable only during noon to 6 p.m. on a summer day, and development of deterioration models for the rest of the time requires development of new thermal models. Further, the stresses vary drastically following onset of joint deterioration; hence, identification of exact physical location of the sensors is required for fine-tuning the models.

17. Key Words: **Sensor Network, Structural Health Monitoring, Rapid Bridge Construction, Vibrating Wires Gauges, Full-Depth Deck Panels, Stress Envelopes, Defect Signature, Finite Element Modeling**		18. Distribution Statement **No restrictions. This document is available to the public through the Michigan Department of Transportation.**	
19. Security Classification (report) **Unclassified**	20. Security Classification (Page) **Unclassified**	21. No of Pages: **150 (excluding the CD of Appendix E)**	22. Price

Intentionally left blank

ACKNOWLEDGEMENTS

DISCLAIMER

The contents of this report reflect the views of the authors who are responsible for the facts and the accuracy of the data presented herein. The contents do not necessarily reflect the official views or policies of the Michigan Department of Transportation, nor Western Michigan University. This report does not constitute a standard, specification, or regulation. Trade or manufacturers' names, which may appear in this report, are cited only because they are considered essential to the objectives of the report. The United States (U.S.) government and the State of Michigan do not endorse products or manufacturers. The invaluable support from graduate students, Cem Mansiz and Eyad Almaita, is highly appreciated.

PROJECT TEAM

Principal Investigator:
Osama Abudayyeh, Ph. D., P.E.
Department of Civil and Construction Engineering
Western Michigan University, Kalamazoo, MI

Co-Principal Investigators:
Haluk Aktan, Ph. D., P.E.
Professor and Chair
Department of Civil and Construction Engineering
Western Michigan University, Kalamazoo, MI

Ikhlas Abdel-Qader, Ph.D., P.E.
Professor
Department of Electrical and Computer Engineering
Western Michigan University, Kalamazoo, MI

Upul Attanayake, Ph. D., P.E.
Assistant Professor
Department of Civil and Construction Engineering
Western Michigan University, Kalamazoo, MI

Intentionally left blank

EXECUTIVE SUMMARY

Bridges are critical components of the transportation infrastructure. There are approximately 600,000 bridges in the United State (FHWA 2008). Regular inspection and maintenance are essential components of any bridge management program to ensure structural integrity and user safety. Even though intensive bridge inspection and maintenance are being performed nationwide, the outcomes are not necessarily impressive. Of the 600,000 bridges in the United States, 12% are deemed structurally deficient, and 13% are declared functionally obsolete (FHWA 2008, BTS 2007, FHWA 2007). Consequently, 25% of the nations' bridges require attention or repair and may present safety challenges. This suggests a need for effective, continuous monitoring systems so that problems can be identified at early stages and economic measures can be taken to avoid costly replacement and minimize traffic delays. Therefore, there is a need for bridge health monitoring technologies and systems to enable continuous monitoring and real time data collection.

Rehabilitation of deteriorated bridge decks causes public inconveniences, travel delays, and economic hardships. Since maintenance of traffic flow during bridge repair requires extensive planning and coordination, it is desirable to adopt techniques for bridge replacement that allow repair work to be completed rapidly at night, on weekends, or during other periods of low traffic volume, thereby reducing accident risks and minimizing travel inconveniences, financial losses, and environmental impact. Rapid bridge replacement with full depth precast deck panels is an innovative technique that saves construction time and reduces user costs. However, this technique needs to be evaluated, and the performance of the bridge needs to be monitored. Sensor networks, also known as health monitoring systems, can aid in the determination of the true reliability and performance of a structure by developing models that predict how a structure would behave internally. This continuous information can greatly increase bridge performance by indentifying signs of early deterioration.

This project focused on continuous monitoring and evaluation of the structural system behavior of the bridge precast deck panels using data from the sensor network installed during construction. Special attention was placed on the durability performance of the joints between precast components as it is believed that the joints may be the weakest link in the deck panel

system, the sensors were installed to monitor both longitudinal and transverse joints as well as mid panel stresses.

Analysis of sensor and load test data showed that the live load effect on the bridge is negligible and that the governing factor is stress induced by thermal loads. Using three years of data from the sensors, stress envelopes were developed. These envelopes serve as the basis for identifying the onset of bridge deterioration. A detailed finite element model was developed and the model was first calibrated using load test data. However, due to the dominance of thermal loads, it was required to calibrate the model using stresses developed in the structural system due to thermal loads. This was a great challenge due to a lack of thermocouples along the depth of bridge superstructure cross-section. A model was identified from literature that is capable of representing the gradient profile from 12 p.m. to 6 p.m. in a summer day. The FE model was calibrated using sensor data and the thermal gradient profile of this specific duration. Debonding of a joint between two deck panels was simulated and a deterioration prediction model was developed combining FE results and sensor data collected over three years. Differential stresses calculated from deteriorated model are greater than 3σ; beyond the 99% confidence level of the data recorded from the sensors. Hence, on-set of deterioration can be identified using sensor data once the differential stress envelopes and FE simulation results are made available for each joint.

One limitation of the deterioration prediction model presented in the report is that it is applicable only from 12 p.m. to 6 p.m. on a summer day. Development of deterioration models beyond this range requires FE model calibration using new structure-specific thermal models. Although differential stress comparison between sensor readings may indicate degradation of panel joint connectivity, there is a potential for the differential stresses fall within the limits of σ due to the location of the sensors. Therefore, further studies are recommended for refining the deterioration prediction model.

Below is a summary of findings and deliverables:

1. Statistical analysis of sensor data collected over a three-year period was useful in evaluating the integrity of deck panel joints and identifying the dominance of thermal load.

2. Using three-year sensor data, longitudinal and transverse stress envelopes as well as the deterioration prediction models were developed.

3. A detailed finite element (FE) model was developed representing the bridge superstructure. The model was calibrated using controlled load test and vibrating wire sensor data collected from the in-service bridge.

4. The calibrated FE model was used to simulate joint deterioration. A deterioration prediction model was developed for a deck panel joint using FE simulation results and vibrating wire sensor data.

Intentionally left blank

LIST OF FIGURES

LIST OF TABLES

Intentionally left blank

1 INTRODUCTION

Bridges are critical components of the transportation infrastructure. There are approximately 600,000 bridges in the United State (FHWA 2008). Regular inspection and maintenance are essential components of any bridge management program to ensure structural integrity and user safety. Even though intensive bridge inspection and maintenance are being performed nationwide, the outcomes are not necessarily impressive. Of the 600,000 bridges in the United States, 12% are deemed structurally deficient, and 13% are declared functionally obsolete (FHWA 2008, BTS 2007, FHWA 2007). Consequently, 25% of the nations' bridges require attention or repair and may present safety challenges. This suggests a need for effective, continuous monitoring systems so that problems can be identified at early stages and economic measures can be taken to avoid costly replacement and minimize traffic delays. Therefore, there is a need for bridge health monitoring technologies and systems to enable continuous monitoring and real time data collection.

Rehabilitation of deteriorated bridge decks causes public inconveniences, travel delays, and economic hardships. Since maintenance of traffic flow during bridge repair requires extensive planning and coordination, it is desirable to adopt techniques for bridge replacement that allow repair work to be completed rapidly at night, on weekends, or during other periods of low traffic volume, thereby reducing accident risks and minimizing travel inconveniences, financial losses, and environmental impact. Rapid bridge replacement with full depth precast deck panels is an innovative technique that saves construction time and reduces user costs. However, this technique needs to be evaluated, and the performance of the bridge needs to be monitored. Sensor networks, also known as health monitoring systems, can aid in the determination of the true reliability and performance of a structure by developing models that predict structure behavior and component interaction. The continuous monitoring of bridge deck health can provide certain stress signatures at the onset of deterioration. The signatures are vital to identify the type of distress and to initiate corrective measures immediately; as a result, bridge service life improves and costly repairs are eliminated.

The bridge is located on Parkview Avenue over US-131 highway in Kalamazoo, Michigan and was recently replaced using full-depth precast deck panel technology. This report focuses on the continuous monitoring and evaluation of the structural behavior of the full-depth deck panel system of the Parkview Bridge deck under traffic and temperature loads using the sensor network installed during construction. A finite element model is developed and calibrated using sensor data to better explain the structural response to thermal and live loading. Further, the transverse joint debonding is simulated, and stress signatures are developed. The stress signatures can be used in conjunction with the stress recorded from the sensor network to identify the onset of deterioration for making efficient and effective maintenance decisions to arrest bridge deck deterioration.

2   STATE-OF-THE-ART LITERATURE REVIEW

2.1   Full-Depth Deck Panel Joint Performance

The most comprehensive study on the performance of precast deck panel systems was conducted by Issa et al. (1995). In the study, several bridges located in 11 states were visually inspected. The observed poor performance of the full-depth deck panel system was attributed to the lack of post-tensioning, panel-to-panel and panel-to-girder connection type, materials used at the joints, and construction practices. The leading durability issue was the leaky joints while the loss of connection between girder and panel aggravated the issue. As a result of this study, the recommended best practices include the following:

- the use of female-to-female type joints between the panels with at least a 1/4-inch opening at the bottom of the joint,
- longitudinal post-tension application to clamp the joints,
- the use of precast concrete girders to reduce the flexibility of the superstructure, and
- the use of a waterproofing membrane over the deck and a wearing surface.

Furthermore, scheduled maintenance has been identified as an important operation to extend the service life of the bridge.

2.2   Bridge Deck Deterioration Prediction

The maintenance and management of bridges in the U.S. have been the focus of many studies from the time that their deterioration reached a point that impaired performance, roughly the 1980's. The effectiveness of a bridge management system (BMS) depends heavily on the accuracy and quality of the deterioration model utilized to determine which maintenance action, if any, should be taken. The American Association of State Highway Transportation Officials. recommends that each department of transportation (DOT) incorporates a deterioration model into its BMS (AASHTO 1993).

The deterioration models most often employed today may be categorized as either deterministic or stochastic. Two types of input data are required for each element by each of the above-mentioned models: (1) a condition rating and (2) a transition probability. Condition rating, is

established by inspection. The rating is the same for both deterministic and stochastic models. The transition probabilities are where the two models differ. A deterministic model is essentially a mathematical model that gives a solution based on defined conditions or states. The input for each parameter must be a single numerical value. By definition, deterministic models fail to account for the random behavior of the components. This means that given the same input of initial conditions, the model will always arrive at the same result, or final condition. This is not realistic in infrastructure deterioration models due to the random nature of the loadings and responses of the structure. The deterministic model assigns a single numerical value to each probability, while a stochastic one assigns a distribution to each probability. Stochastic models are considered as simulations rather than mathematical models. It is through the probabilities that a stochastic model accounts for variability, which is the main advantage of this type of model. Inherently, given the same input, stochastic models will not arrive at the same result. Within each of the aforementioned models, the options of state-based or time-based analysis are available. The state-based analyses provide the probability of the transition from the current state to the next one. The time-based analysis present the probabilistic time that the subject will remain in its current state.

2.2.1 Pertinent Research in Deterioration Modeling

The stochastic infrastructure deterioration model is most often used by DOTs. , Specifically, the stochastic model uses the Markovian distribution. Morcous et al. (2003) summarized the Markovian deterioration models used in bridge management systems. Markovian Chain models are specific types of Markov Processes in which the development is through several transitions between several states. With the goal of simplifying the decision process as well as reducing the need to analyze the bridge deck as a continuous condition state, discrete parameter Markov Chains are used for bridge deterioration (Bogdanoff 1978; Madanat and Ibrahim 1995). Bridge deterioration is a non-stationary process, yet Markov Chain Models assume that the probability of a future state depends only on the current state, inherently neglecting the history of the deteriorating element (Lounis and Mirza 2001). Discrete Markov Chains define discrete transition time intervals and distinct states of condition. The output of these models is the

probability of the component to remain in its current state, or transition to another state, under given environmental and initial conditions. The transition probabilities, which are at the core of such models, require the expert judgment of several experienced bridge engineers (Thompson and Shepard 1994).

As can be expected, there are continual efforts toward increasing the accuracy and consistency of these models. There are several proposals documented in the literature to overcome the commonly accepted limitations of the current Markovian chain models implemented by departments of transportation for bridge deck deterioration. The first limitation to be discussed is the estimation of the transition probabilities, which influences the output of the models. To improve the estimation, the use of the ordered probit technique was proposed by Madanat et al. (1995). The second limitation is the inherent characteristic of Markovian models to disregard the condition history of the structure. Robelin and Madanat (2006) proposed that this could be rectified through state augmentation. The final limitation to be discussed is the subjectivity of the input, the inspection data. The input is affected by several variables, from the weather and lighting conditions, to the experience of the inspector.

In Michigan, the condition of the bridge deck is evaluated using a rating system, which describes the current condition through discrete ordinal value, 0 through 9 (Nowak et al. 2000). This method fails to capture the non-stationary characteristic of the deterioration process. The ordered probit technique is useful and often applied when the dependent variable is discrete and ordinal (McElvey and Zavoina 1975). The ordered probit technique assumes the presence of a latent, unobservable, and time-dependent variable. The difference in two consecutive condition ratings is taken as an indicator of the aforementioned latent variable, describing the non-stationary deterioration. The study by Madanat et al. (1995) demonstrated the approximation of transition probabilities with increased accuracy compared to the alternative method based on linear regression.

The main argument against the use of Markov Chain Models in modeling bridge deterioration is the assumption that the history of the structure has no effect on its future performance. There are several suggestions to modify the Markov Chain models to include aspects of the bridge's history. Robelin and Madanat (2006) proposed the "formulation of a history-dependent deterioration model as a Markov model," through state augmentation. Previous Markov models, as mentioned before, assign an integer value to the current condition of the bridge deck. Robelin and Madanat propose to have four parameters dictating the state of the bridge: the current condition of the bridge, the condition index immediately following the last maintenance procedure, an integer indicating the type of maintenance last performed, and the time since that procedure was performed. Monte Carlo simulation is implemented to obtain the transition probabilities.

Visual inspection remains the most common manner of rating concrete bridge decks. The human effect is not removed by the use of nondestructive testing (NDT). Interpretation of the NDT results requires experience as well as in depth understanding of the deterioration phenomena (Tarighat and Miyamoto 2009). This is because inspectors, through varying levels of experience and interpretations of damage levels, will influence the model outcome, and therefore the safety of the bridge. In an effort to account for the subjectivity associated with inspection data, the application of fuzzy logic with bridge deck condition rating was proposed by Tarighat and Miyamoto (2009). A fuzzy inference system, having proved effectiveness in dealing with imprecise and uncertain data, shows great potential in this application. Tarighat and Miyamoto (2009) suggested that the condition rating may be estimated through the application of the Mamdani-type fuzzy inference.

Research today suggests that the future of deterioration modeling will be through one of three methods:
- further improvements to Markovian Chain Models,
- time-dependent reliability index, or
- case-based reasoning (discussed below).

As discussed above, research is underway to improve the Markovian Chain Models used today.. In addition to those proposed improvements, Noortwijk and Frangopol (2004) stated that "reliability-based models will be the future of bridge management systems." The load carrying capacity of a bridge is also referred to as the structural reliability, and the majority of the maintenance work required by bridges is influenced more by a structural reliability of a bridge than the condition rating (Noortwijk and Frangopol 2004). Therefore, the time-dependent reliability index is favorable in that the load carrying capacity is directly accounted for, as opposed to indirectly through condition states of individual components, as is done with the current models. Moreover, Artificial Intelligence (AI) methods, though having lost support in the past, continue to be explored. Morcous et al. (2002) proposed the use of case-based reasoning (CBR) for bridge management systems. CBR, an AI technique, searches BMS databases for bridges similar to the bridge in question. CBR is gaining support due to its ability to capture the deterioration history and component interaction through the use of "examples" contained in the databases.

There are unique bridges that have limited durability performance records due to their limited in-service numbers or their very recent construction. In such cases, it is not practical to use deterioration models that require an existing database to verify or calibrate the models. There is a potential to develop deterioration models based on limited data and simulation results. For example, Gualtero (2004) studied performance, causes, and trends of deterioration in bridge decks with partial depth precast, prestressed concrete panels. This particular study was initiated due to localized failures observed in several bridges that were built during the late 70's and early 80's. A detailed study of five bridges and forensic investigations of another eight bridges allowed documenting causes of deterioration and distress types specific to this particular deck configuration. A deck failure mechanism model was developed based on the data collected from these 13 bridges. The model includes 13 deterioration stages specific to this bridge type and is helpful in identifying potential local failures to implement effective preventive maintenance strategies. Gualtero (2004) recommended enhancing the accuracy of the deterioration model by fine-tuning the model using finite element simulation results of the deterioration process.

7

2.2.2 Summary

The current use of deterioration models in BMS is not effective due to the lack of data; hence, existing models are unable to predict potential signatures of future damages or deteriorations of a new bridge with a specific configuration. In order to overcome this challenge, Lu et al. (2007) developed a sensor based structural health monitoring system that captures strain/stress time history data to establish a baseline distribution which can be refined by data collected within the first two years. The change in structural response due to damage or deterioration is identified when strain/stress distribution deviates from the established baseline distribution. The prediction accuracy by the baseline distribution can be enhanced by developing strain/stress envelopes as well as defect signatures through finite element simulation of potential deterioration scenarios. This would also provide a comprehensive understanding of the type and extent of deterioration, particularly when a recorded strain/stress response of a structure mimics an established signature or deviates from the stress envelope, thus assisting in accurate maintenance decisions.

3   OVERVIEW OF STATISTICAL METHODS

Statistical methods are used to analyze and better understand the Parkview sensor network data in the four categories: longitudinal, transverse, panel joint, and closure grout stresses. These methods (and categories) include mean, standard deviation, Gaussian distribution, correlation, and correlation factors (Abudayyeh 2010 and Spanos 2003).

3.1   The Mean and Standard Deviation

The mean is the summation of all observations divided by the number of observations. In mathematical representation:

$$\bar{X} = \frac{\sum_{i=1}^{n} X_i}{n}$$
<div align="right">Eq. 3-1</div>

where, $\bar{X}$ is the mean, X_i is the ith observation, and n is the number of observations (samples).

The standard deviation measures the spread of the data around the mean. A small value of standard deviation for a given data set indicates data clustering around the mean for that data set. On the other hand, a high value of standard deviation indicates that the data is widely spread around the mean, suggesting a large variability in the data. The standard deviation for a data set can be calculated as:

$$\sigma = \sqrt{\frac{\sum_{i=1}^{n}(X_i - \bar{X})^2}{n}}$$
<div align="right">Eq. 3-2</div>

where, σ is the standard deviation, X_i is the ith observation, $\bar{X}$ is the mean of the data set, and n is the number of data points in the data set.

3.2   Correlation

The correlation is a strength index for the relationship between two or more random variables. In other words, correlation is a measure of linear dependency between two or more variables. Usually, the correlation is described by a correlation coefficient between -1 to +1, where a +1 value means a perfect increasing linear relationship between the two variables, a -1 value means

a perfect decreasing linear relationship between the variables, and a 0 value means no linear relationship between the variables. The correlation coefficient, based on Pearson's product-moment, can be calculated as

$$\rho_{X,Y} = \frac{Cov(X,Y)}{\sigma_X \sigma_Y} = \frac{E[(X-\mu_X)(Y-\mu_Y)]}{\sigma_X \sigma_Y} \qquad \text{Eq. 3-3}$$

where $\rho_{X,Y}$ is the correlation factor between X and Y random variables, $Cov(X,Y)$ is the covariance matrix, σ_X and σ_Y are the standard deviations for the variables X and Y, E is the expected value or the statistical mean of the variable in the [ ], and μ_X and μ_Y are the statistical means for the variables X and Y.

3.3 Fast Fourier Transform (FFT)

Fast Fourier Transform (FFT) is an algorithm for efficiently calculating the Discrete Fourier Transform (DFT). There are several algorithms for calculating FFT. DFT is a transformation of a signal from the discrete time domain into the discrete frequency domain. DFT is used to obtain knowledge about the spectrum of a given signal. That is, it gives information on the frequency content of the original signal. Mathematically, computing the DFT of N points (H_n) of a signal h_k can be accomplished by:

$$H_n = \sum_{k=0}^{N-1} h_k e^{i2\pi kn/N} \qquad \text{where, } n = 0,1,2, ..., N\text{-}1 \qquad \text{Eq. 3-4}$$

3.4 Gaussian Distribution

Gaussian distribution, or normal distribution, is a symmetric bell shaped curve that is completely described by its mean (μ) and variance (σ^2). The Gaussian distribution peaks at the mean value and is symmetric around its mean as shown in Figure 3-1. The probability density function (PDF) for the Gaussian distribution is:

$$PDF_{\mu,\sigma}(X) = \frac{1}{\sigma\sqrt{2\pi}} e^{-\frac{(X-\mu)^2}{2\sigma^2}} \qquad \text{Eq. 3-5}$$

10

One of the important properties of the Gaussian distribution is the relationship between the standard deviation and the confidence interval. A 68% confidence interval can be obtained within one standard deviation from the mean ($\overline{X} \pm \sigma$). This means that the probability of a sample point (reading) falling within this region is 0.68. A 95% confidence region can be obtained within two standard deviations ($\overline{X} \pm 2\sigma$).
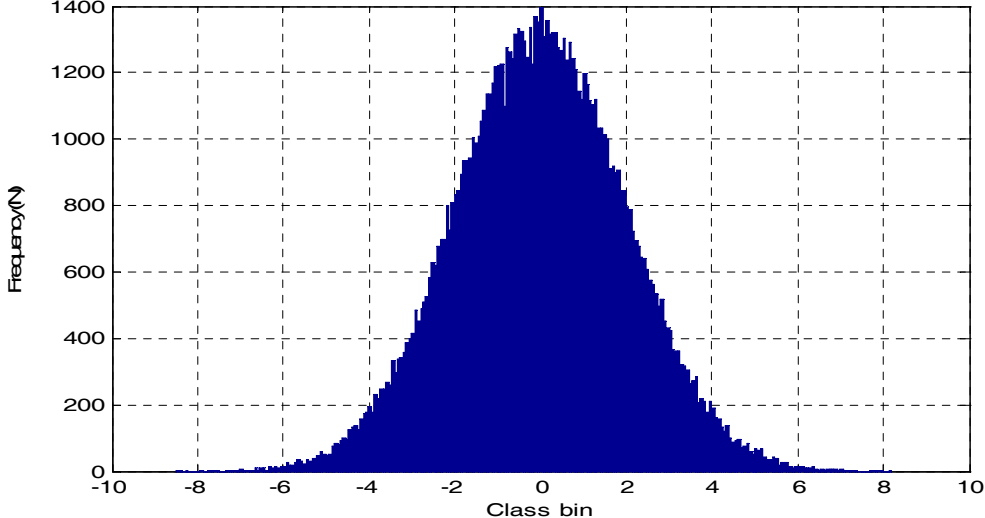

Figure 3-1. Gaussian distribution with μ=0, and σ =2

4   SCOPE AND OBJECTIVES

This work represents an additional 2 years of health monitoring n the Parkview Avenue bridge deck that was performed to accomplish the full realization of the benefits of this technology. The main objectives of the proposed work were to:

1. Evaluate the structural response and behavior of the Parkview Bridge under loads for an extended period of time (2 years) beyond the one year that was completed in January 2010. This was accomplished using the data collected by the sensor network that was installed during construction.
2. Develop a finite element (FE) analysis model of the bridge and calibrate using sensor data for structural performance assessment and validation (reality check) of design assumptions. Special consideration was given to the precast component joint performance.
3. Develop a deterioration prediction model for the Parkview Bridge using three-year health monitoring data and FE simulation results.

The work elements related to each objective listed above are discussed in Sections 5, 6, and 7, respectively.

5 HEALTH MONITORING USING THE SENSOR NETWORK

The Parkview Bridge is the first totally prefabricated bridge in Michigan to take advantage of the accelerated bridge construction (ABC) techniques and sensor network technology. This section provides an overview of the Parkview Bridge design features along with the configuration of the structural health monitoring (SHM) instrumentation. It then discusses the sensor network data types, analysis, and reduction.

5.1 Overview of the SHM Sensor Network Design and Deployment

The Parkview Bridge is located in Kalamazoo, Michigan next to the Engineering Campus at Western Michigan University with US-131 being the featured intersection. After many years of service, this bridge needed replacement. A decision was made to replace the existing bridge using rapid bridge construction techniques. The new Parkview Bridge was designed with four spans and three traffic lanes, with all its major bridge elements including substructure prefabricated off site. The superstructure is composed of 7 Type III AASHTO girders and 48, 9-inch thick precast reinforced concrete deck panels. These panels are labeled as North and South. Once the North and South panels were installed on-site, the transverse continuity between north and south panels were established using a reinforced concrete cast-in-place longitudinal closure pour. The deck was post-tensioned after grouting the transverse joints between panels and the haunch, and completing the closure. Waterproofing membrane was placed over the deck and a 1-1/2 inch asphalt wearing surface was placed. Figure 5-1 illustrates the various prefabricated elements of the bridge including multi-section abutments, single segment pier columns, single section pier caps, pre-stressed concrete I-girders, and post-tensioned full-depth deck panels. The actual construction began on April 7th, 2008, and the bridge was re-opened to traffic on September 8th, 2008.
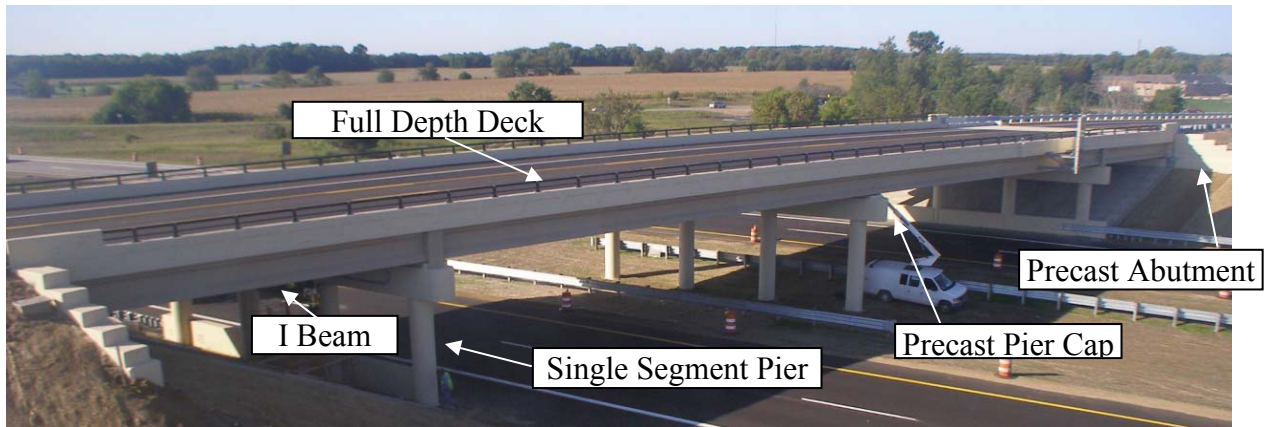
Figure 5-1. Completed Parkview Bridge

The structural health monitoring system was implemented following the completion of the construction. This enabled the remote collection of continuous strain and temperature data at ten-minute intervals. Strain and temperature measurements were chosen in this project for efficiency and cost effectiveness. The SHM system is composed of the following:

- 184 Geokon Vibrating-Wire Strain Gauges (sensors) Model VCE-4200 with built-in thermocouples installed in the bridge deck panels,
- 2 Geokon MICRO-10 Data Loggers Model Number 8020-1-1,
- 12 Geokon Multiplexers Model 8032-16-1S,
- 2 modems,
- a remote computer workstation in a laboratory with communication software, and
- necessary wiring for communication and data transfer (Abudayyeh 2010).

The two data loggers are contacted weekly through the modems and the telephone lines are dedicated to downloading and archiving the sensor data for future analysis. The SHM system started to function in December 2008. Therefore, data archiving for a period of three years has been completed, and a baseline for future continuous monitoring of this bridge's health condition has been developed. Figure 5-2 provides a schematic view of the system configuration.
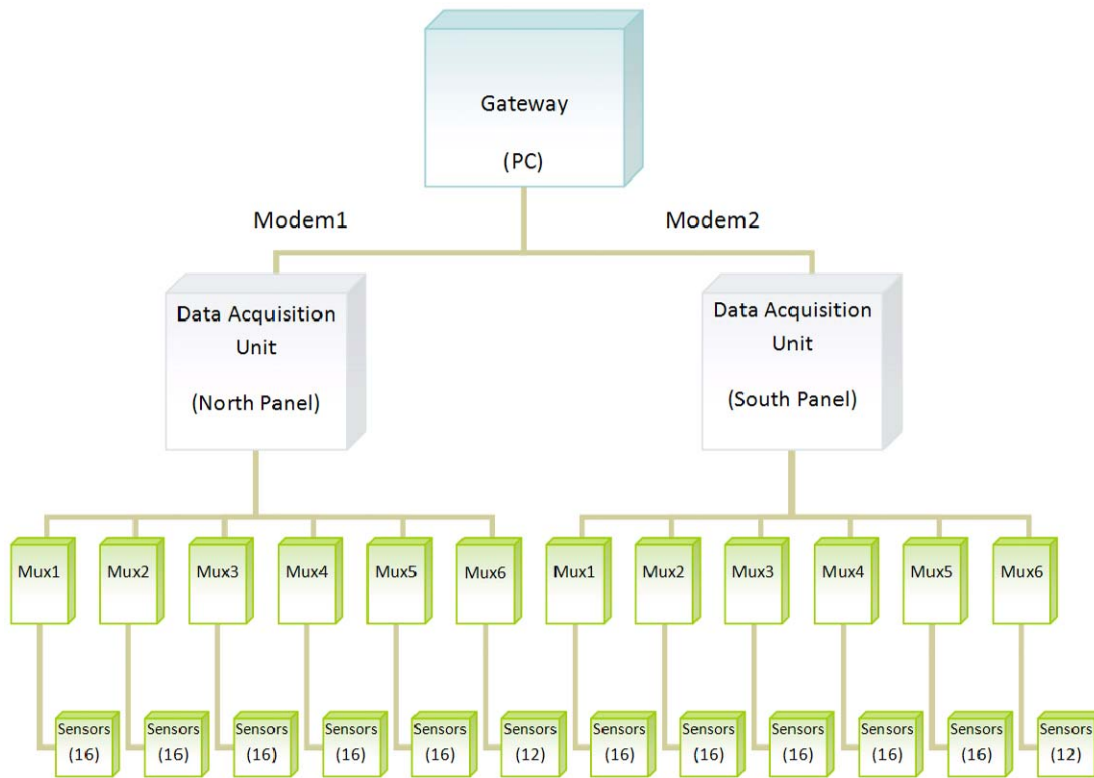
Figure 5-2. Schematic view of the Parkview Bridge SHM system configuration

To effectively monitor the bridge performance under varying load conditions, sensors were grouped, depending on their locations, to address the structural monitoring needs outlined earlier. In this study, four groups of sensors were used to monitor the bridge performance:

- Group 1 – Longitudinal stresses at mid spans and over the piers,
- Group 2 – Transverse stresses at mid spans,
- Group 3 -- Stresses at joints between panels (parallel-to-edge), and
- Group 4 -- Stress at both sides of the cast-in-place closure between North and South panels (Abudayyeh 2010).

Figure 5-3 shows the locations and labels of all the sensors in the panels, and provides the group number for each sensor in parentheses. The construction details in terms of the plans and specifications for the design and installation of the selected instrumentation are provided in (Abudayyeh 2010).
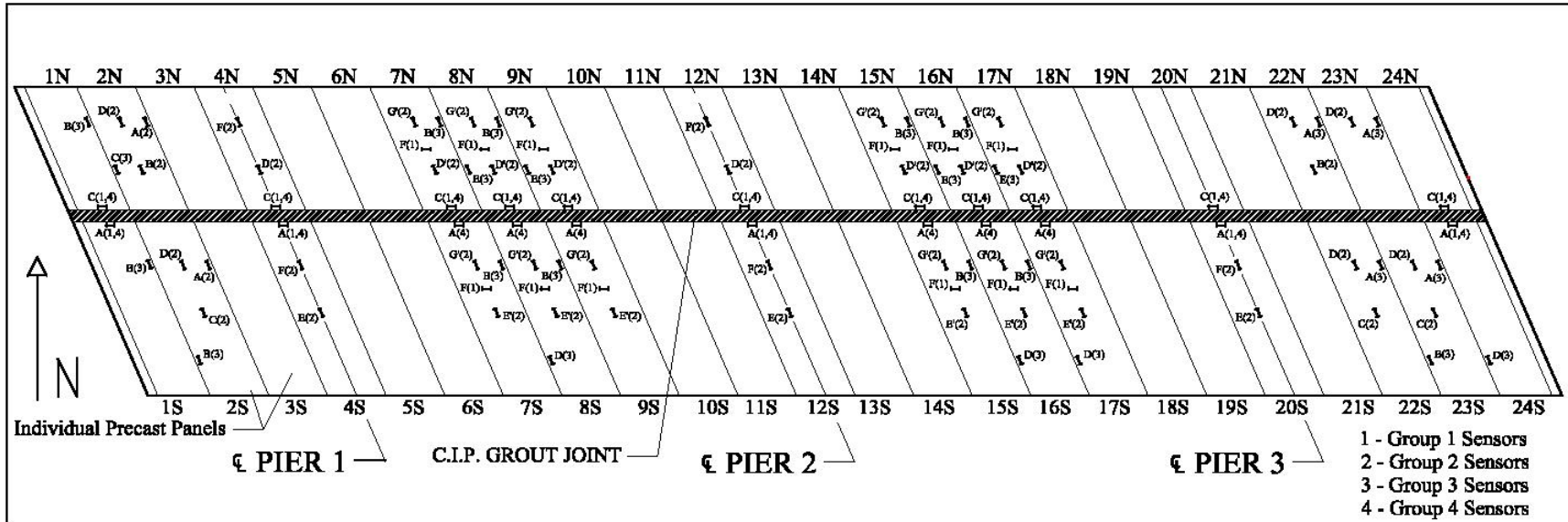
Figure 5-3. Parkview Bridge deck layout*

*Note: the number between ( ) represents the group number(s) that the sensor belongs to.

16

5.2 SHM Configuration Setup

Typically, sensor data are clearly organized and sorted by month due to the large number of readings recorded (Abudayyeh 2010). This provided accessibility to all data for each month and each sensor. The vibrating wire strain gage sensors record restrained deformation under thermal loads; hence the strain readings were converted to stress values by multiplying the strains with the modulus of elasticity of the deck panel concrete calculated from Eq. 5-1. The temperature data is also acquired at the sensor locations and stored along with the stresses. (Note that the sensors read temperatures in degrees Celsius.) The average 28-day compression strength (f'_c) was recorded as approximately 8,000 psi. The Modulus of Elasticity (*E*) was then calculated using the American Concrete Institute's equation:

$$E = 57{,}000\sqrt{f'_c} \approx 5{,}000\ ksi \qquad\qquad \text{Eq. 5-1}$$

This value was then used to convert strain readings into stress values using:

$$Modulus\ of\ Elasticity\ (E) = \frac{Stress\ (\sigma)}{Strain\ (\epsilon)} \qquad\qquad \text{Eq. 5-2}$$

Also, the maximum allowable stresses in the concrete are calculated as:

$$\text{Compression:}\quad f \le 0.45 f'_c\ = -3{,}600\ psi \qquad\qquad \text{Eq. 5-3}$$
$$\text{Tension:}\quad f_t \le 6\sqrt{f'_c}\ = 537\ psi \qquad\qquad \text{Eq. 5-4}$$

After strain values are converted to stresses, allowable design values provided by the designer are compared to actual measured values. Since bridge condition and performance are the primary concern, monthly recorded values are sorted and filtered to make sure allowable stresses are not exceeded and to ensure that no sudden changes in the pattern are observed. This process is performed after the data are normalized and ready to be interpreted for further examination.

5.3   SHM Data Analysis and Reduction

The Parkview sensor network is composed of 184 sensors that collect data points in ten-minute intervals in four main categories: longitudinal, transverse, panel joint, and closure grout stresses. Each data point consists of two readings (strain and temperature). This results in a large data set that needs mining and processing for trend and deterioration prediction analyses. Therefore, the goal is to reduce the number of data points for further analysis without compromising the overall quality. The reduction of the number of data points makes manipulation more efficient and can help in the optimal design of future bridge monitoring systems. The data reduction process involves two steps:

- investigating the types of data collected by the sensors, and
- reducing the number of sensors needed for data collection.

The following techniques are used in achieving the data analysis and reduction goals:

- statistical correlations between sensor data (stresses and temperatures), and
- Fast Fourier Transform (FFT).

5.3.1 Data Types (Static versus Dynamic)

In the Parkview Bridge sensor network, the static data type refers to measured data that result from low frequency loads such as temperature, dead load, and post-tensioning. The dynamic data type, on the other hand, refers to measured data that result from high frequency loads such as traffic loads. The data frequency range that can be measured by a monitoring system is a function of the system's sampling rate capabilities. The number of sensors plays a major role in determining the sampling rate. As the number of sensors goes up, the time needed to read the sensors increases, resulting in lower sampling rate. Unfortunately, the vibrating-wire sensor monitoring system used in the Parkview Bridge is only capable of low sampling rates and is set to one reading every 10 minutes, limiting its ability to capture dynamic data types.

5.3.2 Dynamic Data Analysis

Although the Parkview Bridge monitoring system is designed to capture static data types, the research team investigated the possibility of mining any traffic load (dynamic data)

18

impacts on the bridge deck. Two analyses were performed for this data mining investigation: the Fast Fourier Transform (FFT) and the correlation between the stress and temperature signals.

5.3.2.1 FFT Data Analysis

FFT transforms a signal from discrete time domain to discrete frequency domain. In other words, it allows for computing the spectrum of a discrete signal. FFT is investigated in this project to provide information about the frequency content in the data to allow for relating the data variation to temperature and traffic changes. The dynamic part of the data, high variations in time domain, will be mapped into the high frequency range in the transformed domain (i.e. frequency domain). In the Parkview Bridge data, the dynamicity of the aggregated data would predominately be attributed to traffic load and the natural frequency of the bridge within a small time frame. This assumption is based on the fact that temperature will not drastically change in a small period of time.

Two different sensors were used to investigate the dynamic nature of the data collected by the sensor network. In other words, this investigation seeks to determine what portion of the stress measured by a given sensor is due to traffic loads (dynamic) and what portion is due to temperature (static). The stresses measured by the two sensors were transformed to the frequency domain using the FFT method. The data set used for the investigation was for a one-month period and was selected randomly. The experiment was repeated five times (i.e. five different months) for each of the two sensors. Figure 5-4 and Figure 5-5 show the output from the FFT method for the N-7-C and N-8-F sensors for the months of October-2009 and March 2009, respectively. As the figures illustrate, the data did not contain any high frequency components, reinforcing the earlier assumption that vibrating wire sensors are not capable of capturing stresses from dynamic data types (traffic loads) and are mainly measuring stresses from static loads.
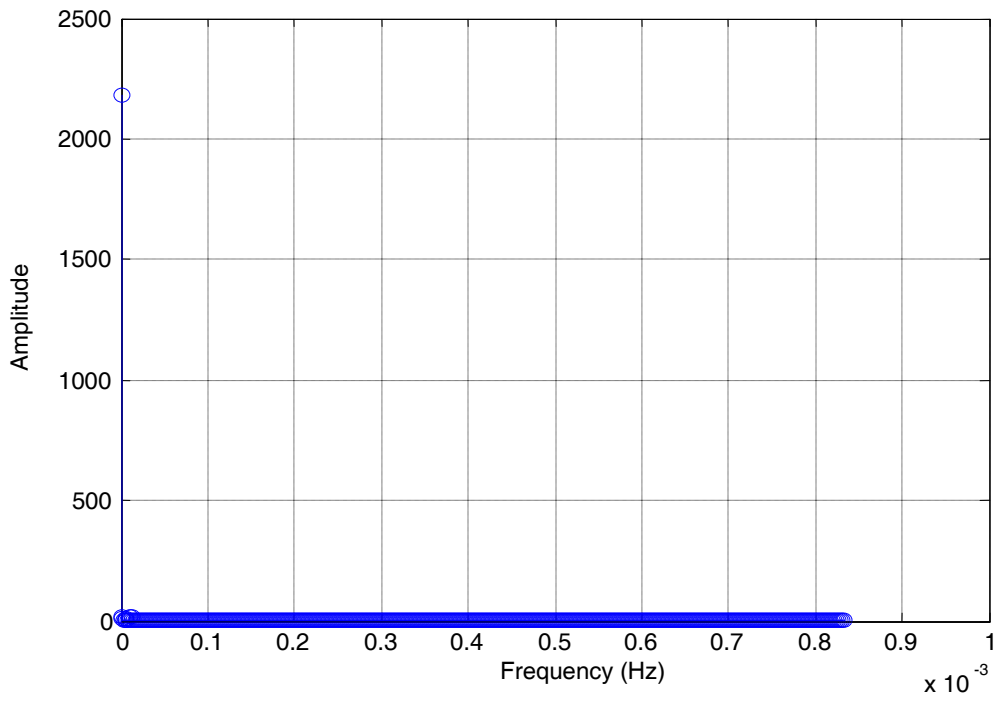
Figure 5-4. FFT for the N-7-C sensor during the month of October 2009
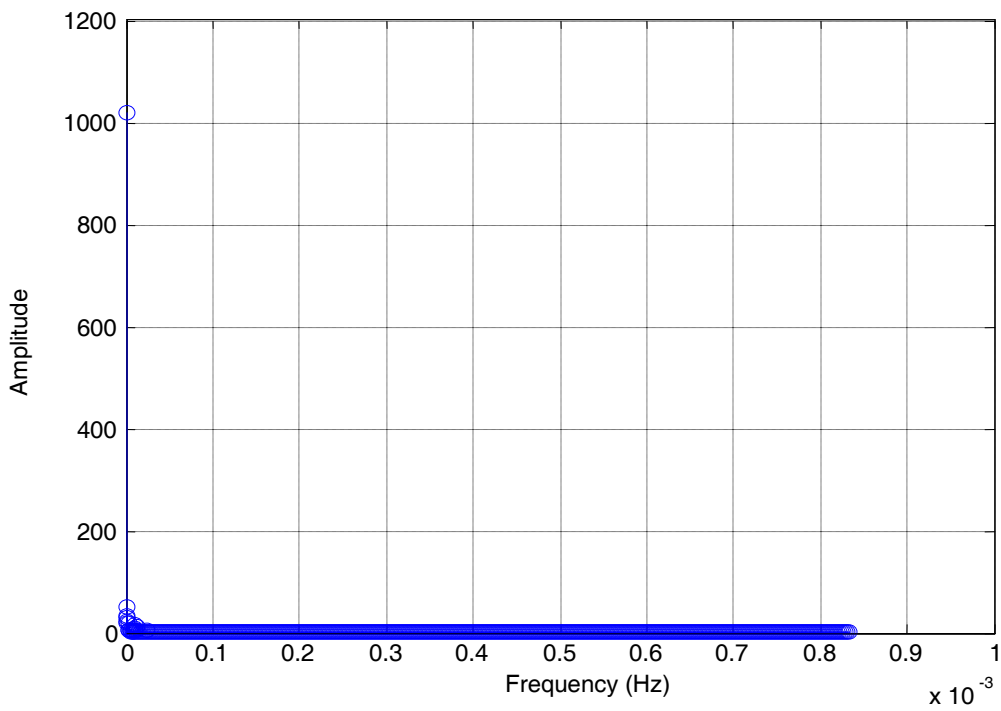
Figure 5-5. FFT for the N-8-F sensor during the month of March 2009

5.3.2.2 Stress-Temperature Correlation Analysis

While the FFT analysis of the sensors data clearly indicated that the Parkview Bridge monitoring sensor network is unable to capture traffic loads, the research team conducted one more investigation using correlation analysis to reinforce this conclusion. Simply stated, if changes in the recorded stress values for a given sensor result predominately from temperature changes, then a high correlation factor between the measured stresses and their corresponding temperatures would be obtained. Table 5-1 through Table 5-4 show the correlation between the stress and temperature readings for sensors located in the north and south sides of spans 2 and 3 during three randomly selected months. It is clear from the tables that the sensor stress changes are highly correlated with the corresponding temperature readings, suggesting that temperature gradients are the predominate loads on the bridge.

Table 5-1. Correlation Factor between Stress and Temperature in North Side of Span 2

Sensor Name	N-7-C	N-8-C	N-9-C	N-7-F	N-8-F
Jan-09	-0.9597	-0.9611	-0.9898	-0.9553	-0.9741
June-09	-0.9900	-0.9906	-0.9895	-0.9784	-0.9695
Nov-09	-0.9715	-0.9738	-0.9737	-0.9352	-0.9308

Table 5-2. Correlation Factor between Stress and Temperature in North Side of Span 3

Sensor Name	N-15-C	N-16-C	N-17-C	N-15-F	N-16-F
Jan-09	-0.9640	-0.9876	-0.9882	-0.9839	-0.9772
June-09	-0.9905	-0.9882	-0.9894	-0.9882	-0.9746
Nov-09	-0.9731	-0.9685	-0.9735	-0.9546	-0.9190

Table 5-3. Correlation Factor between Stress and Temperature in South Side of Span 2

Sensor Name	S-7-F	S-8-F
Feb-09	-0.9801	-0.9794
May-09	-0.9266	-0.9270
Oct-09	-0.9273	-0.9133

Table 5-4. Correlation Factor between Stress and Temperature in South Side of Span 3

Sensor Name	S-15-F	S-16-F
Feb-09	-0.9747	-0.9757
May-09	-0.9472	-0.9545
Oct-09	-0.8975	-0.9088

5.3.3 Data Reduction

After establishing the fact that the Parkview Bridge monitoring system is primarily capturing static data, the next step is to identify the best representative sensor(s) from each category. Choosing the most representative sensor for each category allows dealing with a manageable set of data without overlooking important information, if there is a need in future to reduce the amount of data required to monitor the integrity of the connection between precast components. A high correlation factor between the sensors in a given area or category suggests a high redundancy in the data. Therefore, the representative sensor for such a group would be the one with the highest stress values.

Table 5-5 shows the results of the correlation factor analysis for the north side of span 2 in the longitudinal direction for the 2009 year. It is clear from Table 5-5 that the sensors' data are highly correlated, and one representative sensor (N-7-C) can be selected for this group.

Table 5-5. Correlation Factor between North Side Sensors for Span 2 in the Longitudinal Direction (Year 2009)

	N-7-C	N-8-C	N-9-C	N-7-F	N-8-F
N-7-C	1	0.99741362	0.99898519	0.98296	0.971859
N-8-C	0.997414	1	0.99728037	0.98975	0.982331
N-9-C	0.998985	0.99728037	1	0.984669	0.974425
N-7-F	0.98296	0.98974975	0.98466873	1	0.996258
N-8-F	0.971859	0.98233097	0.97442515	0.996258	1

The correlation factors between the sensors in each span in the longitudinal and transverse categories were computed in a similar manner and found to be highly correlated within each category. The representative sensors for each span in these two categories are shown in Table 5-6. As shown from the table, the number of sensors has been reduced from 22 to 14 for the longitudinal category and from 72 to 13 sensors in the transverse category.

Table 5-6. Representative Sensors for Transverse and Longitudinal Categories

Transverse			
North Panel	**Representative Sensor**	**South Panel**	**Representative Sensor**
Span1	N-2-D	Span1	S-2-C
Pier1	N-4-F	Pier1	S-4-E
Span2	N-8-Gp	Span2	S-7-G
Pier2	N-12-D	Pier2	S-12-E
Span3	N-15-Dp	Span3	S-15-Gp
Pier3	–	Pier3	S-20-E
Span4	N-23-D	Span4	S-22-D
Longitudinal			
North Panel	**Representative Sensor**	**South Panel**	**Representative Sensor**
Span1	N-1-C	Span1	S-1-A
Pier1	N-4-C	Pier1	S-4-A
Span2	N-7-C	Span2	S-7-F
Pier2	N-12-C	Pier2	S-12-A
Span3	N-15-C	Span3	S-15-F
Pier3	N-20-C	Pier3	S-20-A
Span4	N-24-C	Span4	S-24-A

6   FINITE ELEMENT SIMULATION OF THE BRIDGE SUPERSTRUCTURE

6.1   Objective and Approach

The objectives of this section are to present design details of the Parkview Bridge superstructure, to display and discuss the finite element (FE) modeling of components and their interactions, to show model calibration using sensor data, and to elaborate upon the simulation of identified distress types to develop stress/strain contours. The analysis results, in conjunction with sensor data, are used to identify signatures of potential performance issues of the full-depth deck panel system.

6.2   Bridge Configuration and Details

The twenty three degree (23^0) skew Parkview Bridge has four spans with seven simply supported PC-I Type III girders (Figure 6-1). Expansion is allowed only at piers 1 and 3. Fixed bearings are used at the abutments and pier 2. One inch nominal diameter dowel bars are used to prevent backwall sliding over the abutment stems, making them integral abutments (Figure 6-2). In addition, staggered threaded inserts are provided between girder webs and the backwall allowing shear transfer. Concrete diaphragms are used to encase beam ends over the piers, but asphalt felt with roofing tar/asphalt is used to debond beam ends (Figure 6-3). Joints between beam ends over the piers are filled with concrete to form the diaphragms.

Furthermore, the pier diaphragm detail allows girder ends to translate along the girder longitudinal axis (provided that the expansion bearings are used) and to rotate about a horizontal axis perpendicular to the girder's longitudinal axis. However, the beam ends over the abutments are not debonded using asphalt felt. ASTM A709 grade 36 structural steel sections (MC 18×42.7) are used as intermediate diaphragms for span 2 and 3 (Figure 6-4).

Deck width is made up of two full-depth panels, referred as north and south panels, which are connected using a 2 ft wide cast-in-place closure pour (Figure 6-5). Once the panels are placed and leveled, transverse joints between panels were grouted, and the

24

longitudinal joint was formed with cast-in-place concrete. The full-depth deck panel assembly was post-tensioned in the longitudinal direction using tendons placed through 14 ducts. The haunches and deck shear connector pockets were grouted after the longitudinal post-tension application. Finally, bridge construction was completed by placing a waterproofing membrane, a 1.5 in. asphalt wearing surface, and safety barriers.

Initial post-tension force applied at each location was 182.8 kips. The spacing between post-tension ducts is shown in Figure 6-5. The post-tension tendon size, tendon length, stressing force, stressing end, and stressing sequence are shown in Table 6-1.

Table 6-1. Post-tension Details

PT Designation	Tendon Size	Tendon Length	Stressing Force (kips)	Stressing End	Stressing Sequence
L1	4×0.6"	245'-6 ¼"	182.8	ABUT A	6
L2	4×0.6"	245'-6 ¼"	182.8	ABUT B	14
L3	4×0.6"	245'-6 ¼"	182.8	ABUT A	1
L4	4×0.6"	245'-6 ¼"	182.8	ABUT B	8
L5	4×0.6"	245'-6 ¼"	182.8	ABUT A	5
L6	4×0.6"	245'-6 ¼"	182.8	ABUT B	11
L7	4×0.6"	245'-6 ¼"	182.8	ABUT A	3
L8	4×0.6"	245'-6 ¼"	182.8	ABUT B	10
L9	4×0.6"	245'-6 ¼"	182.8	ABUT B	12
L10	4×0.6"	245'-6 ¼"	182.8	ABUT A	4
L11	4×0.6"	245'-6 ¼"	182.8	ABUT B	9
L12	4×0.6"	245'-6 ¼"	182.8	ABUT A	2
L13	4×0.6"	245'-6 ¼"	182.8	ABUT B	13
L14	4×0.6"	245'-6 ¼"	182.8	ABUT A	7
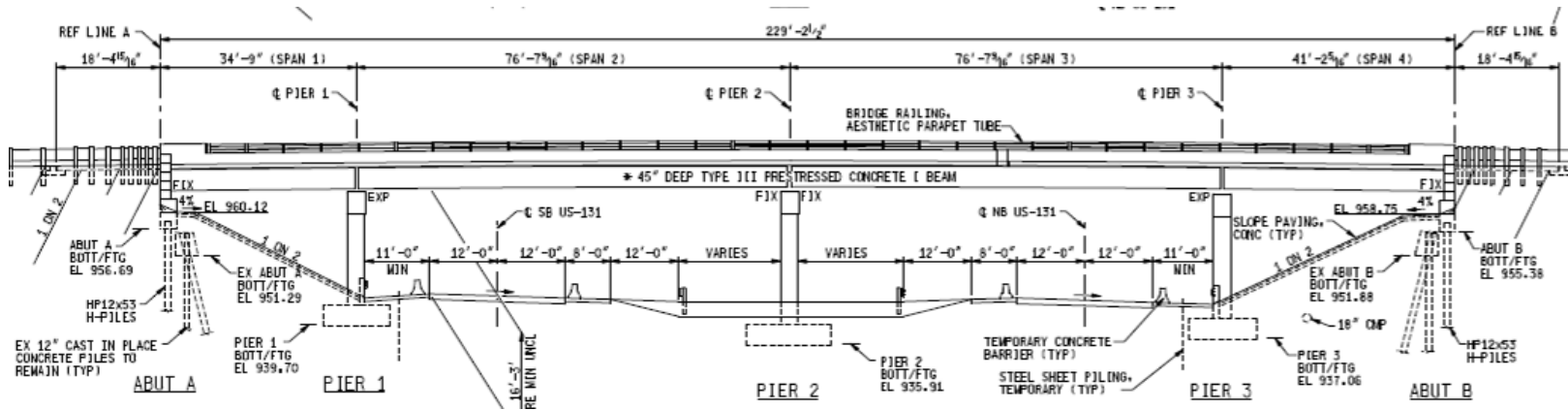
Figure 6-1. Parkview Bridge elevation
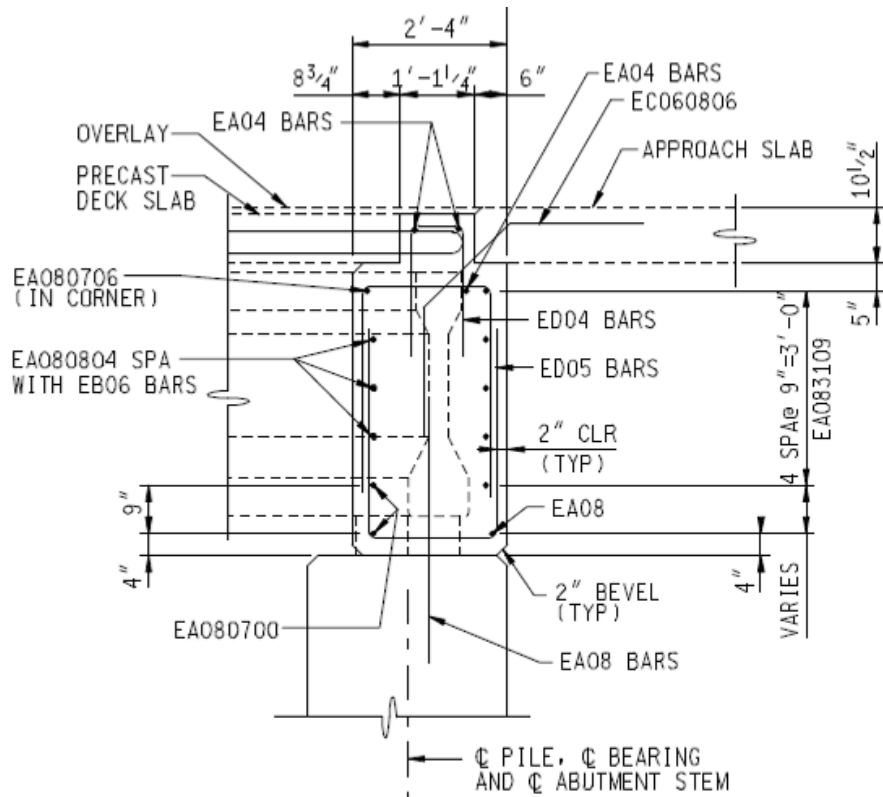
Figure 6-2. Backwall-abutment connection details
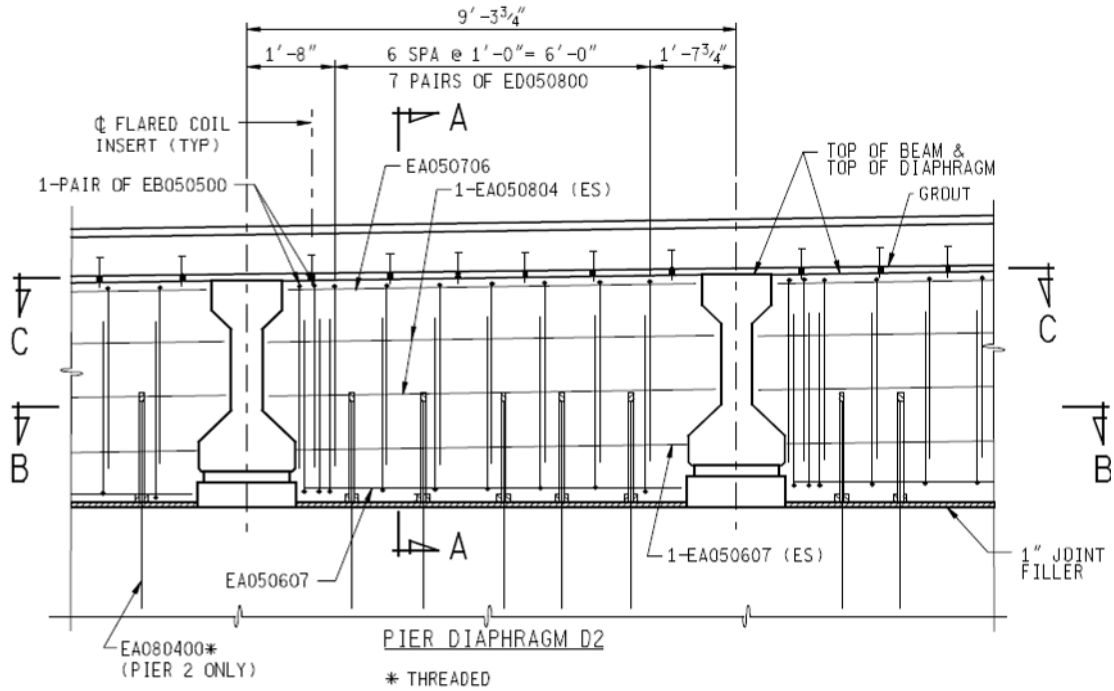
Figure 6-3. Pier-diaphragm-beam end connection details
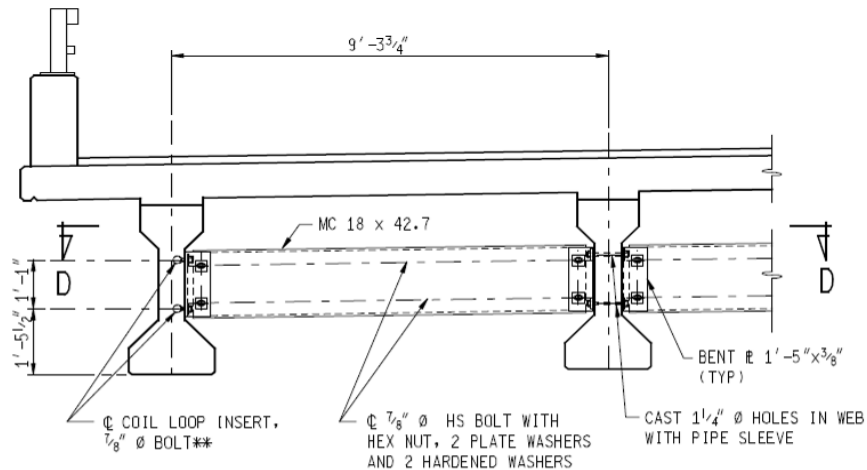
Figure 6-4. Intermediate diaphragm details

28
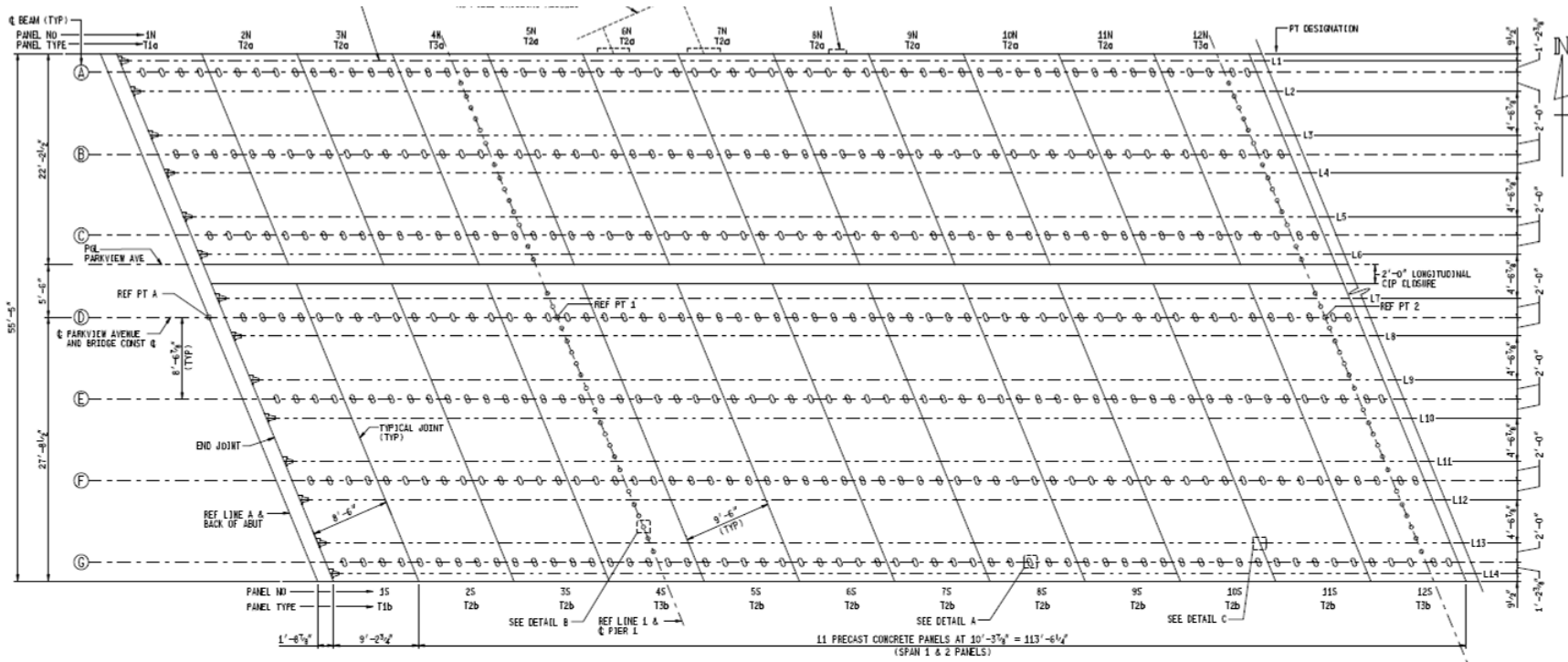
Figure 6-5. Deck panel and post-tension layout

6.3 Material Properties

Table 6-2 shows the material properties used in the model.

Table 6-2. Material Properties

Description		Density (lb/ft^3)	Strength (psi)	Modulus of elasticity (ksi)	Poisson's ratio
Deck Panel		150	8,000	5,000	0.2
Haunch		150	8,000	5,000	0.2
I-beam	at release	150	5,700	4,303	0.2
	at service	150	7,000	4,769	0.2
Prestress strands (0.6" φ, 270 ksi low relaxation)		491	270,000	28,500	0.3
Post-tension tendons (0.6" φ, 270 ksi low relaxation)		491	270,000	28,500	0.3
Grout			8,000	5,000	
CIP closure		150	6,000	4,415	0.2
Intermediate diaphragm		491	60,000	29,000	0.3

Thermal expansion coefficient (AASHTO LRFD 2007):

$$\text{Concrete and grout materials} = 6 \times 10^{-6} \, (\text{in/in/}^0\text{F})$$
$$\text{Steel} \qquad\qquad = 6.5 \times 10^{-6} \, (\text{in/in/}^0\text{F})$$

6.4 Analysis Loads

The load types used in the analysis include the bridge self weight, the trucks used for load testing, and thermal gradient. As discussed in Chapter 5, live load effect is not captured by the sensors. Further, the static truck load testing data presented in Abudayyeh (2010) shows that the bridge is very stiff, and the live load has a negligible effect on the structure response to loading.

6.4.1 Self-weight

Material densities and component geometries are used to introduce the self-weight of bridge components, except the asphalt wearing surface, diaphragms, and barriers. The weight of the asphalt wearing surface is applied as a uniformly distributed load. Barrier load is applied as a uniformly distributed strip load along the deck edge.

6.4.2 Truck Loads

The FE model calibration under static loads is performed using load test data. Four single-direction and six bi-directional load scenerios are considered. Two types of trucks were used in load testing (Figure 6-6).

Type I truck for single-directional testing   Type II truck for bi-directional testing

Figure 6-6. Truck types used for load testing

Trucks were placed to develop ten loading scenerios (Table 6-3). The truck positions are shown in Figure 6-7. Trucks were placed to maximize the span moments of the loaded spans. Dimensional details of the Truck I and Truck II are illustrated in Figure 6-8 and Figure 6-9, respectively. Axle weights given in Table 6-4 were measured in field.

According to Yap (1989) tire contact area and pressure distribution can be changed due to the state of loading and tire production methods. Therefore, tire contact pressure distribution may differ even within the same type of tire produced by same company. Due to difficulty in knowing the exact pressure distribution, it was decided to use the tire pressure distribution and the patch dimension of 20 in.×10 in. specified in the AASHTO (2010).

Table 6-3. Load Testing Scenarios

Testing Scenario	Truck Type 1 Location (Single-Directional – 1 Truck)	Truck Type II Location (Bi- Directional – 2 Trucks)
1	47	
2	42	
3	49	
4	40	
5		45,44
6		47,42
7		49,40
8		51,38
9		47,40
10		45,33

31
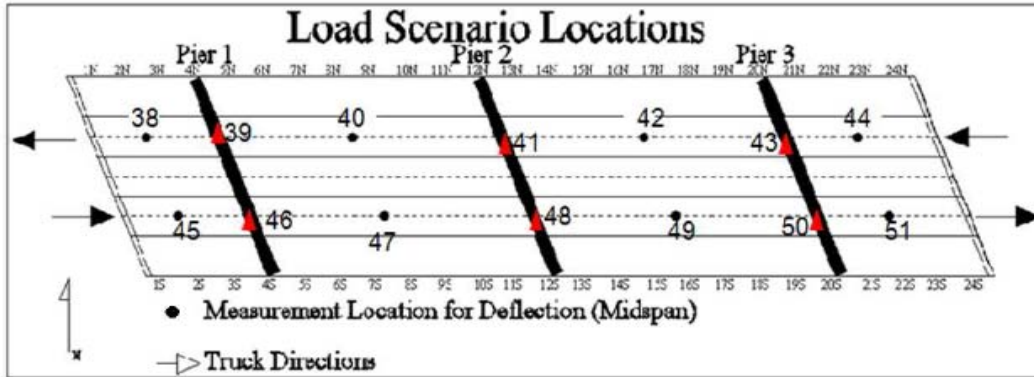
Figure 6-7. Truck positions
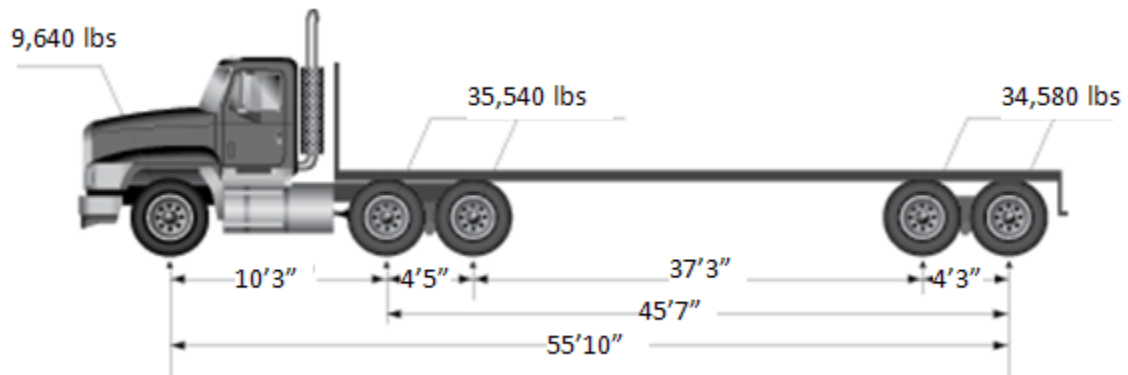
Figure 6-8. Truck type I truck configuration

Figure 6-9. Truck type II configuration

Table 6-4. Axle Weight of Type I and II Trucks

Axle #	Single Directional Truck Type 1 Weights (lbs)	Bi-Directional Truck Type 1 Weights (lbs)	
Front Axle	9,640	17,850	18,350
#2 Axle	35,540	18,050	18,600
#3 Axle		17,800	18,250
#4 Axle	34,580	-	-
#5 Axle		-	-
Gross Weight	79,760	53,700	55,200

6.4.3 Thermal Gradient Load

The thermal gradient profiles specified in AASHTO (2010) are defined for design purposes. The analysis performed in this project is to understand the structural performance; hence, the use of thermal gradient profile through the depth of bridge superstructure, at the time of interest, is important. This is a great challenge as there were no temperature sensors placed through the cross-section depth. Extensive literature review was performed and various recommendations were reviewed in order to identify thermal gradient profile representatives of a day in summer and a day in winter. Priestly (1976) proposed that vertical temperature gradient, during a period that the deck heats up follows a fifth-degree parabola (Figure 6-10). The example presented by Priestly (1976) is a box-girder in which the temperature reaches ambient value at a depth of 47.24 in. along the web during an early afternoon of a hot summer day.

$$T(y) = T_{top}\left(\frac{y}{1200}\right)^5$$

Units: Temperatures are in degrees Celsius and lengths in mm

$$(1\,°C = 1.8\,°F,\ 1\,mm = \frac{1}{25.4}\ in)$$
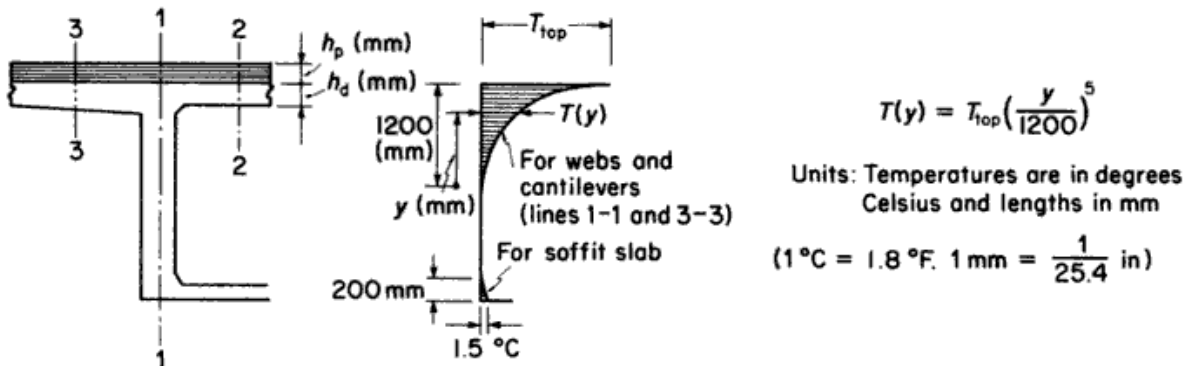
Figure 6-10. Temperature profile proposed by Priestly (1976)

Based on a set of data collected over a period of 18 hours from the I-35W St. Anthony Falls Bridge, French et al. (2009) developed thermal gradients through the depth at midnight, 6 a.m., noon and 6 p.m. (Figure 6-11). The data collected at noon closely represents the fifth-order model presented by Priestly (1976). The profile at 6 p.m. closely represents a second-order curve.
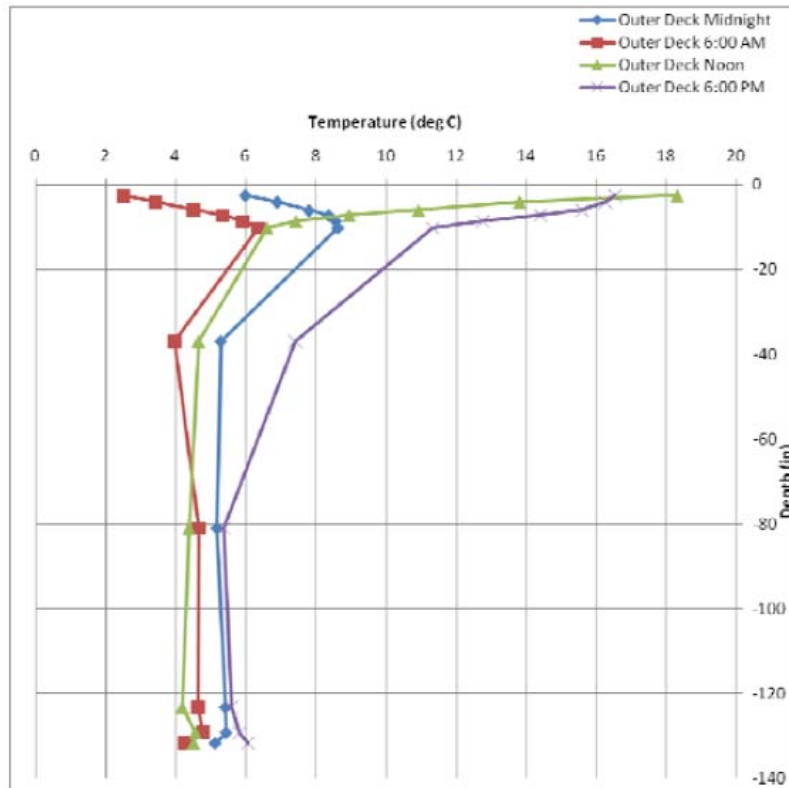
Figure 6-11. Thermal gradient profiles at different times of a day (Source: French 2009)

Vibrating wire gages embedded in the deck panels contain thermistors and records strains as well as temperature. Within a limited area, vibrating wire gages are attached to top and bottom reinforcements of the deck panels. However, bottom layer sensors are not available above the girders. Literature recommended the fifth and second-order thermal profiles for concrete girders to represent thermal gradient profile at noon and 6 p.m. during a summer day. Hence, the fifth and second-order thermal profiles that were calibrated with the measured temperature at the depth of vibrating wire gages were used for thermal gradient load at noon and 6:00 p.m. for the girders and the deck above the girders (Figure 6-12). On the other hand, the temperature records from top and bottom thermistors were used for the rest of the deck (Figure 6-13). Even though different temperature profiles were used to represent temperature distribution within concrete elements, a constant temperature was assigned to the top surface of the entire deck. There are no

34

reliable models to represent temperature profile during winter. Hence, temperature and stress data recorded during summer were used for model calibration.
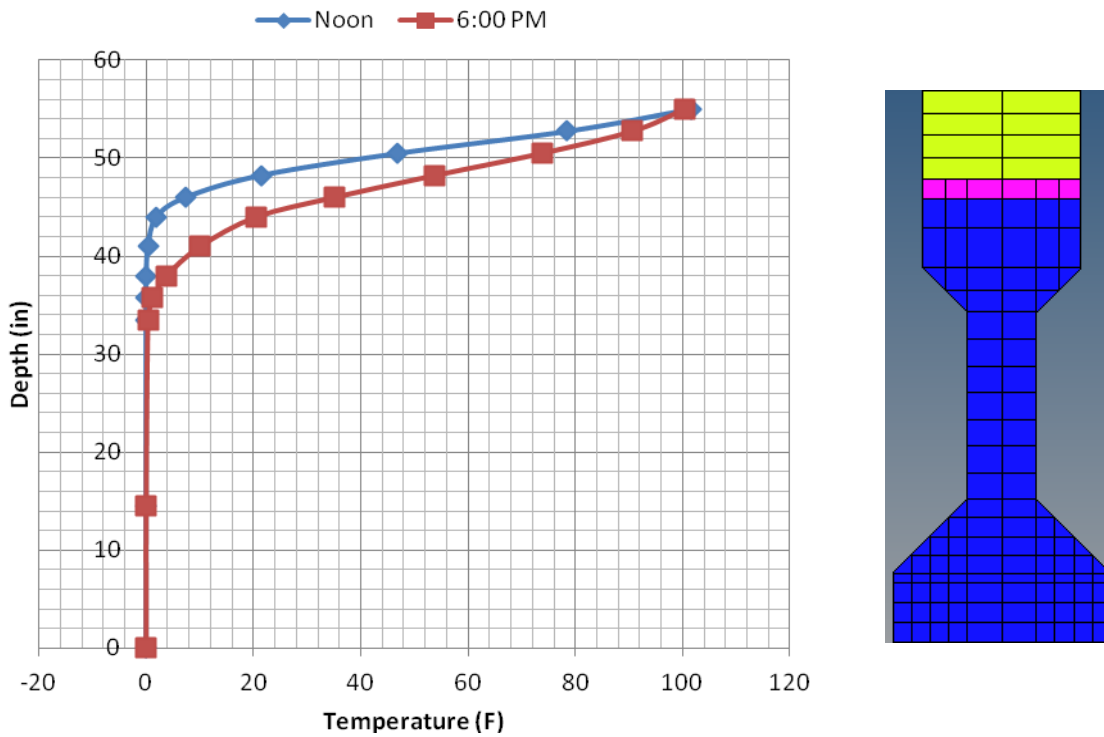
Figure 6-12. Temperature distribution along the depth of a girder and the deck above the girder
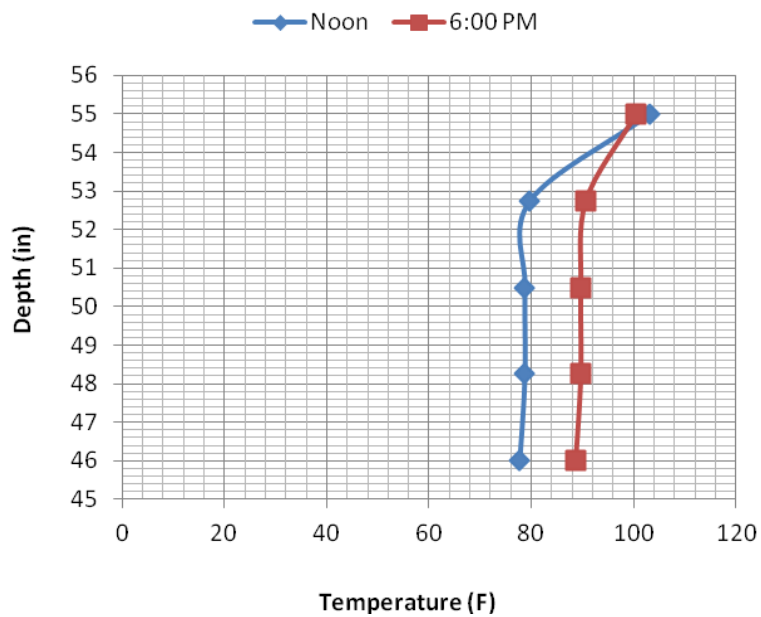
Figure 6-13. Temperature distribution along the depth of deck located in between girders

6.5   Finite Element Modeling

Altair HyperMesh version 10 (Altair 2010) is used as the finite element pre/post-processor while Abaqus version 6.10 (Simulia 2010) is used as the solver. The finite element model consists of full-depth deck panels, PC-I girders, prestress strands, post-tension tendons, diaphragms, shear keys and haunch. Concrete components are modeled by using, incompatible mode, 8-node linear brick elements (C3D8I). The behavior of incompatible mode elements is similar to quadratic elements with lower computational demand compared to quadratic elements. Their disadvantage is the sensitivity to element distortion, which may result in stiffer elements. The element types listed in the following table are used in the model. In addition to the individual components models, component interaction models is vital to understanding the structural system behavior and implications of potential issues on structural durability such as debonding at panel joints or at the haunch. The boundary interaction between the components is modeled by contact options in Abaqus. A detailed discussion of contact analysis options, their use, and selection and verification is given in Romkema et al. (2010).

Table 6-5. Element Types used in FE Modeling

Components	Element Types	Definition
Deck Panel	C3D8I	8-node linear brick element
Haunch	C3D8I	8-node linear brick element
I-beam	C3D8I, C3D6	8-node linear brick element, 6-node linear triangular prism
Prestress strands Post-tension tendons	T3D2	2-node linear 3-D truss
Grout	C3D8I	8-node linear brick element
Intermediate diaphragm	B31	2-node linear beam
End diaphragm	MPC, Beam	Rigid Beam Element

6.5.1 PC-I Girder

Simply supported PC-I girder models with prestressing strands are developed representing girder geometries and prestressing strand profiles for each span. The girder models are verified against the camber calculated from basic relations given in the PCI Bridge Design Manual (PCI 2003). Further, the girder cambers are compared against those stated in the bridge plans.

Girder end stresses are not needed in this particular study. Hence, strands are lumped into groups. They are modeled in groups maintaining the strand eccentricity by considering the total cross-

section area of strands (Table 6-6) and debonded lengths (Table 6-7) that matches the camber and stresses under self-weight and prestressing forces. The C3D8I and C3D6 elements represent girder geometry while T3D2 elements represent the strands.   Moreover, the FE mesh configuration is developed by limiting the maximum aspect ratio to 5 for more than 90 percent of the elements used in girder models (Figure 6-14). Material properties are assigned as per Table 6-2. The girder design details and FE models are shown in Figure 6-14, Figure 6-15 and Figure 6-16.

Table 6-6. Strand Locations and Total Number of Strands

Span	Midspan					End					Total
	Bottom			Top		Bottom			Top		
	1	2	3	1	2	1	2	3	1	2	
1	0	8	0	0	0	0	8	0	0	0	8
2	8	10	6	2	0	8	10	6	2	0	26
3	8	10	6	2	0	8	10	6	2	0	26
4	0	8	2	0	0	0	8	2	0	0	10

Table 6-7. Strand Debond Length

Span	Row	Number of strands	Debonded length (ft)
2 and 3	1	2	20
2 and 3	2	2	10
2 and 3	2	2	5
2 and 3	3	2	5

Section view

Isometric view
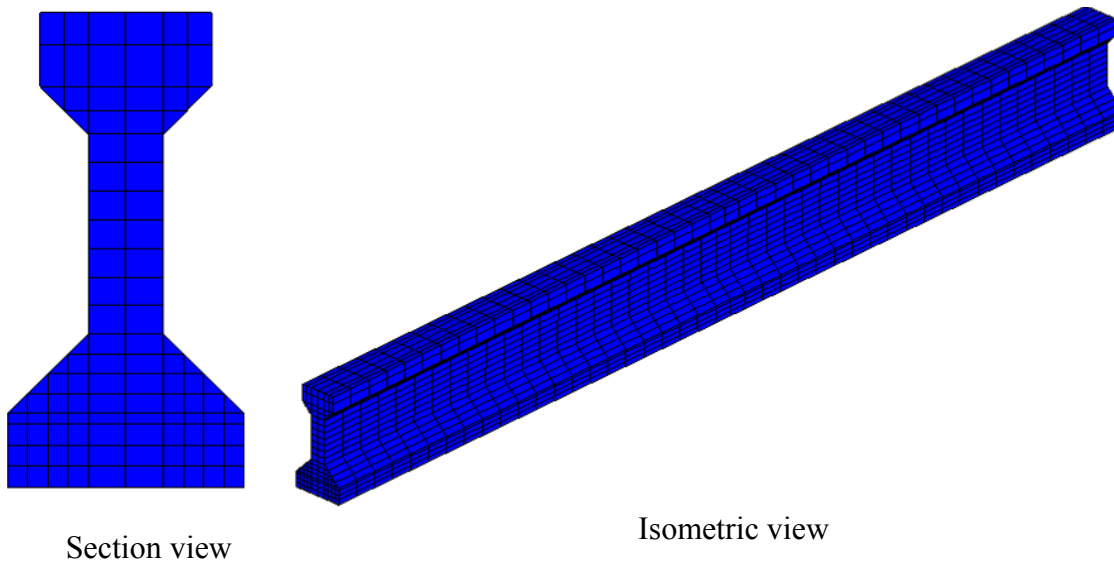
Figure 6-14. General views of PC-I girder FE models
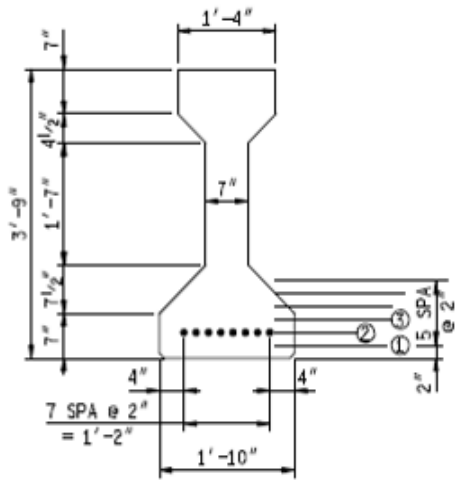
Span 1 girder details
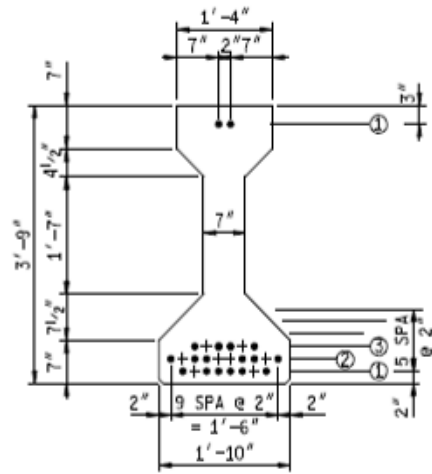
Span 2 and 3 girder details (end section)
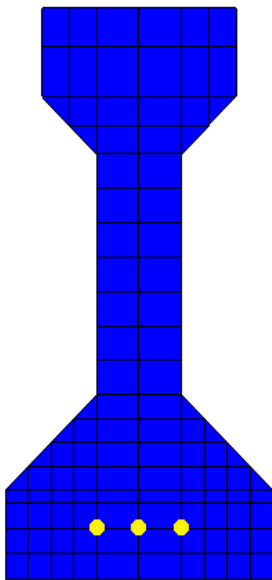
Span 1 FE model
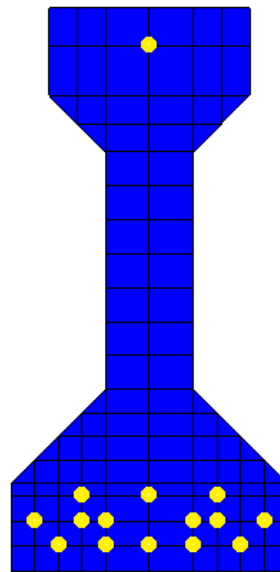
Span 2 and 3 FE model (end section)

Figure 6-15. Span 1 and span 2 and 3 end section girders details and FE models
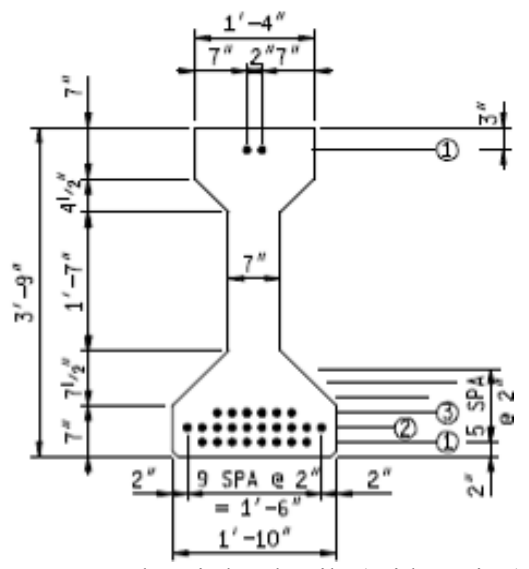
Span 2 and 3 girder details (mid section)
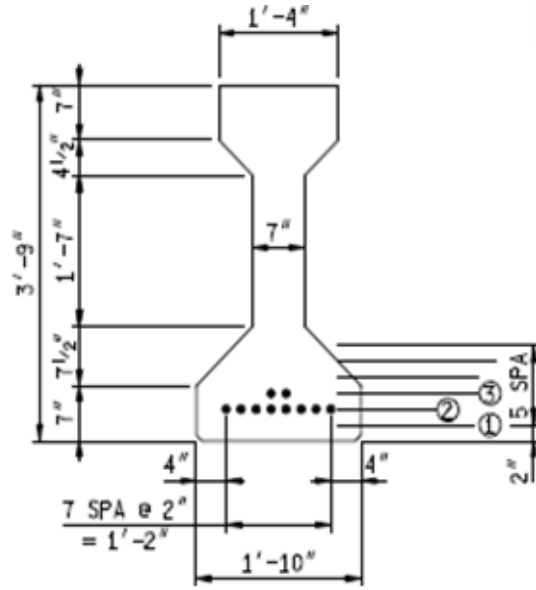
Span 4 girder details
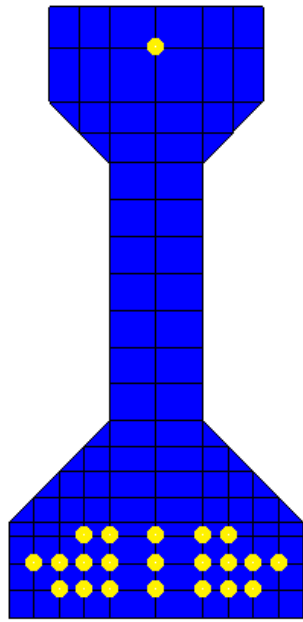
Span 2 and 3 FE model (mid section)
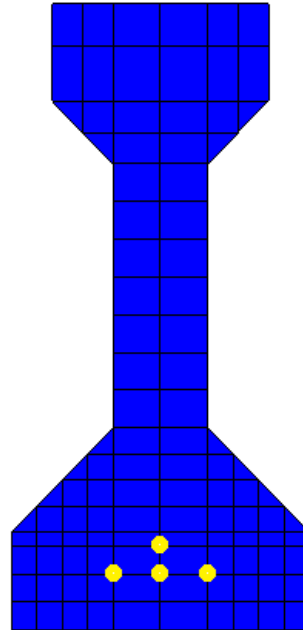
Span 4 FE model

Figure 6-16. Span 2 and 3 mid section and span 4 girders details and FE models

6.5.2 Girder End Boundary Conditions

Movement is allowed over pier 1 and 3 while fixed bearings are used over pier 3 (Figure 6-1). Girder movement is allowed in the direction of the girder centerline by providing a slotted sole plate based on bearing details provided in Figure 6-17 and Table 6-8. Note that elastomeric pads are not used over the abutments. Further, dowels are used to connect the backwall to the abutment developing integral abutment details (Figure 6-18). As per the design plans, the shear moduli of plain elastomeric bearings and laminated elastomeric bearings are 200 psi (+/- 30 psi) and 100 psi (+/- 15 psi), respectively. Elastomeric bearing design is based on a maximum pressure of 500 psi under dead load and 800 psi under combined dead and live loads.

Plan view of a bearing

Section C-C   Section D-D
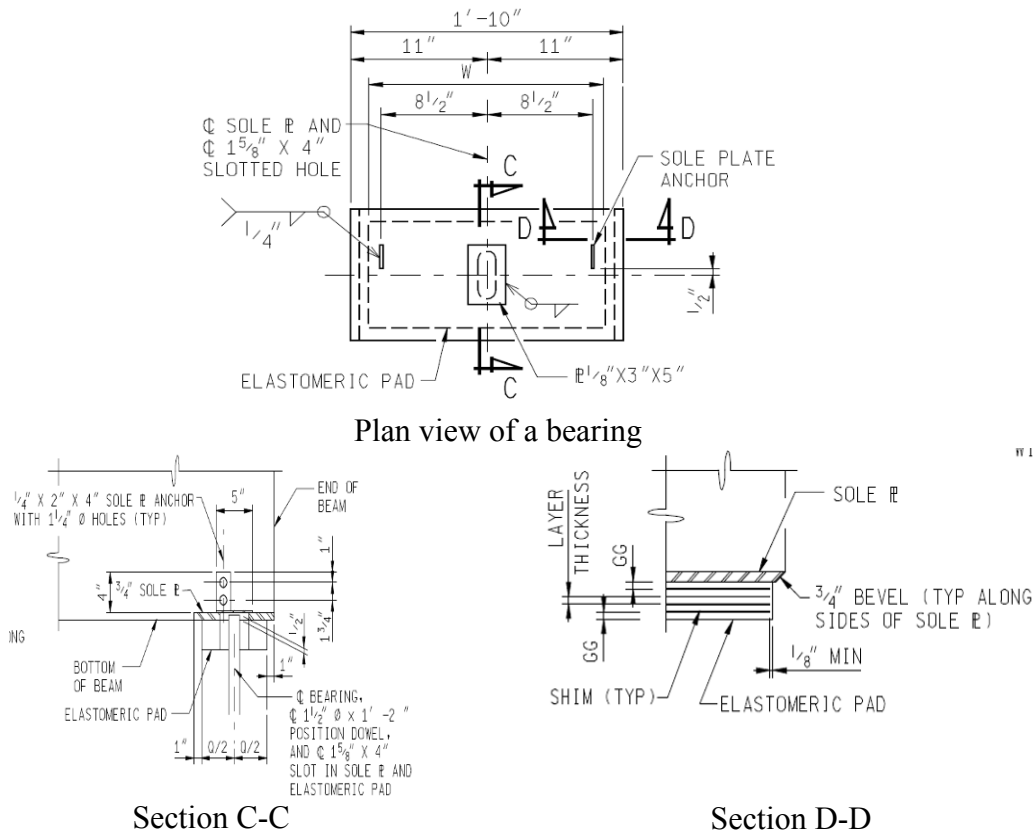
Figure 6-17. Bearing details

Table 6-8. Elastomeric Pad and Shim Dimensions

	Span 1		Span 2	Span 3	Span 4	
	ABUT A	PIER 1	PIER 1 & 2	PIER 2 & 3	PIER 3	ABUT B
Thickness (in.)	0.125	2	2.5	2.5	2	0.125
(Q) Parallel to beam (in.)	12	8	10	10	8	12
(W) Perpendicular to beam (in.)	20.5	19	19	19	19	20.5
GG (in.)	-	0.25	0.25	0.25	0.25	-
Layers	-	3@0.36"	4@0.37"	4@0.37"	3@0.36"	-
Shims	-	4@0.1046"	5@0.1046"	5@0.1046"	4@0.1046"	-
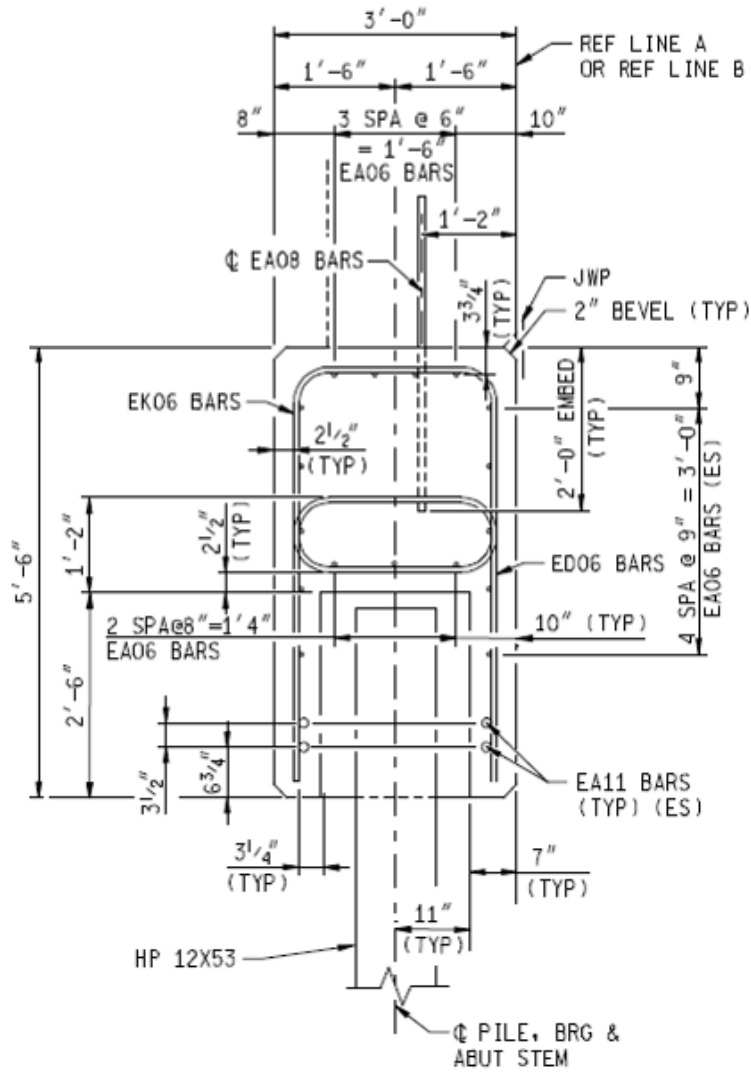
Figure 6-18. Abutment and backwall connection details

41

6.5.3 Full-Depth Deck Panels, Joints, and Haunch

The 9 in., full-depth deck panels are designed to span over the girders. The deck panels are modeled having node lines along the post-tensioning duct locations to accommodate post-tensioning tendons depicted in Figure 6-5. The typical deck panel joint detail, described in the plans, is simplified in the model since its effect on the global structural response is negligible. Simplified flat contact, 2 in. wide joint detail represents grouted joints between deck panels (Figure 6-19).
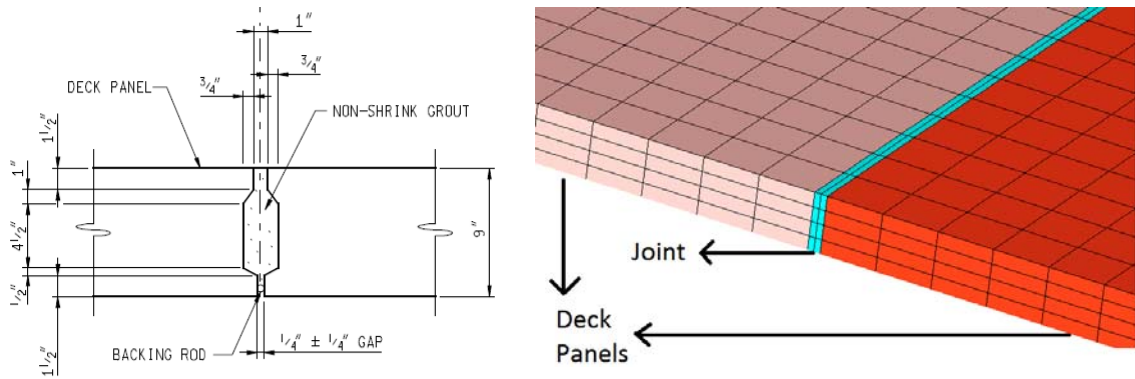
(a) Typical joint detail

(b) FE deck panel model with a panel joint

Figure 6-19. Typical joint details and FE representation

Furthermore, haunch thickness changes as detailed in the plans, but a 2 in. uniformly thick haunch is incorporated into the model (Figure 6-20). The element type of C3D8I is selected for all of the deck panels, joints, and haunch in this model.
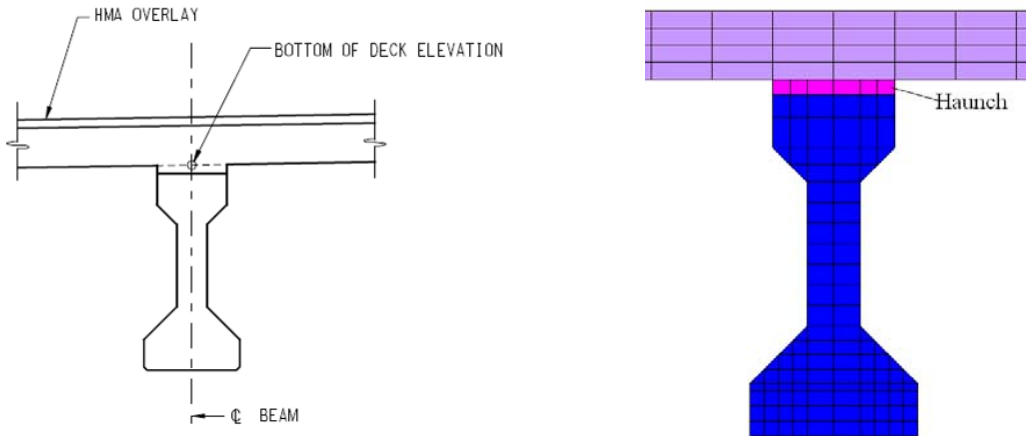
Figure 6-20. Girder, deck panel, and haunch model

6.5.4 End and Intermediate Diaphragms

The intermediate diaphragms are modeled using beam element, which has an equal cross-section and moment of inertia to the MC 18x42.7 steel section. For end diaphragms, instead of using solid elements, rigid elements are used. Ends of the rigid elements are connected to the beam as shown in Figure 6-21. The rigid element configuration, shown in Figure 6-21, is selected to avoid potential over-constrained problems. Concrete fill material shown in Figure 6-21 is defined at the pier location between girder ends by using C3D8I elements.
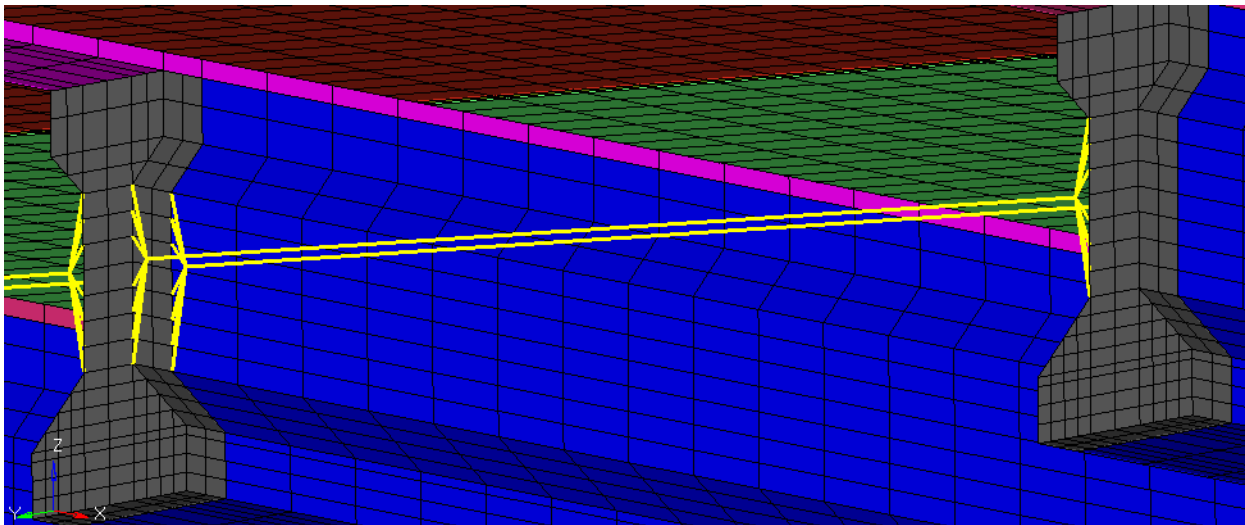
Figure 6-21. Diaphragm and concrete fill

6.5.5 Bridge Model

During the construction, prestress I-beams were erected and shim packs were installed on top of the girders. Deck panels were placed on top of the shim packs allowing horizontal movement of the panels. Subsequently, deck panel joints were grouted and the CIP closure concrete was placed. After CIP and grout joints reached 3500 psi, post-tensioning tendons were installed and stressed. Finally, haunch and shear pockets were grouted. This process allowed compressing only the deck panel system without creating any secondary stresses on rest of the components.

The FE model represents the entire bridge superstructure. Abaqus version 6.10 allows removing and adding elements during analysis. This option in abaqus was implemented to model the construction process by first removing elements from the full bridge models and adding them back on gradually. First, surfaces were generated. Then, the self-weight of the haunch and deck panels was calculated. Then, the haunch was removed, and the self-weight of haunch and deck

43

panels was applied to the top of the beam. At the same time, tendons in I-beam and deck panels were stressed to induce prestress and post-tension effects. During this particular analysis step, deck panels were supported on temporary supports such that there was no load transfer between the deck panels and the I-beams. Afterwards, the haunch was added to the structure, and uniform load and temporary boundary conditions were removed. Consequently, the complete superstructure model was developed without inducing secondary stresses.

6.5.6 Contact Surface Modeling

The bridge has a 23 degree skew. Girders are placed parallel to the bridge's longitudinal axis, and their ends are perpendicular to its longitudinal axis. Deck panels are placed parallel to pier or abutment axes. Because of these reasons, two different mesh configurations were developed for the girders and deck panels. Furthermore, a refined mesh configuration is used for deck panels to maintain their maximum aspect ratio of less than five. Five is considered to be the critical aspect ratio for stress analysis since we are interested in deck panel stresses under the aforementioned loads.

Interaction between dissimilar meshes can be established using contact interaction. Abaqus allows three different types of contact analysis which are general contacts, contact elements and contact pairs. According to Romkema (2010), the contact pair option requires a surface to be created at each interface but will yield more accurate results; hence, interaction between two dissimilar meshes was defined by using contact pair option in Abaqus. Details of this modeling process can be found in Romkema et al. (2010) and Simulia (2010). Master and slave surfaces were generated between the beam and haunch and haunch and deck panels (Figure 6-22).
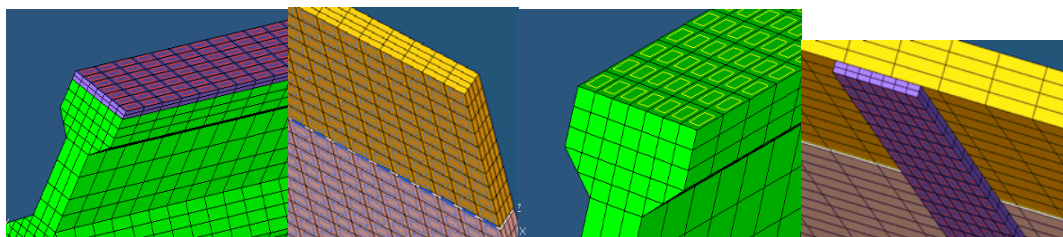
Figure 6-22. Contact surfaces

6.6   FE Model Calibration

6.6.1   Calibration with Load Test Data

Three sensor groups were monitored during load testing. As stated previously, data was collected during all 10 loading scenarios. The three sensor groups are: (1) all C sensors embedded in the north panels and located closed to the closure joint; (b) A sensors embedded in south panels and located over the piers; and (c) F sensors embedded in south panels and located at the mid-span of spans 2 and 3 (Figure 6-23). These three sensor groups are labeled as North C, South A, and South F, respectively for the purpose of comparison with FE results. The measured stress from sensors during each of the 10 loading scenarios was compared with the FE results. Figure 6-24 is an example of the comparison of stresses measured using North C, A, and F sensors and the FE analysis results for loading scenario 1.

Similar comparisons were performed for all loading scenarios and included in Appendix B. FE analysis results correlate well with sensor data except in scenarios 2 and 9. During these two loading scenarios, several C and F sensors show tensile stresses of up to 40 psi, while they are expected to be under compressive stresses. As seen from the Figure 6-24, the change in stress under static truck load is very small. Accuracy of the Vibrating Wire Sensors embedded in concrete is at $\pm$ 0.5%. Initial readings of the sensors, before placing the trucks, were about -2000 psi; therefore, a $\pm$10 psi deviation would be within the resolution accuracy and not discernible. Hence, most of the load testing data lies within the noise level of the sensors, an indication of the negligible impact of live load on stresses that develop in the deck panels.

For joint durability, thermal loads play a significant role, and further analysis was required to calibrate the model under temperature loads.
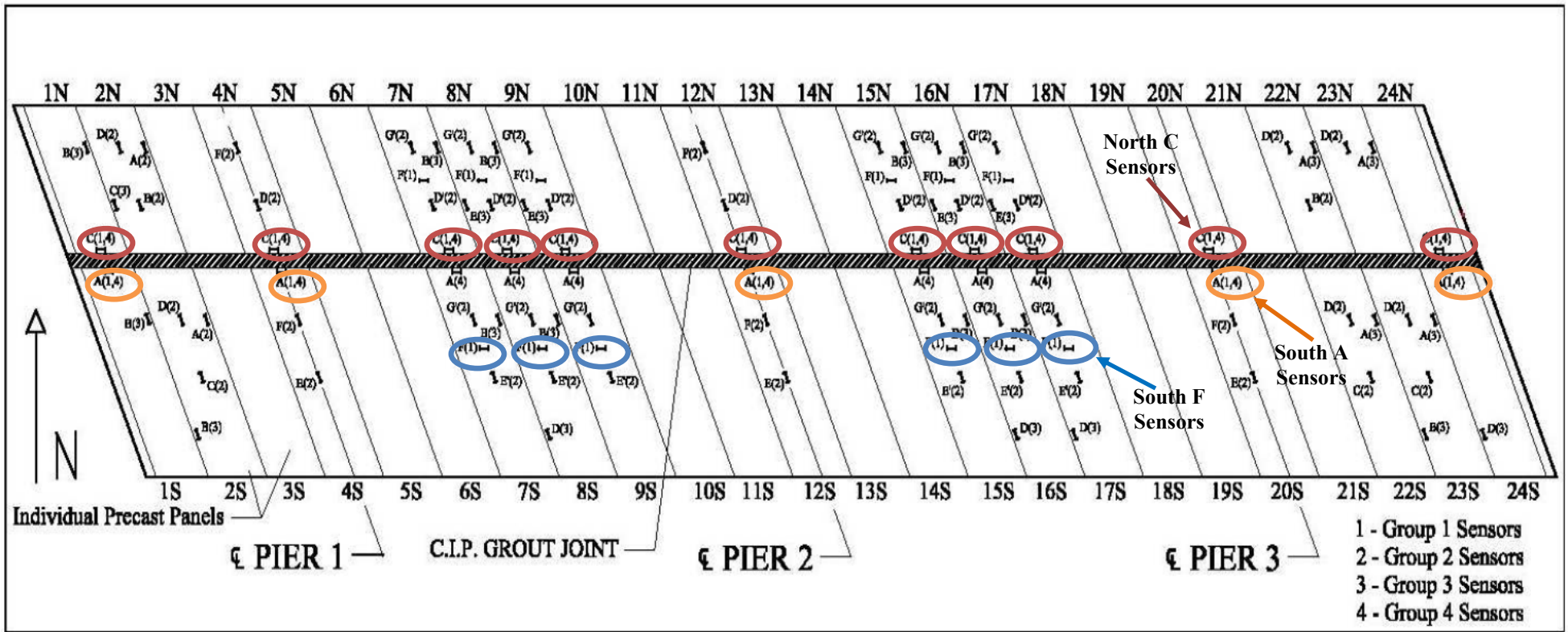
Figure 6-23. Sensor locations and deck layout
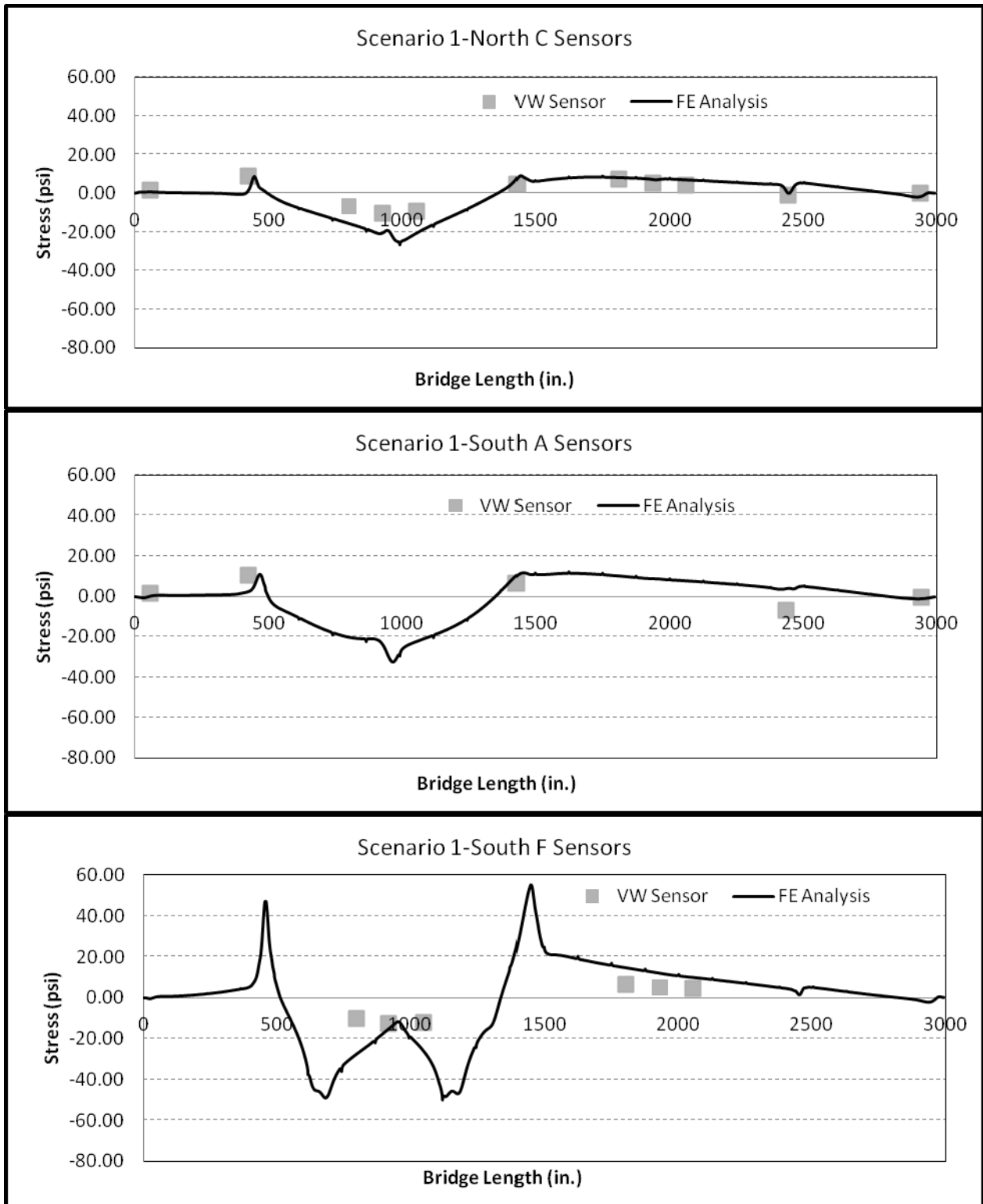
Figure 6-24. Comparison of load test data and FE analysis results – Scenario 1

6.6.2 Calibration with Thermal Loads

A parametric analysis was conducted evaluating various mesh configurations, temperature profiles, and boundary conditions. As per the abutment design details, girder ends are encased with a cast-in-place concrete backwall which is connected to the abutment wall through a single layer of dowels. Note that, in this bridge, the girder ends are not constrained from rotation. Therefore, only horizontal shear and vertical forces are transferred from the bridge superstructure to the abutment. Backfill and the piles provide some restraint to bridge movement. Ideal boundary conditions, pin and roller supports, were used at the abutments to establish the upper and lower bound constraints. A pin support was used at pier 2 while rollers were used at pier 1 and 3. As shown in Figure 6-25, the sensor data lies within the upper and lower bounds established using pin and roller boundary conditions. Note that the data shown in Figure 6-25 represent the change in stress from noon to 6 p.m.

The FE analysis results can be improved by modeling soil-structure interaction using nonlinear springs; however, required modeling efforts and increase in analysis time do not justify the potential outcome as the upper and lower bound results do not change significantly within 2nd and 3rd spans. Further, a good correlation between analysis results and the sensor data was achieved. In addition, a slight change in temperature profile changes the stresses developed in the deck. The temperature profiles, discussed in section 6.4.3, are for a section without an asphalt wearing surface. Presence of an asphalt cover affects the surface temperature (Fouad 2007). However, due to unavailability of temperature profiles for bridge decks with asphalt wearing surface, the temperature profiles and values given in section 6.4.3 were used for further analysis.

According to the design details, bridge superstructure is restrained for vertical, lateral, and transverse directions at pier 2. Expansion bearings are used at pier 1 and 3 which do not prevent uplift of girders. Hence, analysis was performed by allowing uplift and longitudinal translation at pier 1 and 3 while maintaining pin supports at pier 2 and the abutments. The results are identical to the stresses calculated from the model without uplift (Figure 6-25). Hence, further analysis was performed using the model without uplift at pier 1 and 3 which drastically reduced the analysis time.

The change in transverse stress from noon to 6 p.m. was calculated and compared with the sensor data (Figure 6-26). The model was analyzed using the temperature profiles and values presented in section 6.4.3. The roller boundary conditions at pier 1 and 3 and pin boundary conditions at pier 2 and the abutments were used in the model.

The differences observed in analysis results and sensor data can be attributed to the difference in actual temperature variation within the deck and the temperature profiles used in the analysis and potential movements at the abutments.
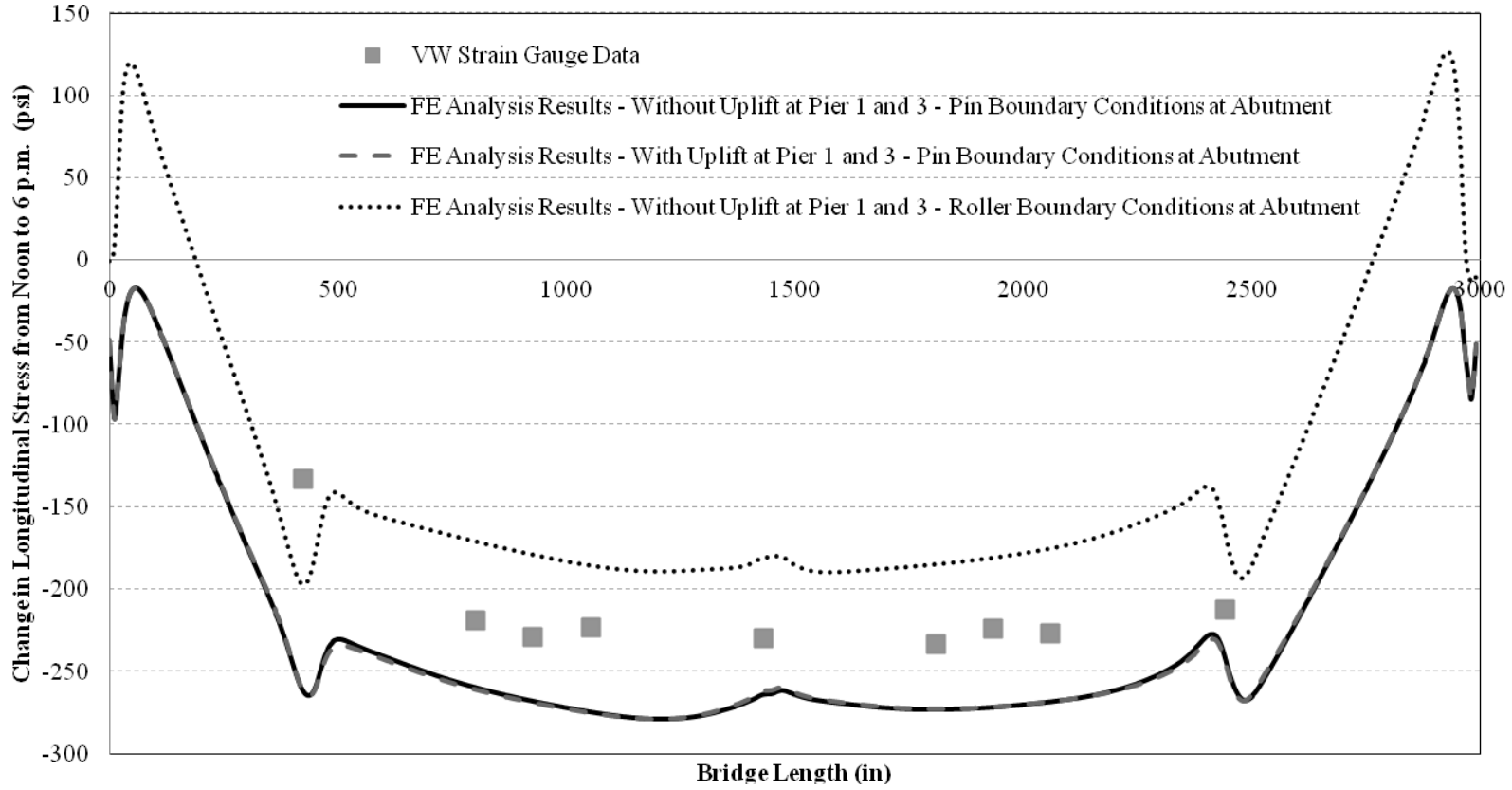
Figure 6-25. Change in longitudinal stress from noon to 6 p.m. under thermal load

50
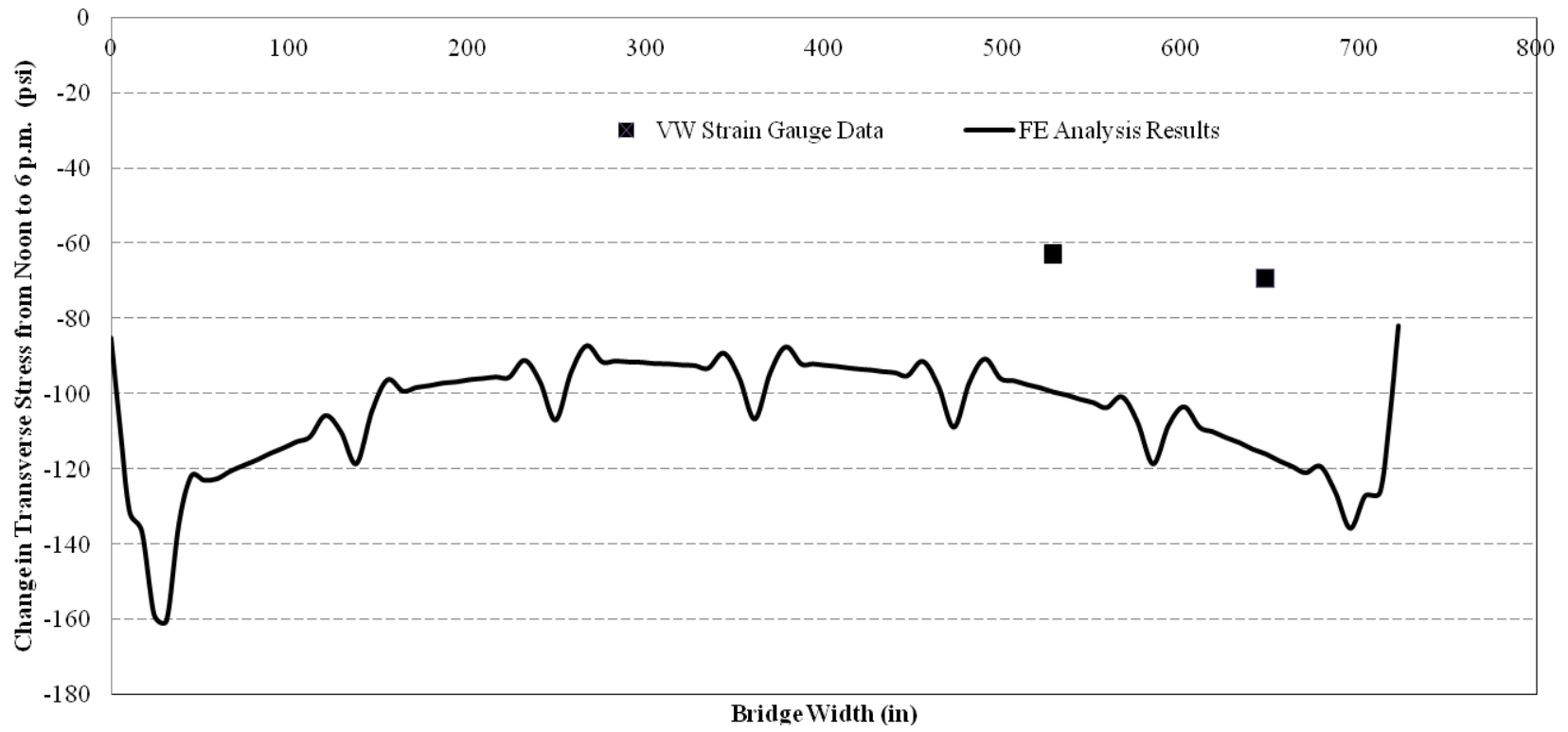
Figure 6-26. Change in transverse stress from noon to 6 p.m. under thermal load

6.7   Bridge Deck Stresses at the End of Construction

After model was calibrated, the bridge deck stresses at the end of construction were calculated through a construction process simulation. Stress contours were developed under self-weight and post-tension (Figure 6-27). Tensile stresses were developed at the edge of the deck panel over the abutments and located in between the post-tension ducts. Bridge deck top surface longitudinal stress variation, between two post-tension ducts, under self-weight and post-tension is shown in Figure 6-28. As shown in Figure 6-28, all the deck panel joints are in compression and the values are around -400 psi, as expected from the design.
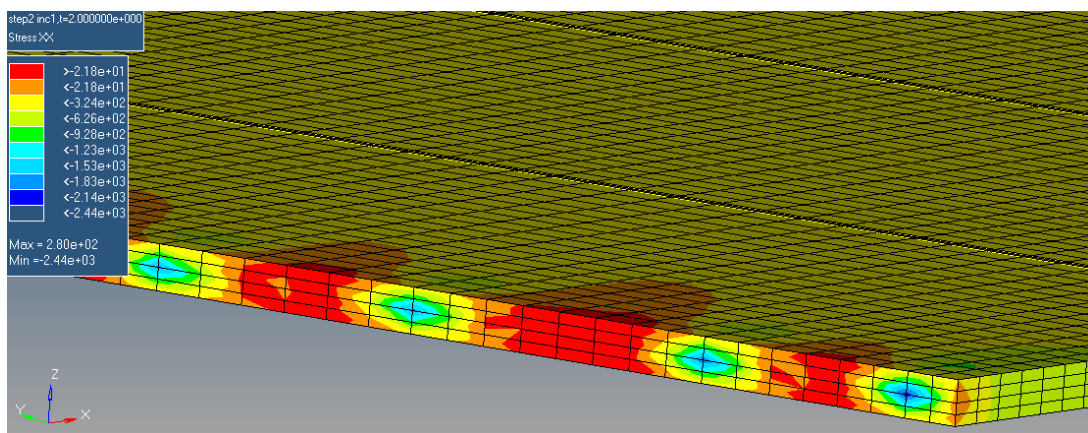
Figure 6-27. Deck panel stress at the end of construction under self-weight and post-tension (psi)
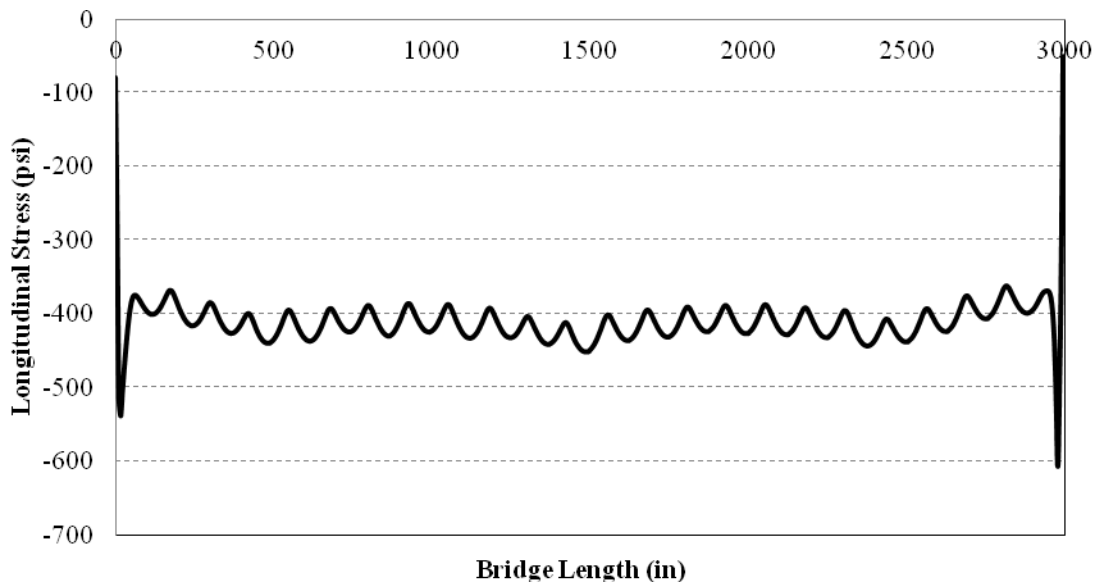
Figure 6-28. Bridge deck stresses at the end of construction

6.8   Modeling Panel Joint Defects

The long-term durability and serviceability of full-depth deck system is questionable as deterioration starts at the transverse joints between deck panels. Most of the durability problems are associated with construction quality control and quality assurance issues related to panel joint grout and grouting procedures (Sneed 2010). After careful consideration of the design details and performance of existing full-depth deck panel systems, in terms of durability, the weakest link in the Parkview Bridge is identified as the transverse joints between deck panels. Hence, it was decided to simulate only the debonding of transverse deck panel joints and develop deterioration prediction models.

As discussed previously, the impact of traffic load is insignificant and not considered in deterioration modeling. Due to lack of models representing temperature variation through the deck during an entire 24-hr cycle, discrete loading was applied simulating stress variation between noon and 6 p.m. As presented in Section 6.4.3, change in thermal gradient from noon to 6 p.m. in a summer day was used. The analysis yielded only one data point a day. Analysis did not include creep and shrinkage as their impact on stress variation is minimum within such a short period of 6 hours in a precast system.

Deterioration of joint between panel 7 and 8 on the north span (i.e., 7N and 8N in Figure 6-23) was considered. Considering the worst case scenario, joint separation was simulated. Abaqus version 6.10 allows changing material properties between analysis steps. This option was used and grout modulus of elasticity was changed to a very small value so that there was no load transfer across the joint. Post-tension strands were continued through the joint, irrespective of the joint condition. Stress variation in panel 7N and 8N without and with deterioration is shown in Figure 6-29 and Figure 6-30, respectively. Stresses shown in the figures are due to change in temperature from noon to 6 p.m., as discussed in Section 6.4.3. When there is no deterioration at the joint, panel 7N and 8N behave monolithically while the deck panels remain compressed (note that the negative values presented in the figures represent compression). On the other hand, panels start to show tensile stresses as monolithic behavior between panels is lost due to deterioration at the joint (Figure 6-30).
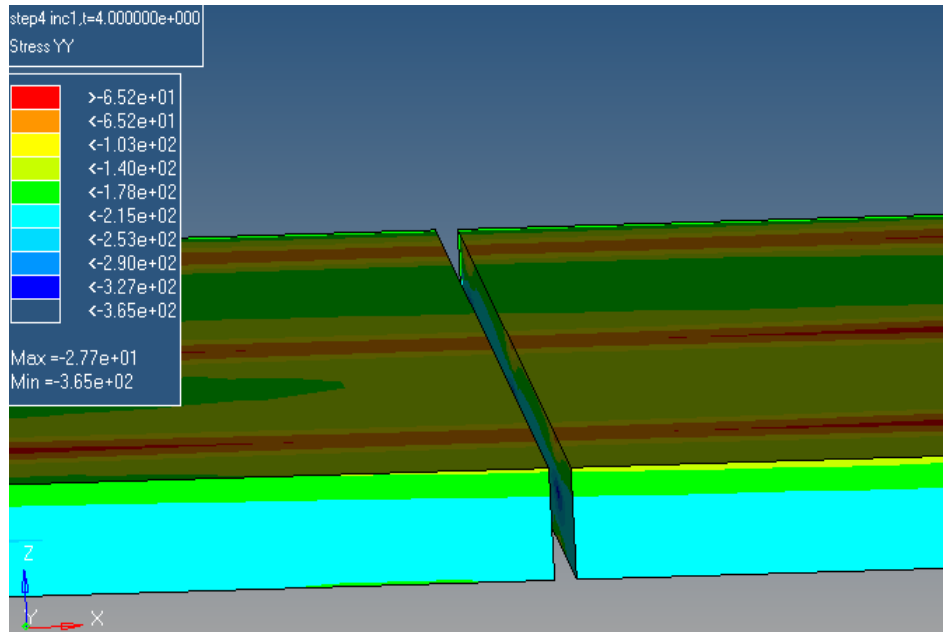
Figure 6-29. Deck panel transverse stress at 6 p.m. - without joint deterioration (psi)
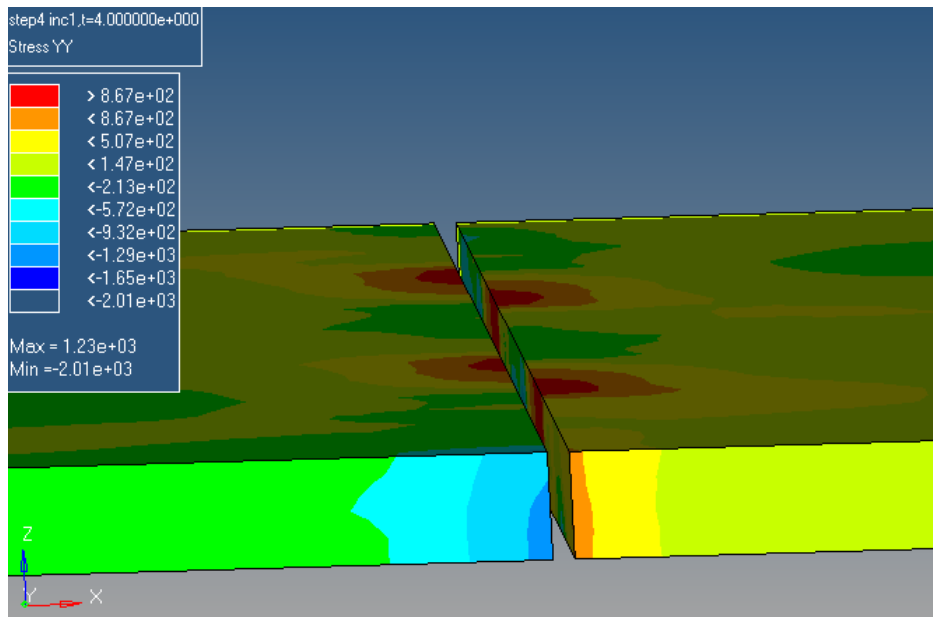
Figure 6-30. Deck panel transverse stress at 6 p.m. - with joint deterioration (psi)

The joint deterioration simulation process discussed in this section was followed, and deterioration prediction models were developed and presented in Section 7.3.

7   DETERIORATION PREDICTION MODEL DEVELOPMENT

The Parkview Bridge deck deterioration prediction model consists of two main modules: 1) stress envelopes from sensor data and 2) finite element joint deterioration signature models.

7.1   Stress Envelopes Development

Data was collected during past three years and analyzed. The stress envelopes were developed to determine baseline performance patterns and conditions. The envelopes are based on the sensor data that was collected and analyzed over a 32-month period. Four stress envelope categories were defined:

2. Longitudinal stress envelopes,
3. Transverse stress envelopes,
4. Panel joint stress envelopes, and
5. Closure grout stress envelopes.

7.1.1   Longitudinal Stress Envelopes

In this category, the stress envelopes were developed for each span and pier locations based on the worst case longitudinal stresses. This was accomplished by using the monthly maximum and minimum stress readings recorded over a 32-month period in the bridge deck within and over the piers. Essentially, the envelopes were developed using the maximum and minimum recorded values within each month rather than using statistical averages. The monthly maximum and minimum stress values were used to develop the stress envelopes for the entire monitoring duration of 32-months. Figure 7-1 shows an example of a stress envelope for the north side of span 1 over a 32 month period. The 32-month envelopes developed for rest of the bridge deck area are provided in Appendix C. Ultimately, the chart in this figure was reduced to a one-year envelope template based on the worst case stress data experienced over the 32-month period of the bridge life-cycle and will be shown later in this section. Note that while the absolute stress envelope for this category can be defined based on the design constraints (i.e. -3600psi to +537psi), we feel that a maximum-minimum stress representation will be a more appropriate baseline since it is not desirable to wait until stresses have reached the design limits.
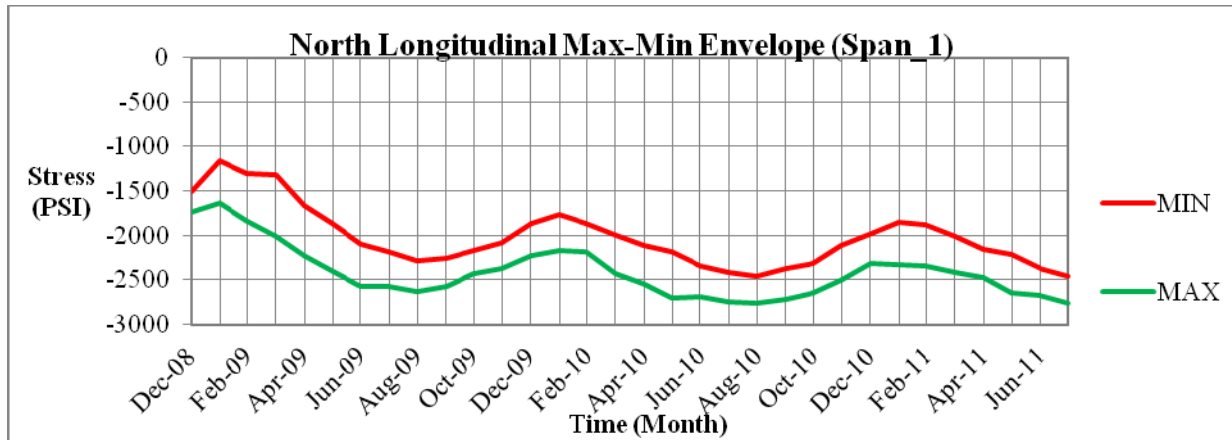
Figure 7-1. Longitudinal max-min stress envelopes for north panels of span 1 (December 2008 to July 2011)

7.1.2 Transverse Stress Envelopes

Using the same process described in the previous section, the transverse stress envelopes were developed using data from the sensors that are placed in the transverse direction of the deck. Figure 7-2 shows an example of a stress envelope for the north side of span 1 over 32 months. The 32-month envelopes developed for rest of the bridge deck area are provided in Appendix C. Again, this chart was reduced to a one-year envelope template based on the worst case stress data experienced over the initial three years of the bridge's life and will be shown later in this section.
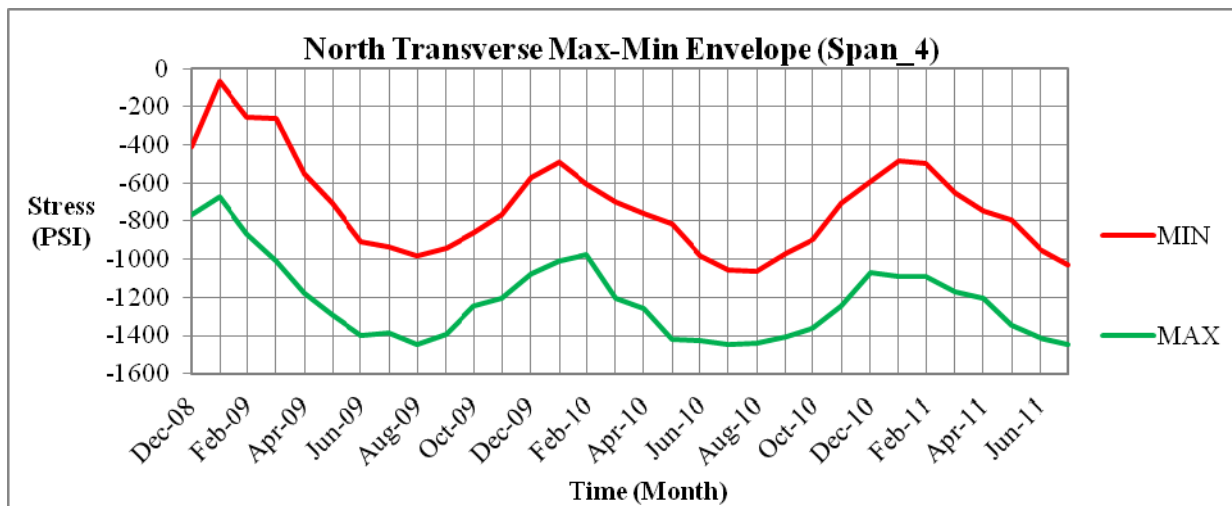
Figure 7-2. Transverse max-min stress envelopes for north panels of span 4 (December 2008 to July 2011)

7.1.3 Panel Joint Stress Envelopes

In this category, the goal was to evaluate the joint integrity between two panels. The basis for the evaluation was the stress patterns measured by the sensors in the panels on both sides of a

joint. If a joint is healthy, the two panels on both sides of the joint would behave monolithically (the design intent), and the stress profiles of the sensors on both sides of the joint would have similar patterns. To formalize the assessment of the joint condition and the creation of the stress envelopes, the following process was developed:

1. Monitor joint sensor data profiles on a monthly basis.
2. Establish correlation between the sensors across the panel joints.
3. Compute the difference in stresses between the sensor readings across panel joints to establish the differential stress envelope by
   – histograms for the differences (frequency analysis) to estimate the data distribution,
   – the mean and standard deviation of the differences,
   – the best random variable model that represents the histograms, and
   – differential stress envelopes based on the best-fit random variable properties, and the mean and standard deviation values.

These sensors are embedded in the bridge deck in the transverse direction and are placed very close to the joints between the panels. Table 7-1 lists the sensor in the transverse direction while Figure 7-3 shows an example of the parallel-to-edge sensors (N-7-B and N-8-E) that monitor the differential stresses across the joint between north panels 7 and 8. Table 7-2 shows that the two sensors (N-7-B and N-8-E) are highly correlated which is an indication of the monolithic behavior of the two north panels (7 and 8). The difference between the sensors' stresses is computed and shown in Figure 7-4. A histogram for the differences is shown in Figure 7-5. The histogram shows that this distribution is Gaussian l. Based on a Gaussian distribution, the limits of difference range, or the stress envelope, for this panel joint is calculated as:

Maximum Stress Limits = Mean - 2*σ (95% confidence)
Maximum Stress Limits = Mean - 3*σ (99% confidence)
Minimum Stress Limits = Mean + 2*σ (95% confidence)
Minimum Stress Limits = Mean + 3*σ (99% confidence)

Figure 7-6 shows the stress envelope for the sensors across the joint between north panels 7 and 8. The chart in this figure is developed as a one-year envelope template based on the normal

distribution differential stress data experienced over the initial three years of the bridge life-cycle as will be shown later in this section.

Table 7-1. Panel Joint Sensors

Span #	North Panel	Sensor	Sensor	South Panel	Sensor	Sensor
Span 1	1	N-1-B		1	S-1-B	
	2	N-2-C		2	S-2-B	
Span 2	7	N-7-B		7	S-7-B	
	8	N-8-E	N-8-B	8	S-8-D	S-8-B
	9		N-9-E	9		S-9-D
Span 3	15	N-15-B		15	S-15-B	
	16	N-16-E	N-16-B	16	S-16-D	S-16-B
	17		N-17-E	17		S-17-D
Span 4	22	N-22-A		22	S-22-A	
	23	N-23-C	N-23-A	23	S-23-B	S-23-A
	24		N-24-D	24		S-24-D
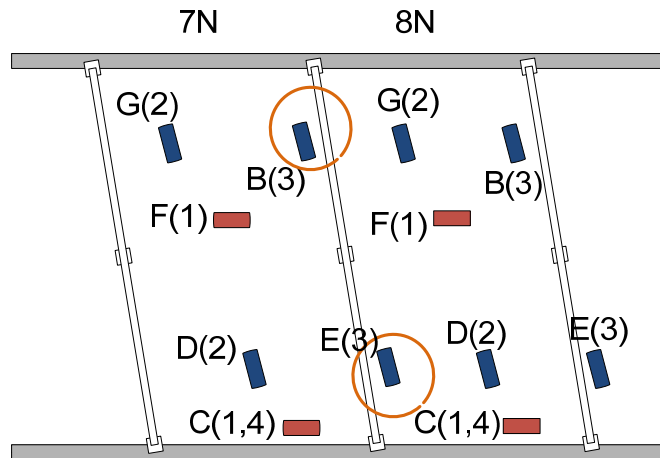
Figure 7-3. Panel joint sensors N-7-B and N-8-E for the joint between north panels 7 and 8

Table 7-2. Sensors Correlation Coefficient for North and South Side Panels for the Cumulative Period from January 2009 through July 2011

Span #	North Panel	Sensor	Sensor	North Panel	Correlation Coefficient	
Span 1	1	N-1-B		1	0.9399	
	2	N-2-C		2		
Span 2	7	N-7-B		7	0.9817	
	8	N-8-E	N-8-B	8		0.9823
	9		N-9-E	9		
Span 3	15	N-15-B		15	0.9896	
	16	N-16-E	N-16-B	16		0.8621
	17		N-17-E	17		
Span 4	22	N-22-A		22	0.9904	
	23	N-23-C	N-23-A	23		0.9660
	24		N-24-D	24		
Span #	South Panel	Sensor	Sensor	South Panel	Correlation Coefficient	
Span 1	1	S-1-B		1	0.9670	
	2	S-2-B		2		
Span 2	7	S-7-B		7	0.9787	
	8	S-8-D	S-8-B	8		0.8076
	9		S-9-D	9		
Span 3	15	S-15-B		15	0.9776	
	16	S-16-D	S-16-B	16		0.9816
	17		S-17-D	17		
Span 4	22	S-22-A		22	0.9358	
	23	S-23-B	S-23-A	23		0.9938
	24		S-24-D	24		
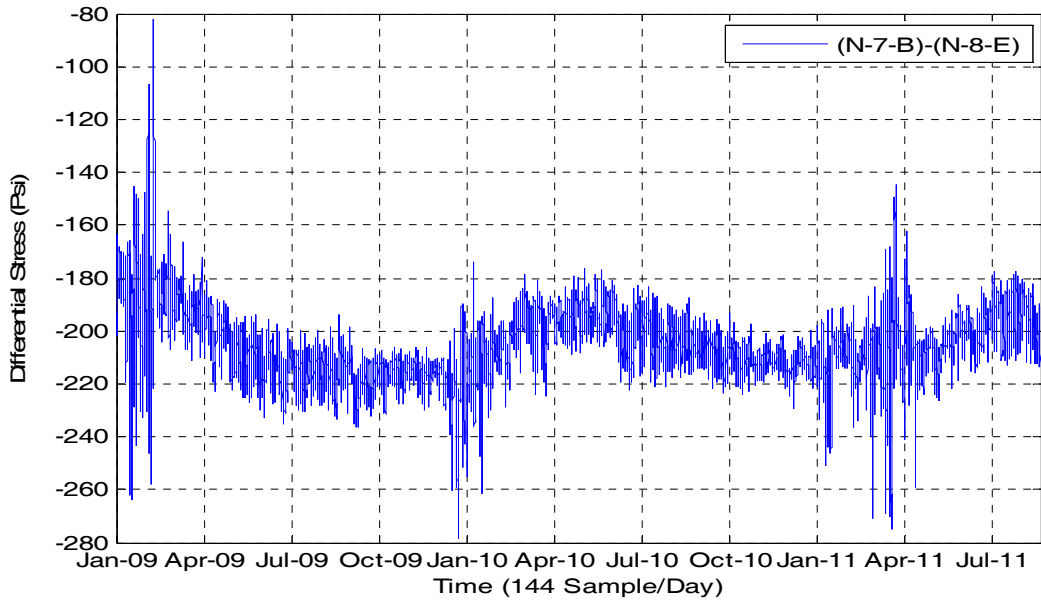
Figure 7-4. Differential stress profile calculated from parallel-to-edge sensors in the north panels 7 and 8 (Span 2) for the period from January 2009 through July 2011
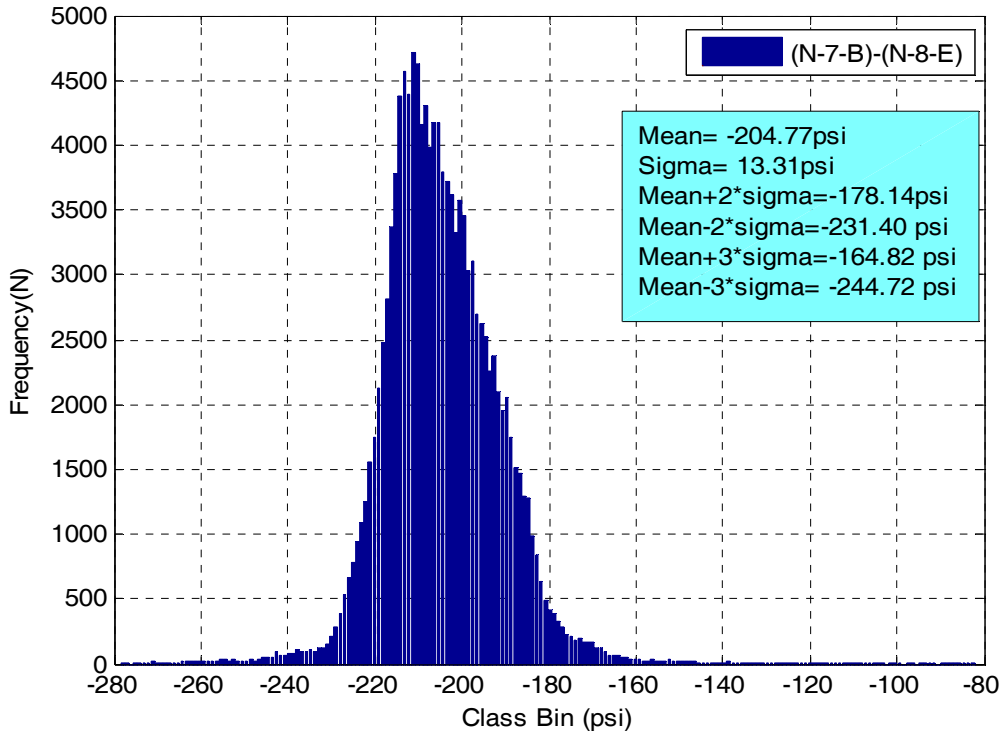
Figure 7-5. Differential stress histogram for parallel-to-edge sensors between north panels 7 and 8 (span 2) for the period from January-2009 to July 2011

60
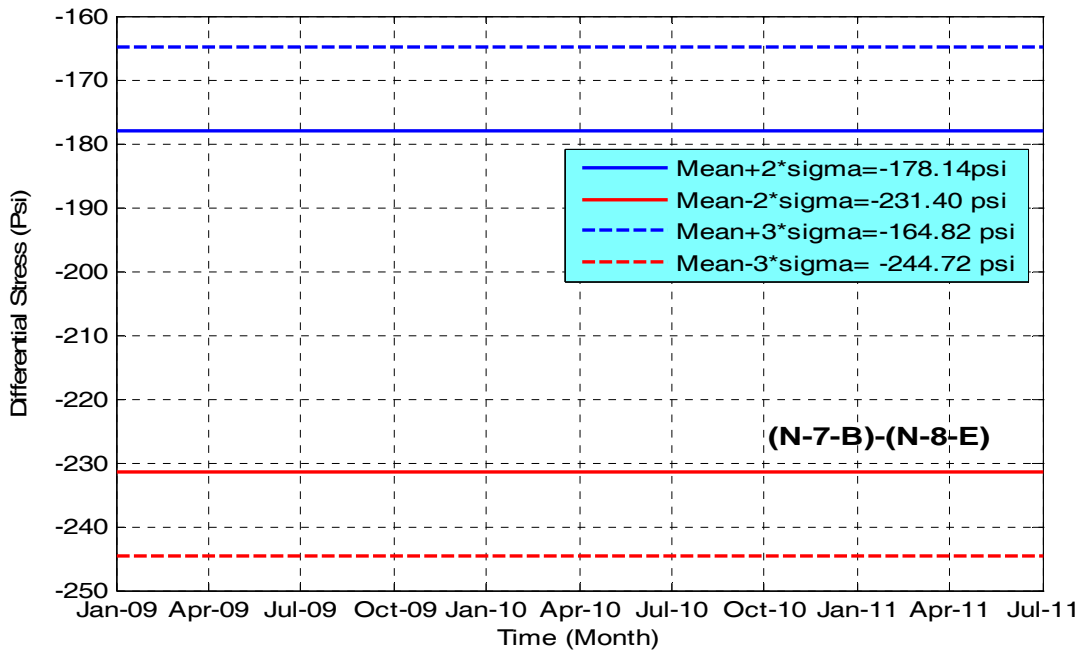
Figure 7-6. Differential stress envelope for parallel-to-edge sensors between north panels 7 and 8 (Span2) for the period from January 2009 through July 2011

7.1.4 Longitudinal Closure Grout Stress Envelopes

The closure grout stress envelopes are generated from the Gaussian distribution model of the sensor data of the longitudinally embedded sensors around the closure area along the Parkview Bridge deck. The goal of these stress envelopes is to monitor the closure grout stresses between the north and south side panels. If the panels on both sides of the closure behave monolithically, the stress profiles of the sensors on both sides would have similar patterns.

Table 7-3 lists the panels on either side (north and south) of the closure and the corresponding sensors that are used in this analysis. It is clear from this table that, to-date, all the sensor pairs across the closure are highly correlated, an indication of the monolithic behavior of the north and south panels across the closure. Furthermore, differential stress histograms were developed. Figure 7-7 shows an example differential stress histogram for the closure grout sensors between north panel 7 and south panel 7 in span 2 (sensors N-7-C and S-7-A). Assuming the histogram is Gaussian, the maximum and minimum stress limits are calculated as:

Maximum Stress Limits = Mean - 2*σ (95% confidence)

Maximum Stress Limits = Mean - 3*σ (99% confidence)

Minimum Stress Limits = Mean + 2*σ (95% confidence)

Minimum Stress Limits = Mean + 3*σ (99% confidence)

Table 7-3. Correlation Coefficient of Closure Grout Sensors for the Cumulative Period from January 2009 through November 2010

Span #	North Panel	Sensor	South Panel	Sensor	Correlation
Span 1	1	N-1-C	1	S-1-A	0.9938
Pier 1	4	N-4-C	4	S-4-A	0.9937
Span 2	7	N-7-C	7	S-7-A	0.9964
	8	N-8-C	8	S-8-A	0.9941
	9	N-9-C	9	S-8-A	0.9949
Pier 2	12	N-12-C	12	S-12-A	0.9604
Span 3	15	N-15-C	15	S-15-A	0.9950
	16	N-16-C	16	S-16-A	0.9943
	17	N-17-C	17	S-17-A	0.9954
Pier 3	20	N-20-C	20	S-20-A	0.9965
Span 4	24	N-24-C	24	S-24-A	0.9928
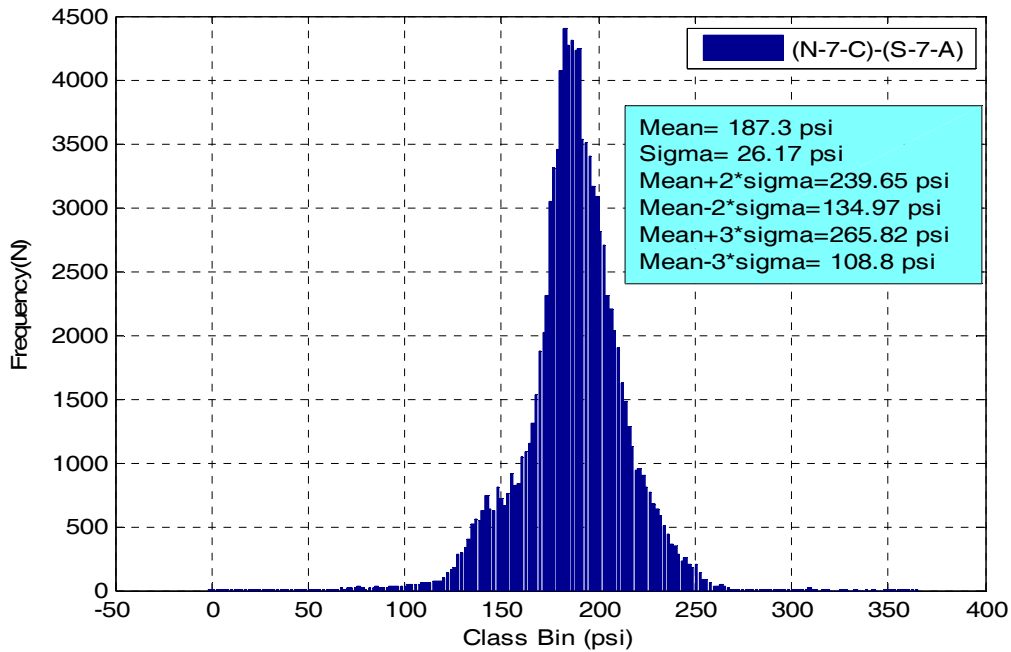
Figure 7-7. Differential stress histogram for the closure grout sensors between north panel 7 and south panel 7 (span 2) for the period from January 2009 through July 2011

Figure 7-8 is developed as a one-year envelope template based on the normal distribution differential stress data experienced over the initial three years of the bridge life-cycle.
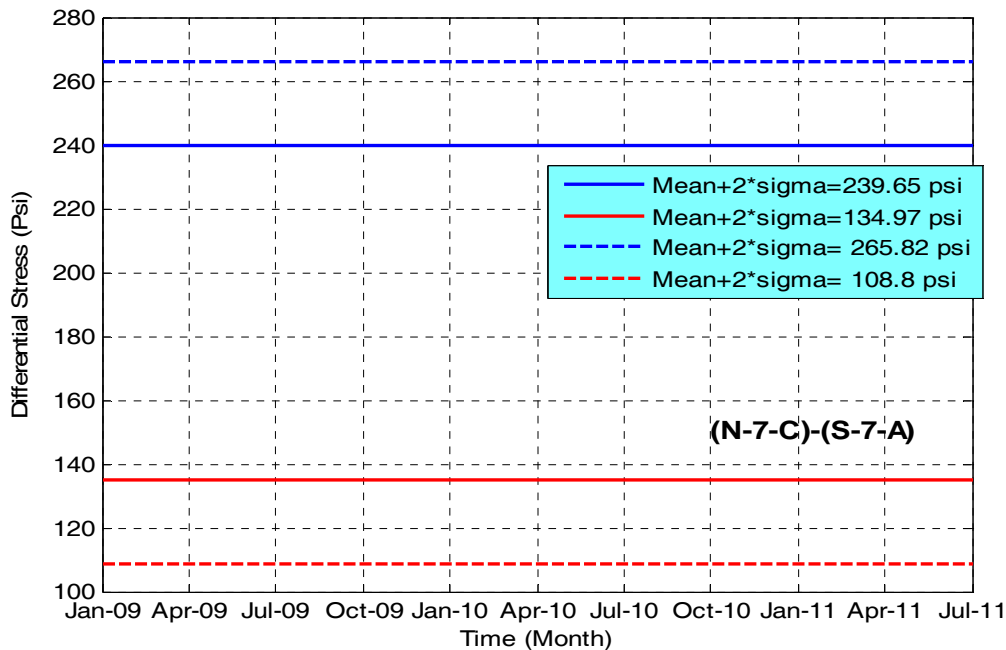
Figure 7-8. Differential stress envelope for grout sensors between north panel 7 and south panel 7 (span 2) for the period from January 2009 through July 2011

7.2   Final Stress Envelopes

This section presents the stress envelopes of the four categories outlined in Section 7.1.   The envelopes are one-year templates (January to December) that represent the limits of acceptable stress values in each category.

7.2.1 Longitudinal Stress Envelopes

Figure 7-9 is an example of a one-year stress envelope for south span 2 in the longitudinal direction. A similar set of envelopes is developed and are presented in Appendix D. Figure 7-10 is an example of stresses collected during August and September 2011 (after the development of the envelopes) and plotted against the limits presented in the envelopes. Note that in some instances on the figure stresses exceeded the maximum envelop limit, meaning that they were higher than the maximum compression experienced by the baseline envelope. However, these stresses do not represent a concern since they are still well below the design limit of -3600psi.
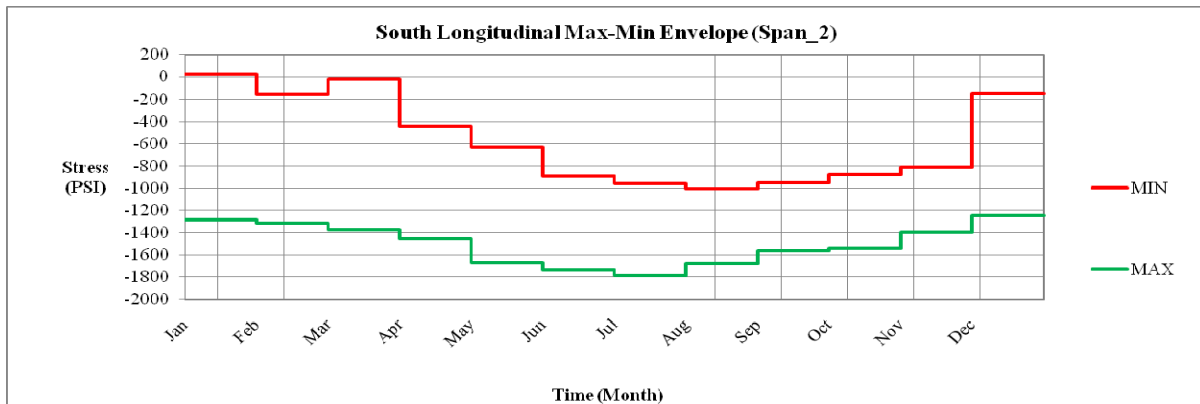
Figure 7-9. One-year envelope for south span 1 in the longitudinal direction
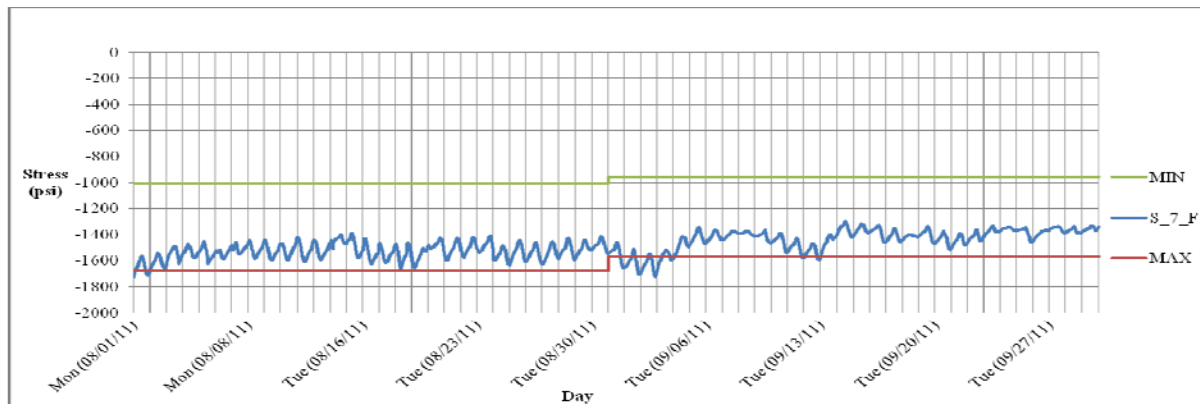
Figure 7-10. An example of the south longitudinal envelope for span 2 with stresses collected during August and September 2011

7.2.2 Transverse Stress Envelopes

Figure 7-11 is an example of a one-year stress envelope for south span 2 in the transverse direction. A similar set of envelopes is developed and are presented in Appendix D. Figure 7-12 is an example of stresses collected during August and September 2011 (after the development of the envelopes) and plotted against the limits presented in the envelopes.
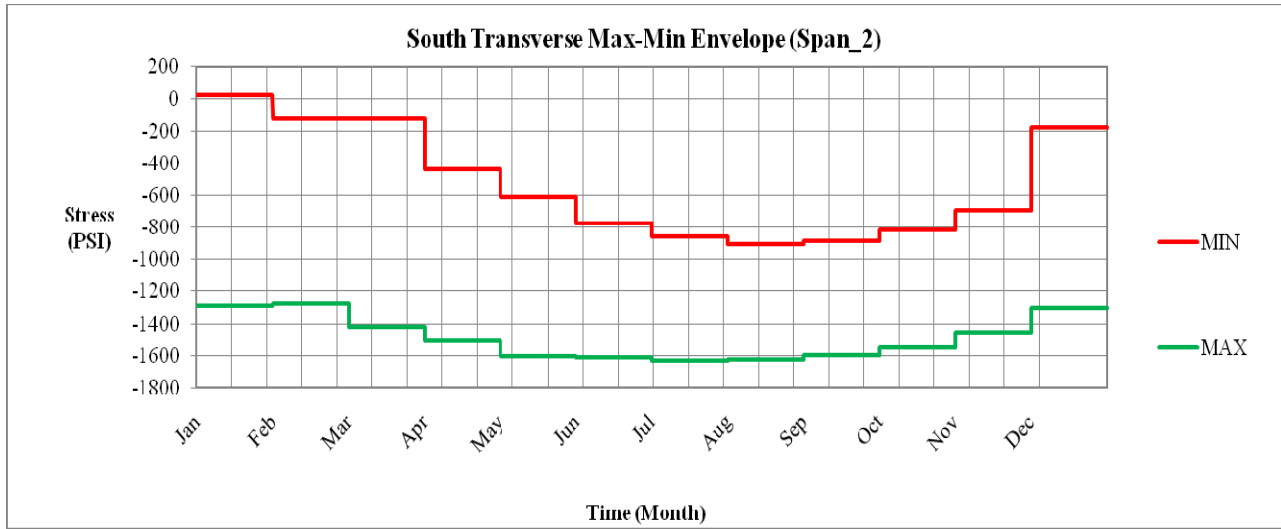
Figure 7-11. One-year envelope for north span 2 in the transverse direction
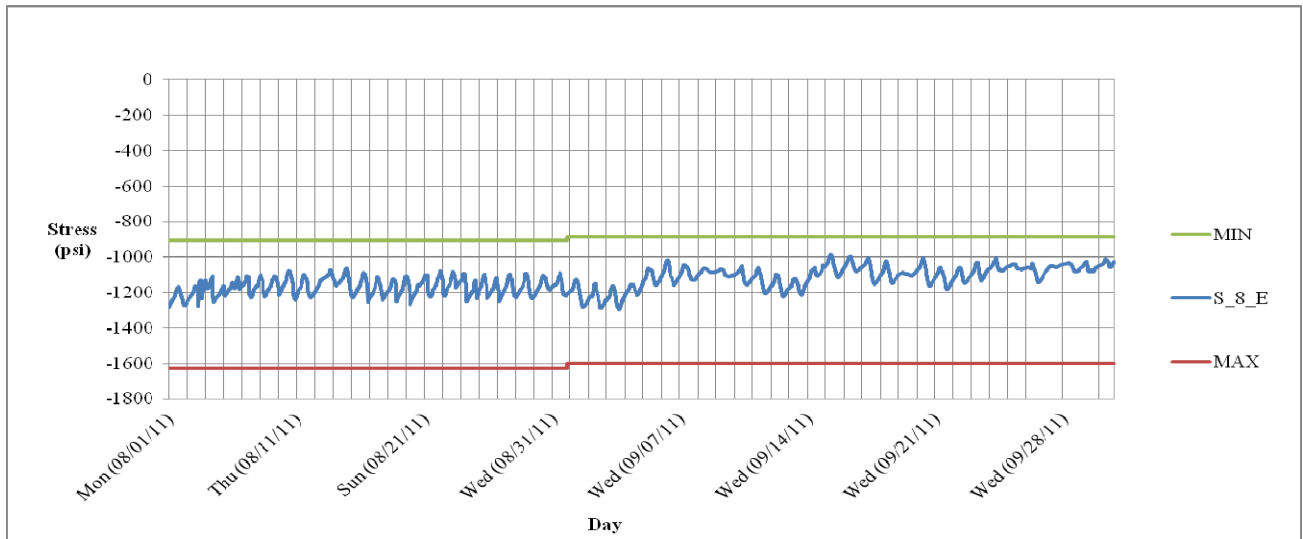
Figure 7-12. An example of the south transverse envelope for span 2 with stresses collected during August and September 2011

7.2.3 Panel Joint Stress Envelopes

Figure 7-13 is an example of a one-year stress envelope for the joint between south panels 7 and 8. A similar set of envelopes is developed for the rest of the panel joints and are presented in Appendix D. Figure 7-14 is an example of stresses collected during August and September 2011 (after the development of the envelopes) and plotted against the limits presented in the envelopes. Note that the stress envelopes presented in Figure 7-13 and Appendix D were based on a Gaussian distribution developed using data collected during the first 32 months of the bridge's life. Generally, it is expected to have differential stresses fluctuating within the boundaries defined by Mean +/- 3*σ (with 99% confidence). Exceeding the Mean +/- 3*σ boundaries for an extended period of time would require a detailed investigation.
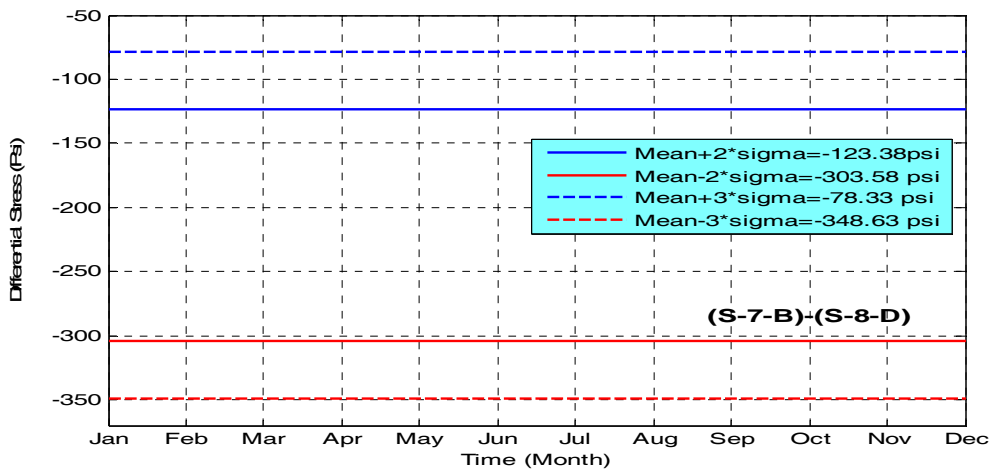
Figure 7-13. One-year differential stress envelope for sensors across the joint between south panels 7 and 8 (Span2).
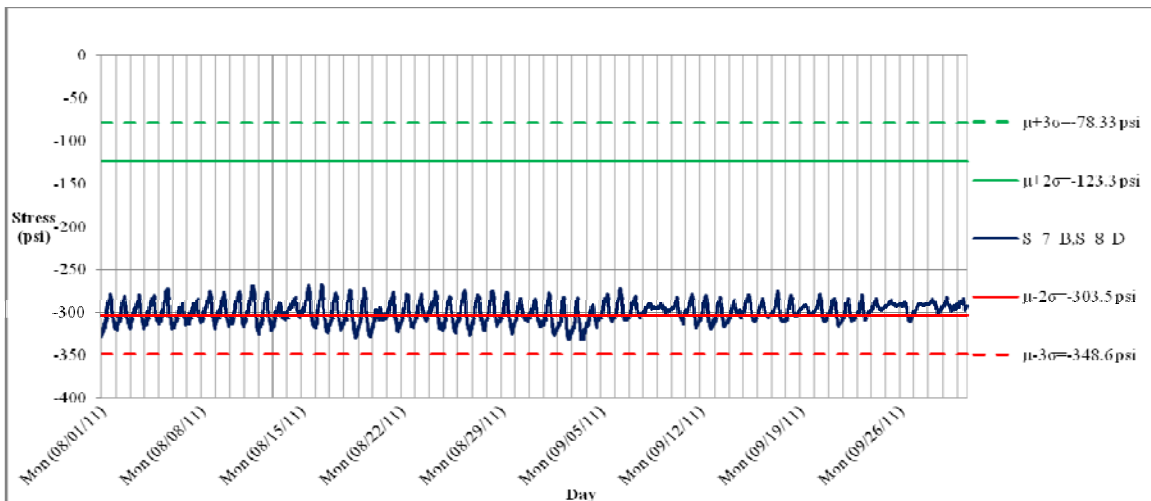
Figure 7-14. An example of the envelope for the joint between south panels 7 and 8 (Span 2) with stresses collected during August and September 2011

66

7.2.4 Closure Grout Stress Envelopes

Figure 7-15 is an example of a one-year stress envelope for the Parkview bridge closure. A similar set of envelopes is developed for the rest of the panel joints and are presented in Appendix D. Figure 7-16 is an example of stresses collected during August and September 2011 (after the development of the envelopes) and plotted against the limits presented in the envelopes. Note that the stress envelopes presented in Figure 7-15 and Appendix D were based on a Gaussian distribution developed using data collected during the first 32 months of the bridge's life. Generally, it is expected to have differential stresses fluctuating within the boundaries defined by Mean +/- 3*σ (with 99% confidence). Exceeding the Mean +/- 3*σ boundaries for an extended period of time would require a detailed investigation.
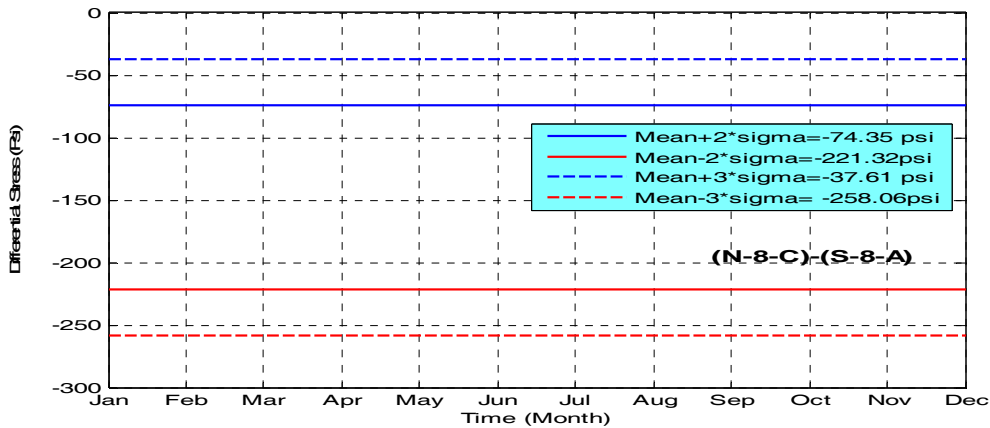
Figure 7-15. One-year differential stress envelope for the closure grout sensors between north panel 8 and south panel 8 (Span 2)
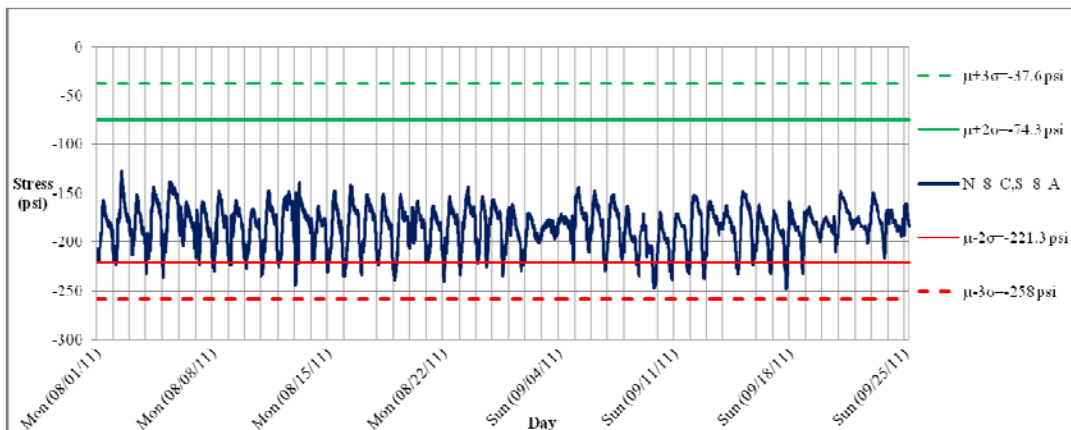
Figure 7-16. An example of the envelope for the closure grout sensors between north panel 8 and south panel 8 (Span 2) with stresses collected during August and September 2011.

7.3 Joint Deterioration Prediction Model

Two different models, with and without deterioration, were analyzed following the procedure discussed in Section 6.8 to monitor the behavior of the structure under thermal loads. According to load test data and the analysis of sensor data, the dominant load is thermal. Hence, the FE analysis was performed under thermal gradient. The temperature data collected from embedded sensors was used for this purpose. Direct comparison of stresses from sensors and FE analysis was not meaningful because the FE model did not include shrinkage, creep and other parameters that might have contributed to the sensor readings. Hence, relative variation of stresses recorded from sensor N-7-B and N-8-E, and FE results of corresponding locations were compared. Relative stresses were calculated using Eq. 7-1 and 7-2. Finite element model was calibrated using temperature data collected during a period of 7 days and stress data collected from vibrating wire sensors during the same period (Figure 7-17). Finite element results and sensor data correlate well. This proves that the FE model is capable of representing bridge superstructure response under thermal gradient.

$$VW_{RS}(t) = |VW(t)| - |VW_M| \qquad \text{Eq. 7-1}$$

where,

$VW_{RS}(t)$ = Relative stress of vibrating wire sensor data at a given time

$VW(t)$ = Vibrating wire sensor reading at a given time

VW_M = Mean value of the vibrating wire sensors data collected during the 7-day period

$$FE_{RS}(t) = |FE(t)| - |FE_M| \qquad \text{Eq. 7-2}$$

where,

$FE_{RS}(t)$ = Relative stress calculated from FE analysis

$FE(t)$ = Stress from FE analysis at time t

VW_M = Mean value of the stress calculated from FE analysis for the 7-day period

Calculation of the transverse stresses from FE results requires a calibration factor between sensor data and the FE analysis. The mean stress values recorded from each sensor are the calibration factors. Hence, the mean stress values calculated from respective sensor data were added to the FE results for transverse stress calculation as shown in Eq. 7-3. Once

calibration factors were introduced, a very good correlation was observed between the transverse stresses calculated along the joint between panel 7 and panel 8 (Figure 7-18). On the other hand, very high stress fluctuations were observed when joint deterioration was simulated in the FE model (Figure 7-18).

$$FE_{TS}(t)_i = |FE(t)_i| + |VW_{Mi}| \qquad \text{Eq. 7-3}$$

where,

$FE_{TS}(t)_i$ = Transverse stress calculated from FE analysis at time t and at sensor location i

$FE(t)_i$ = Stress from FE analysis at time t and sensor location i

VW_{Mi} = Mean stress value of the data collected from a sensor at location i

In order to recommend distress signatures for panel joints, a procedure similar to Section 7.1.3 was followed. The stress differences between sensor N-7-B and N-8-E were calculated from one week's data as shown in Figure 7-19. It is worth reiterating that the FE data shown in Figure 7-19 correspond to the change in stress at sensor locations due to change in temperature from 12 p.m. to 6 p.m. Differential stresses calculated from deteriorated model are greater than 3σ; beyond the 99% confidence level of the data recorded from the sensors. Hence, on-set of deterioration can be identified using sensor data once the differential stress envelopes and FE simulation results similar to Figure 7-19 are made available for each joint. However, before developing FE analysis results simulating deterioration of each joint in the system, it is required to fine-tune the model developed for the joint between panel 7N and 8N. Once long-term monitoring data is available, fine-tuning of distress signatures needs to be performed and further refinements to the 3σ limits needs be evaluated.
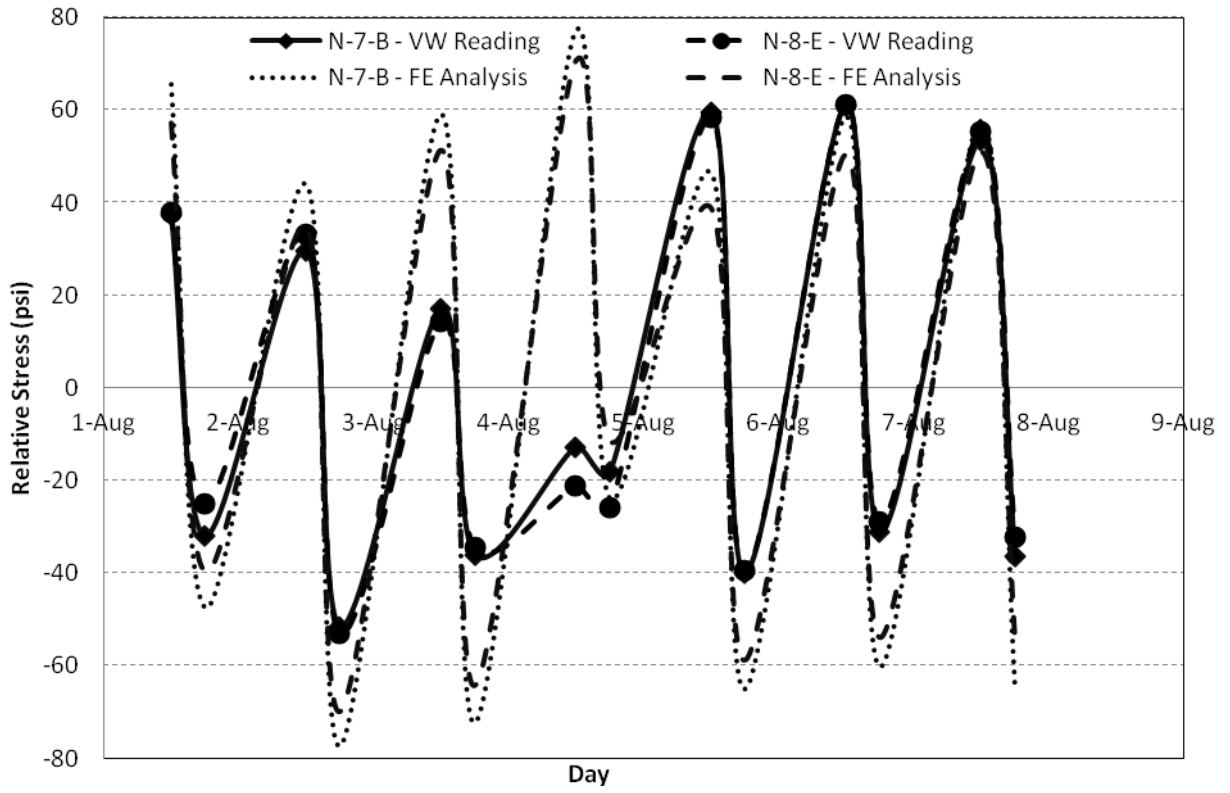
Figure 7-17. Relative stress variation against time
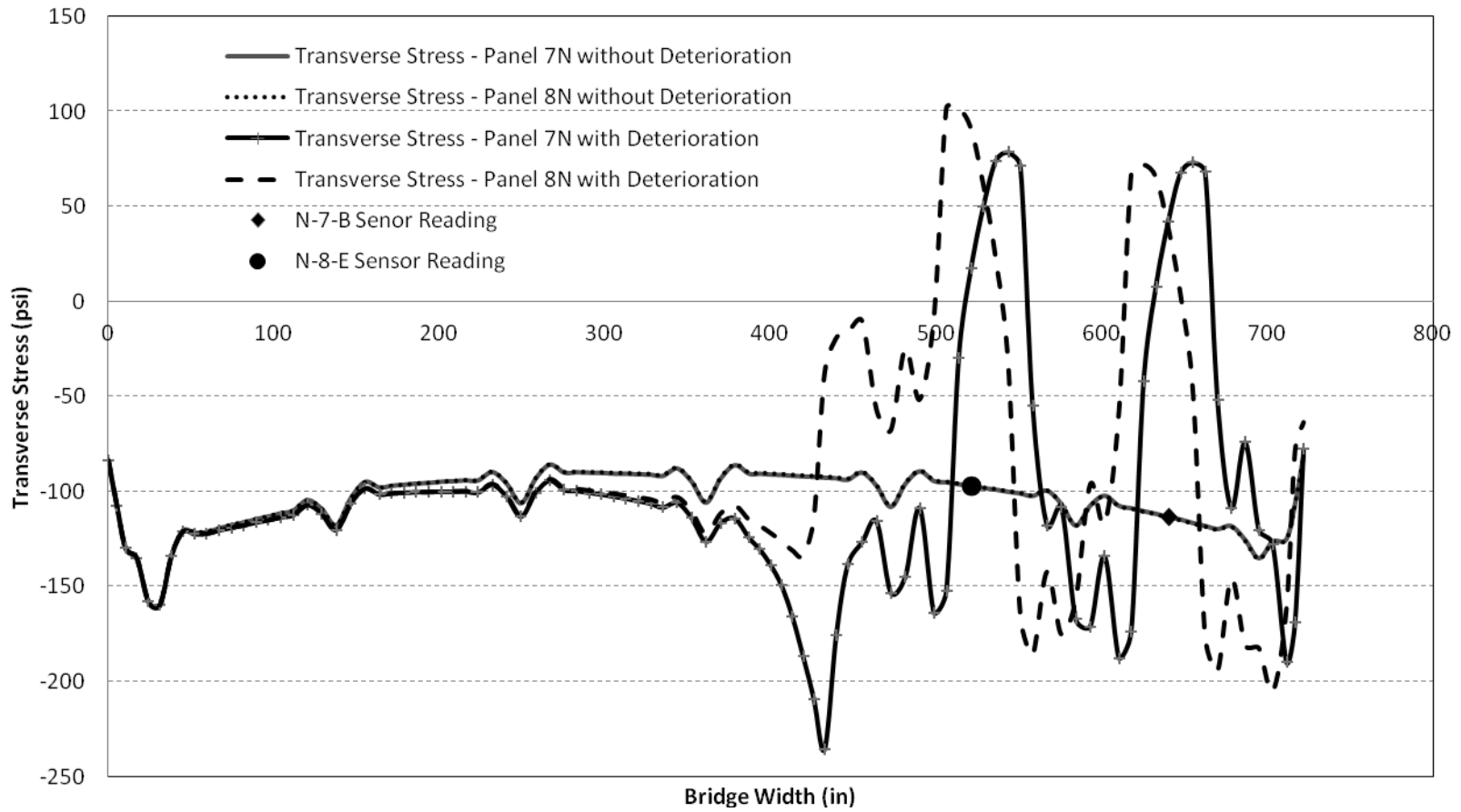
Figure 7-18. Transverse stress variation along the panel joint
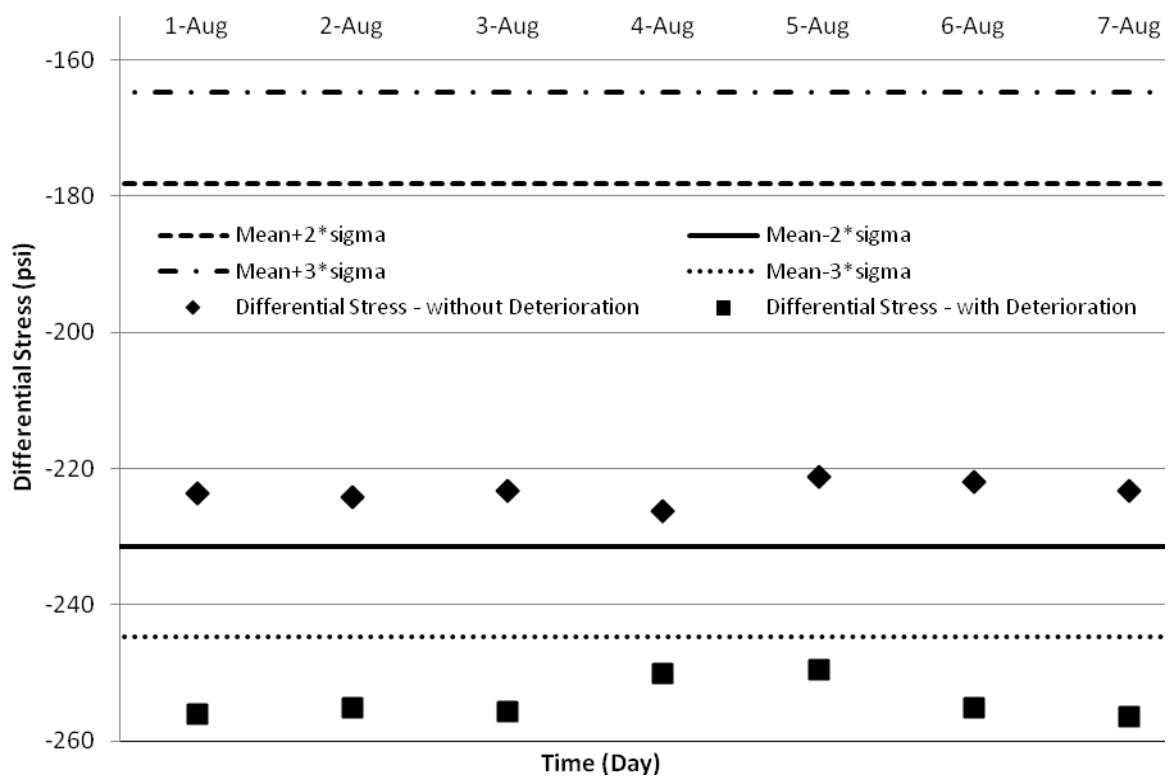
Figure 7-19. Deterioration prediction model for the joint between north panel 7 and 8 (Span2)

8 SUMMARY AND CONCLUSIONS

The Parkview Bridge is the first fully prefabricated full-depth deck panel bridge in Michigan. The bridge was constructed by assembling prefabricated components on site emulating one of the most common accelerated bridge construction (ABC) techniques. Though this innovative bridge construction technique brings many purported benefits in terms of safety, quality, and savings in user costs, one of the major durability concerns in full-depth deck panel systems is joint integrity. Hence, bridge performance monitoring becomes vital in identifying the onset of deterioration to make effective and efficient maintenance decisions to extend the service life of the bridge. After careful evaluation of the design details and construction process, it was determined, in terms of durability, that the transverse joints between deck panels are the weakest links in the system.

Analysis of sensor and load test data showed that the live load effect on the bridge is negligible and that the governing deck panel stresses are due to thermal loads on the structure. Stress envelopes were developed based on statistical analysis of three years' cumulative data. These envelopes serve as the baseline for identifying the onset of bridge deterioration.

A detailed finite element model was developed and the model was first calibrated using load test data. However, due to the dominance of thermal loads, it was required to calibrate the FE model using stresses developed in the structural system due to thermal loads. This was a challenge due to lack of thermocouples along the depth of bridge superstructure cross-section to document the temperature profile. A model was identified from literature that is capable of representing the thermal gradient profile at 12 p.m. and 6 p.m. in a summer day. The FE analysis of bridge superstructure was performed using the thermal gradient profiles. Sensor data was used to calibrate the model. Using the calibrated model, debonding of a joint between two deck panels was simulated and a deterioration prediction model was developed combining FE results and sensor data collected over three years. Differential stresses calculated at the simulated debonded joint were greater than 3σ; beyond the 99% confidence level of the data recorded from the sensors. Hence, on-set of deterioration can be identified using sensor data once the differential stress envelopes and FE simulation results similar to Figure 7-19 are made available for each joint. However, before developing FE models simulating the deterioration of all joints in the

system, the model developed for the joint between panel 7N and 8N must be fine-tuned using long-term monitoring data.

One limitation of the deterioration prediction model presented in the report is that it is applicable only from 12 p.m. to 6 p.m. on a summer day. Refinement of the deck deterioration model for wider applicability requires calibration using new structure-specific thermal models.

Below is a summary of findings and deliverables:

1. Statistical analysis of sensor data collected over a three-year period was useful in evaluating the integrity of deck panel joints and identifying the dominance of thermal load.
2. Using three-year sensor data, longitudinal and transverse stress envelopes as well as the deterioration prediction models were developed.
3. A detailed finite element (FE) model was developed representing the bridge superstructure. The model was calibrated using controlled load test and vibrating wire sensor data collected from the in-service bridge. .
4. The calibrated FE model was used to simulate joint deterioration. A deterioration prediction model was developed for a deck panel joint using FE simulation results and vibrating wire sensor data.

9   RECOMMENDATIONS FOR FUTURE WORK

The focus of this work has been on the development of deterioration prediction models using sensor network data and refined finite element analyses. Sensor data analysis showed that the governing load is thermal. In addition, a deterioration prediction model for a joint between deck panels is presented with limited data which is applicable during a specific time period.

While temperature models for bridge design are available in design specifications, the structural performance assessment requires thermal profile models for a specific bridge configuration and for a specific time of a day in a specific season. Once a structure-specific thermal model is developed, the deterioration prediction model presented in this report will require further verification, fine-tuning, and analysis to identify potential weak zones, in terms of durability. Fine-tuning of the deterioration prediction models require identification of the exact location of sensors and conducting a sensitivity analysis to evaluate the impact of sensor

location and orientation on the accuracy of the model. Therefore, it is recommended to establish a long-term, continuous monitoring program with additional sensors to monitor thermal profile of the bridge superstructure or a parallel study to develop thermal profiles of the specific structure and the research methodology presented in the report.

10 REFERENCES CITED

- AASHTO. (2010). *AASHTO LRFD Bridge Design Specifications*, 3rd Ed., American Association of State Highway Transportation Officials, Washington DC 20001.

- AASHTO. (1993). *Guidelines for Bridge Management Systems*, 1st Ed., American Association of State Highway Transportation Officials, Washington DC 20001.

- Abudayyeh, O. (2010). *A Sensor Network System for the Health Monitoring of the Parkview Bridge Deck*, Final Report Number RC 1536, the Michigan Department of Transportation, Lansing, MI.

- Altair. (2010). Altair Engineering, Inc. http://www.altair.com

- Spanos, A. (2003). *Probability Theory and Statistical Inference,* Cambridge University Press, New York.

- Bogdanoff, J.L. (1978). "New cumulative damage model - I." *Journal of Applied Mechanics, Transactions ASME*, 45(2), 246-250.

- BTS. (2007). *Highway Bridges in the US - an Overview*, BTS Special Report, the Bureau of Transportation Statistics (BTS), Research and Innovative Technology Administration (RITA), U.S. Department of Transportation (US DOT), 1200 New Jersey Avenue, SE, Washington, DC 20590.

- FHWA. (2008). "Deficient Bridges by State and Highway System." National Bridge Inventory (NBI), National Bridge Inspection Program, the Federal Highway Administration (FHWA), U.S. Department of Transportation, 1200 New Jersey Ave SE, Washington, DC 20590. <http://www.fhwa.dot.gov/bridge/defbr07.cfm> (August 1, 2010).

- Fouad, N. (2007), "Temperature loading of concrete bridges due to environmental thermal actions." *Proceedings of the 12th International Conference on Structural & Geotechnical Engineering 2007,* Cairo, Egypt.

- Gualtero, I. A. (2004). *Deterioration process and deck failure mechanism of Florida's precast deck panel bridges*, Master's Thesis, Department of Civil and Environmental Engineering, College of Engineering, University of South Florida.

- Issa, M.A., Issa, M., Khayyat, S.Y., Yousif, A.A., Kaspar, I.I. (1995). "Field performance of full depth precast concrete panels in bridge deck reconstruction." PCI Journal, 40(3), 82-108.

- Lounis, Z., and Mirza, M. S. (2001). ''Reliability-based service life prediction of deteriorating concrete structures.'' *Proceedings of the 3rd International Conference on*

Concrete Under Severe Conditions, Univ. of British Columbia, Vancouver, Canada, vol. 1, 965–972.

- Lu, P., Wipf, T. J., Phares, B. M., and Doornink, J. D. (2007). "A bridge structural health monitoring and data mining system." *Proceedings of the 2007 Mid-Continent Transportation Research Symposium*, Ames, Iowa.

- Madanat, S. and Ibrahim, W. H. W. (1995). ''Poisson regression models of infrastructure transition probabilities.'' *Journal of Transportation Engineering,* 121(3), 267–272.

- Madanat, S., Karlaftis, M. G., and McCarthy, P. S. (1997). "Probabilistic Infrastructure Deterioration Models with Panel Data." *Journal of Infrastructure Systems*, 3(1), 4-9.

- Madanat, S., Mishalani, R., and Ibrahim, W.H.W. (1995). "Estimation of Infrastructure Transition Probabilities from Condition Rating Data." *Journal of Infrastructure Systems*, 1(2), 120-125.

- McElvey, R.D., Zavoina, W. (1975). "A statistical model for the analysis of ordinal level dependent variables." *The Journal of Mathematical Sociology*, 4(1), 103-120.

- Morcous, G., Lounis, Z., and Mirza, M.S. (2003). "Identification of Environmental Categories for Markovian Deterioration Models for Bridge Decks." *Journal of Bridge Engineering*, 8(6), 353-361.

- Morcous, G., Rivard, H. and Hanna, A.M. (2002). "Modeling Bridge Deterioration Using Case-Based Reasoning." *Journal of Infrastructure Systems*, 8(3), 86-95.

- Noortwijk, J. M. V., and Frangopol, D. M. (2004) "Deterioration and maintenance models for insuring safety of civil infrastructures at lowest life-cycle cost." *Life-Cycle Performance of Deteriorating Structures: Assessment, Design and Management*, D.M. Frangopol, E. Bruhwiler, M.H. Faber and B. Adey, eds., Reston, VA, 384-391.

- Nowak, A. S., Szerszen, M. M. and Juntunen, D. A. (2000). *Michigan Deck Evaluation Guide*, Technical Report, University of Michigan, Ann Arbor, MI.

- PCI. (2003). *Precast Prestressed Bridge Design Manual*, Precast/Prestressed Concrete Institute, 175 W. Jackson Boulevard, Chicago, IL 60604.

- Priestley, M.J.N. (1976). "Design of thermal gradients for concrete bridges," *New Zealand Engineering,* 31 (9), 213-19.

- Robelin, C.A. and Madanat, S.M. (2006). "Dynamic Programming based Maintenance and Replacement Optimization for Bridge Decks using History-Dependent Deterioration

Models," *Proceedings of the 9th International Conference on Applications of Advanced Technology in Transportation*, ASCE, Reston, VA., 13-18.

- Romkema, M.A., Attanayake, U. and Aktan, H. (2010). *Incorporating Link Slabs in High Skew Bridges during Repair Activities- Design Recommendations*, Technical Report: CCE-10-01, Department of Civil and Construction Engineering, Western Michigan University, Kalamazoo, MI.

- Simulia (2010). Abaqus 6.10 Analysis User's Manual. http://www.simulia.com/

- Sneed, L., Belarbi, A., and You, Y. (2010). *Spalling Solution of Precast-Prestressed Bridge Deck Panels,* Report Number OR11-005, Missouri Department of Transportation, Jefferson City, MO.

- Tarighat, A., and Miyamoto, A. (2009). "Fuzzy concrete bridge deck condition rating method for practical bridge management system." *Expert Systems with Applications: An International Journal*, 36 (10), 755-8611.

- Thompson, P. D., and Shepard, R. W. (1994). "Pontis." *Transportation Research Circular, 324*, Transportation Research Board, Washington, D.C., 35–42.

- Yap, P., (1989). "Truck tire types and road contact pressures." *The Second International Symposium on Heavy Vehicle Weights and Dimensions*, Kelowna, British Columbia, June 18 – 22.

APPENDIX A: LIST OF ACRONYMS, ABBREVIATIONS, AND SYMBOLS

Abbreviation	Description
AASHTO	American Association Of State Highway And Transportation Officials
ABC	Accelerated Bridge Construction
FFT	Fast Fourier Transform
FEA	Finite Element Analysis
FEM	Finite Element Modeling
FHWA	Federal Highway Administration
PCI	Precast/Prestressed Concrete Institute
SHM	Structural Health Monitoring
VWSG	Vibrating Wire Strain Gages

APPENDIX B: FE MODEL CALIBRATION WITH LOAD TEST DATA
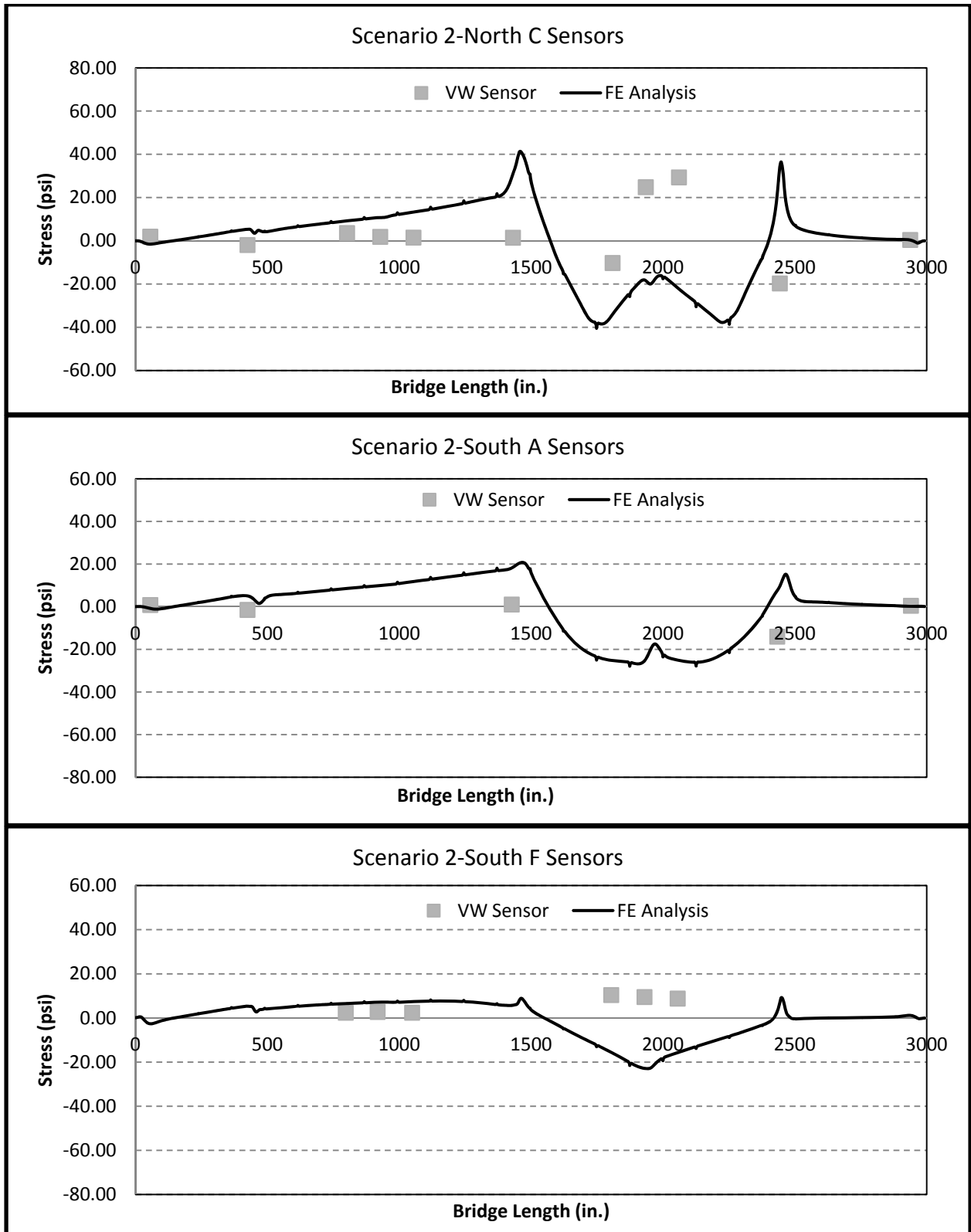
Figure B-1. Comparison of load test data and FE analysis results – Scenario 2
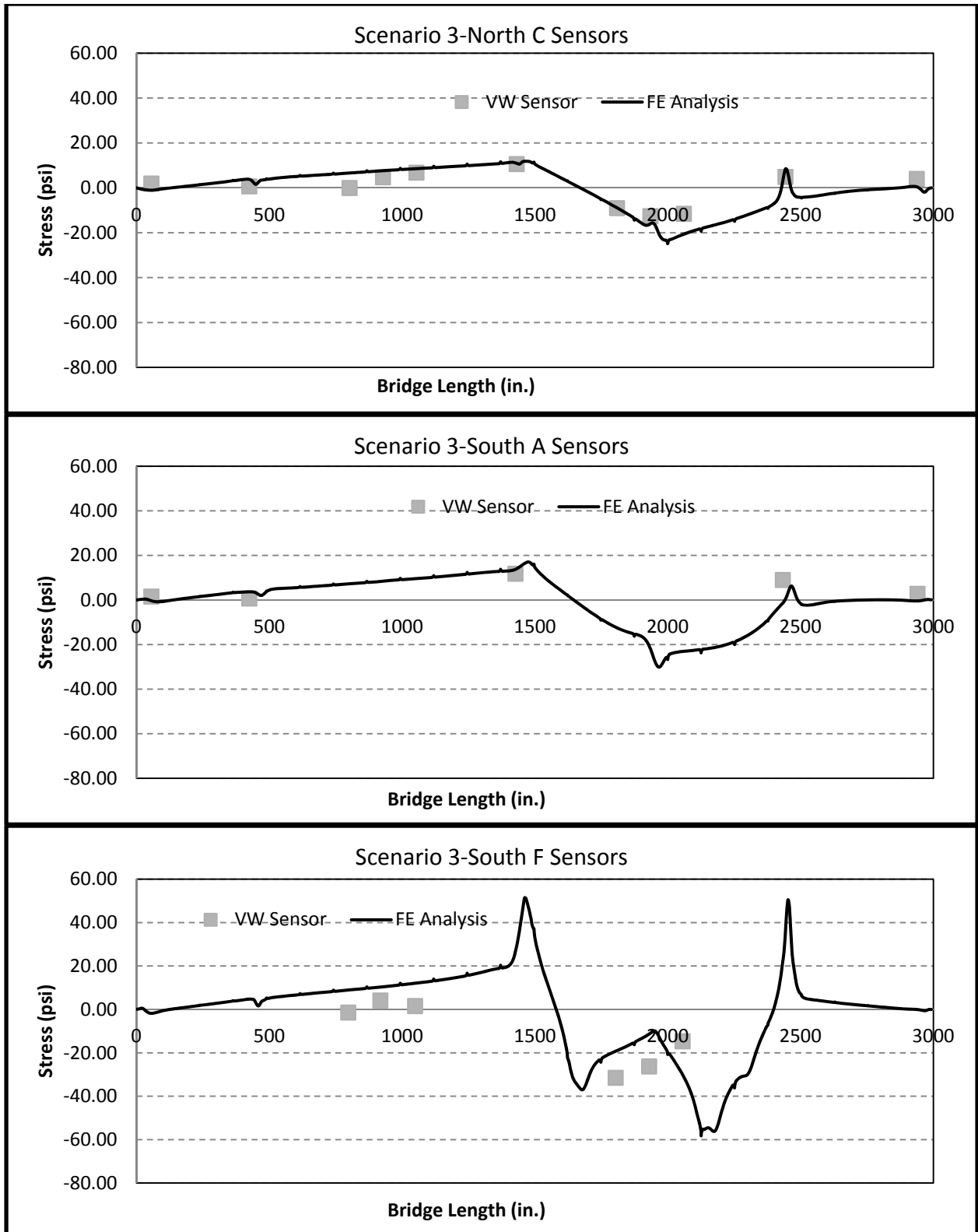
Figure B-2. Comparison of load test data and FE analysis results – Scenario 3
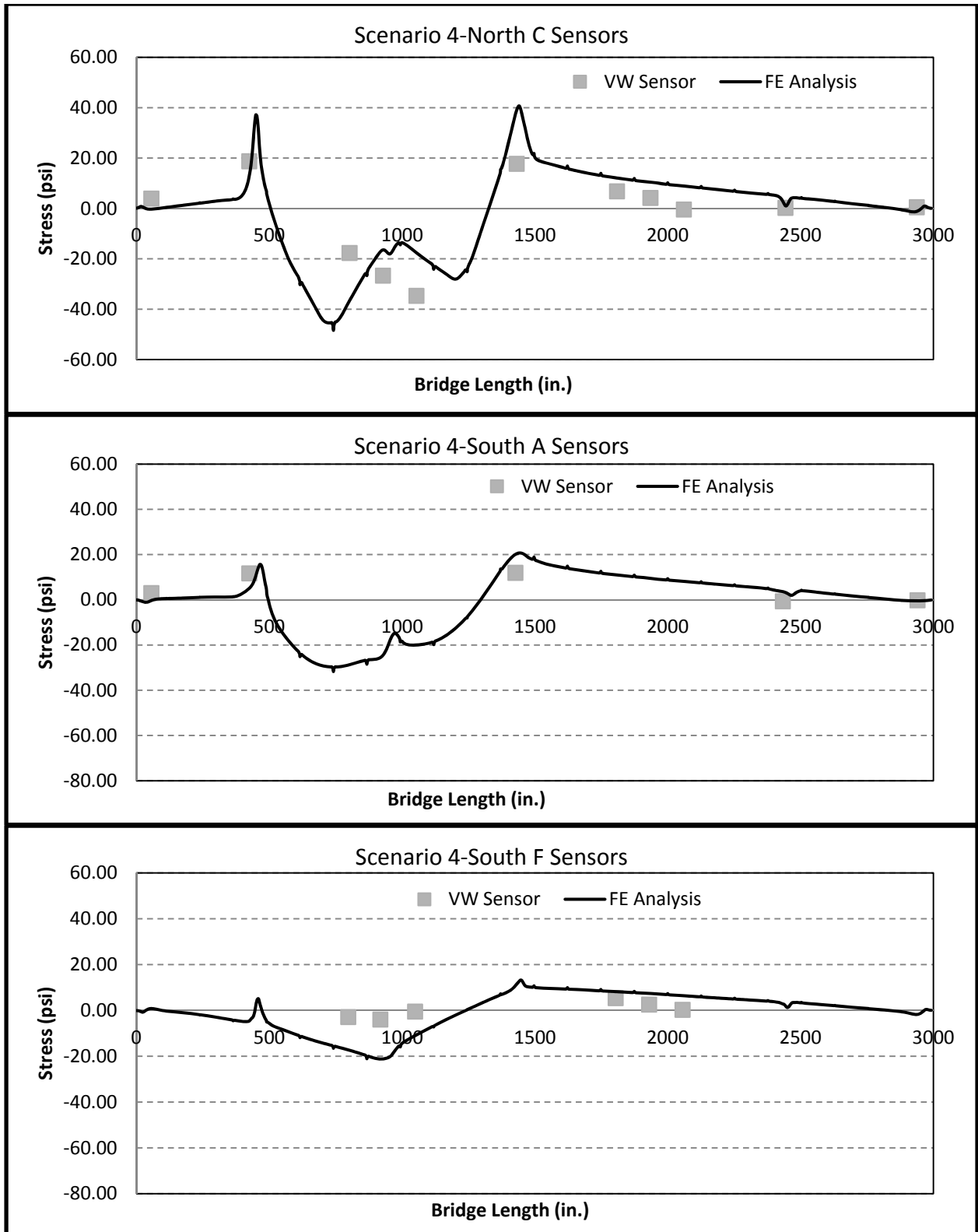
Figure B-3. Comparison of load test data and FE analysis results – Scenario 4
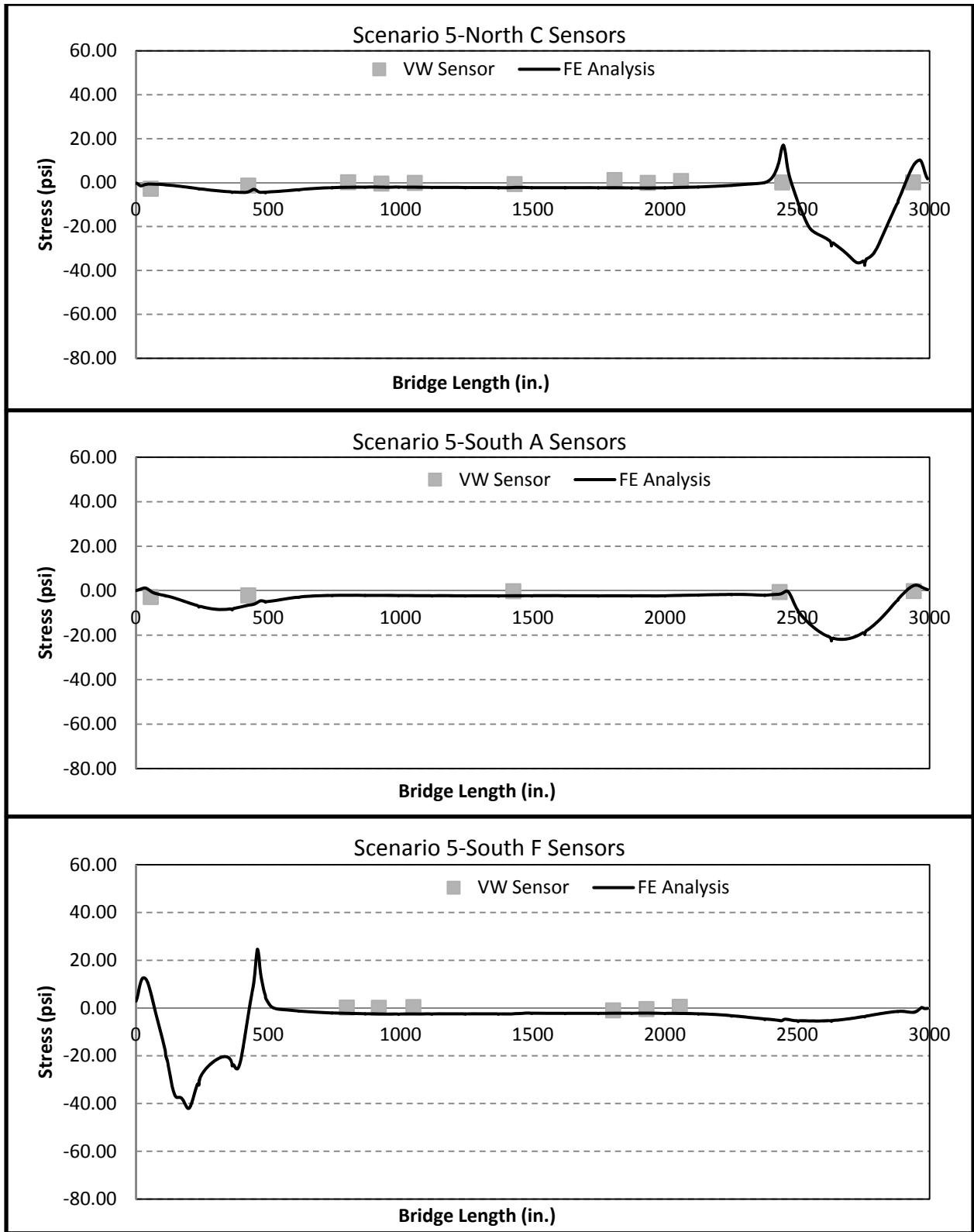
Figure B-4. Comparison of load test data and FE analysis results – Scenario 5

83
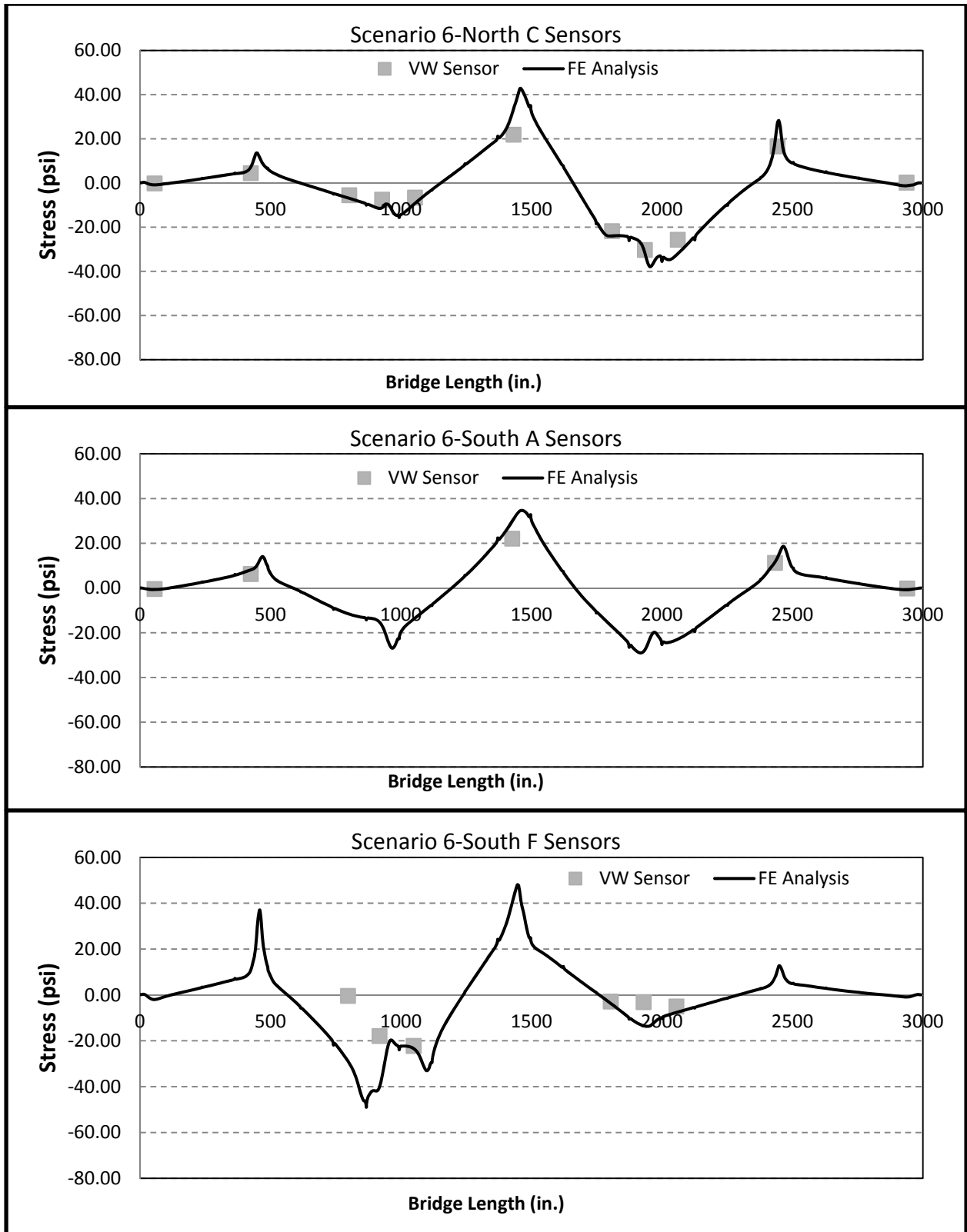
Figure B-5. Comparison of load test data and FE analysis results – Scenario 6
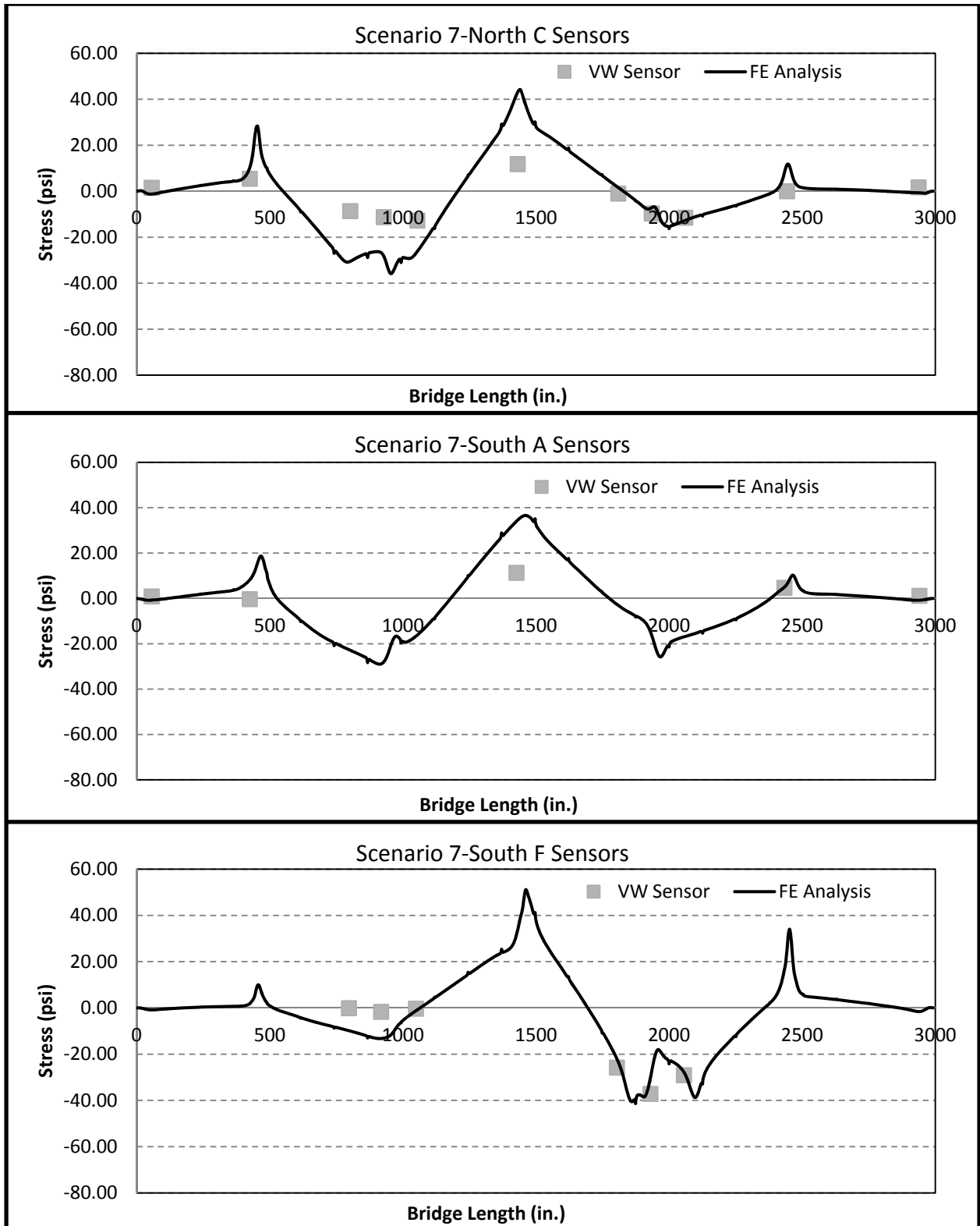
Figure B-6. Comparison of load test data and FE analysis results – Scenario 7
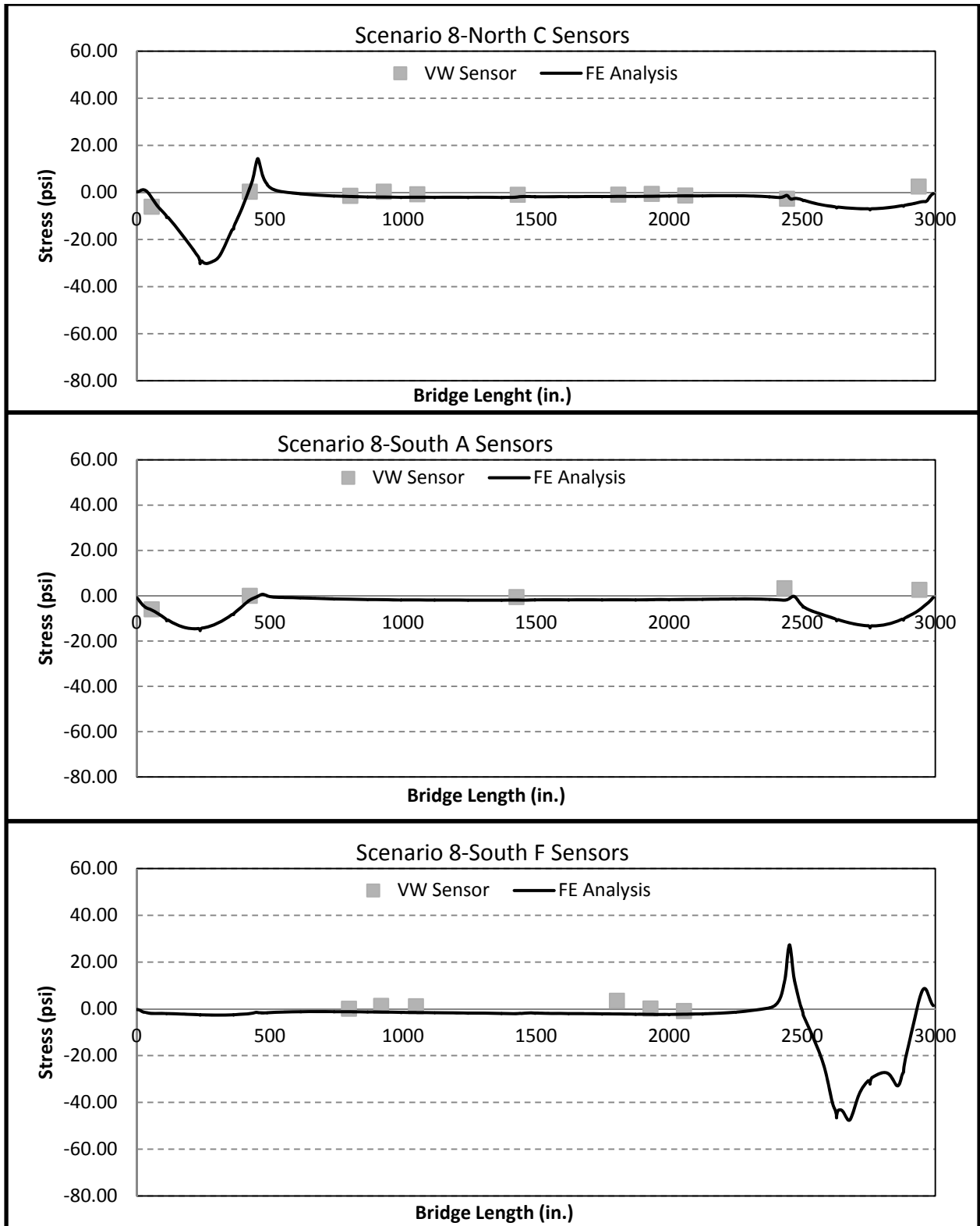
Figure B-7. Comparison of load test data and FE analysis results – Scenario 8
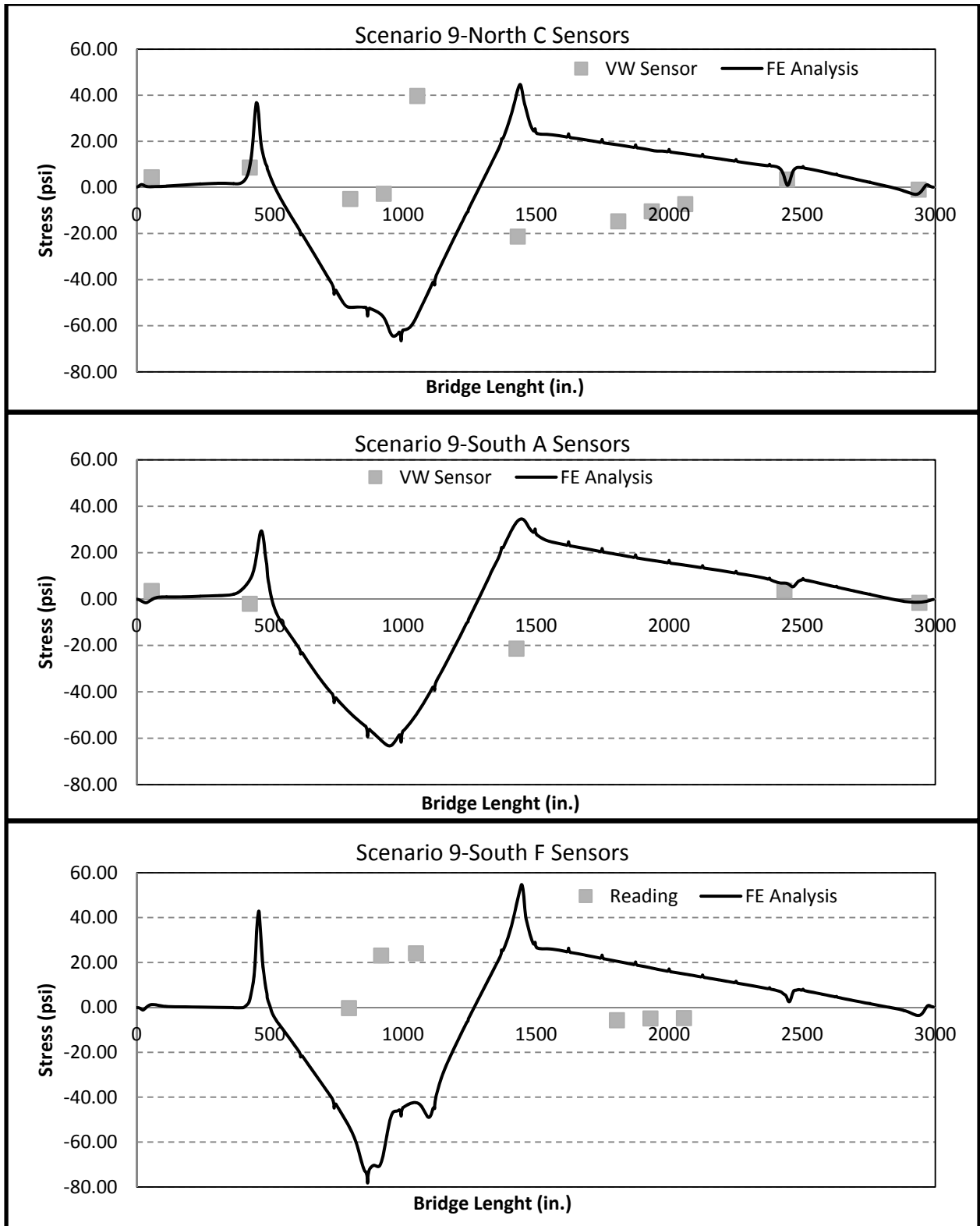
Figure B-8. Comparison of load test data and FE analysis results – Scenario 9
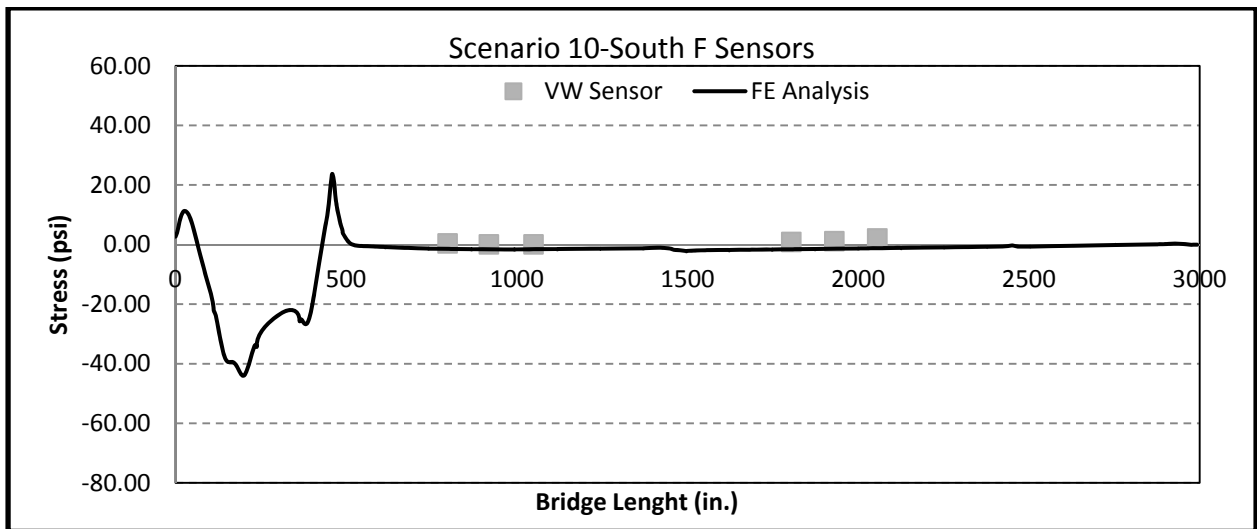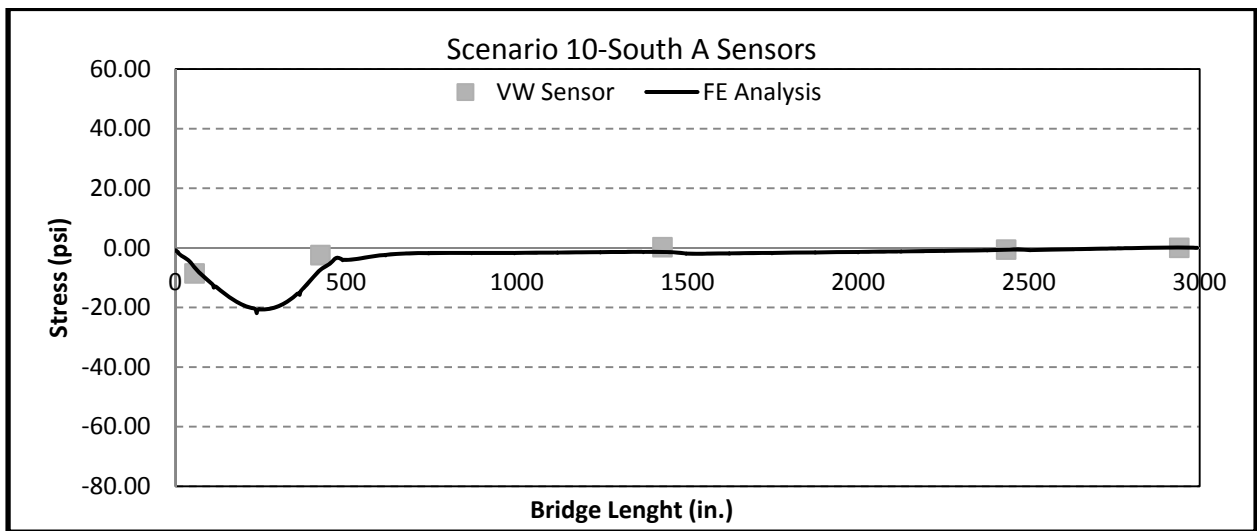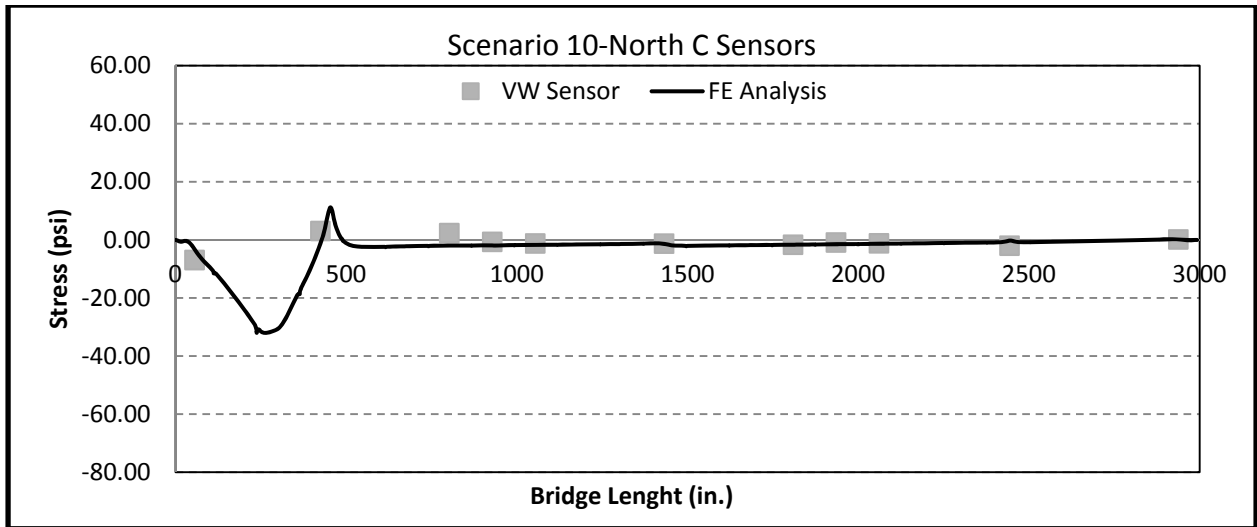
Figure B-9. Comparison of load test data and FE analysis results – Scenario 10

88

APPENDIX C: THREE-YEAR STRESS ENVELOPES
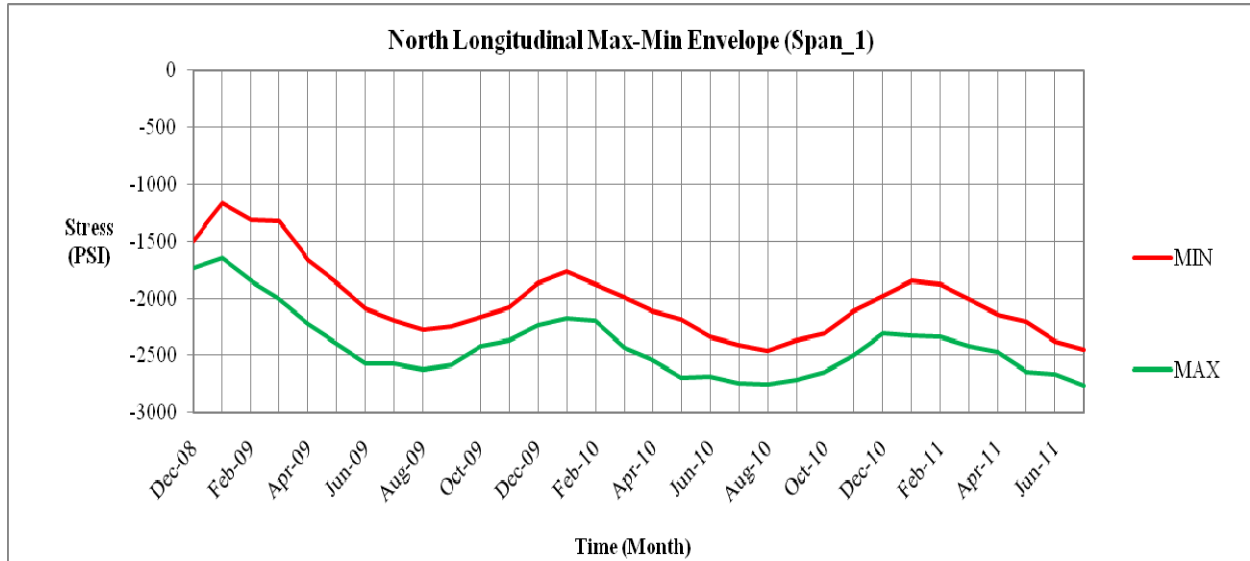
Figure C-1. Three-year envelope for north span 1 in the longitudinal direction
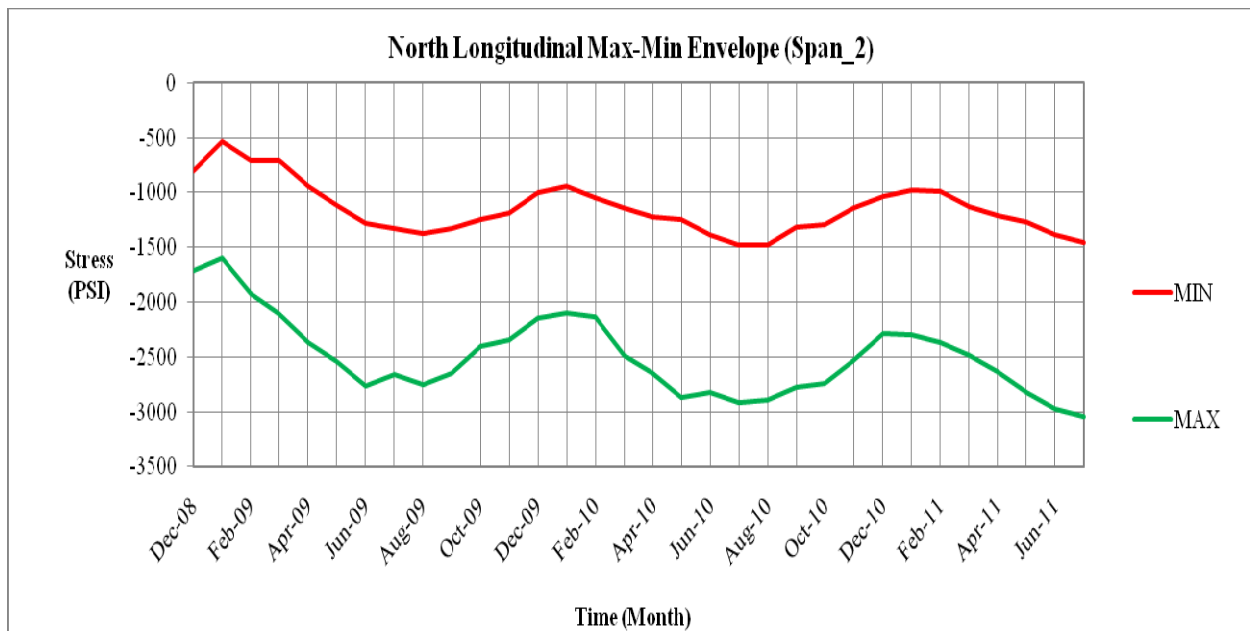
Figure C-2. Three-year envelope for north span 2 in the longitudinal direction

89
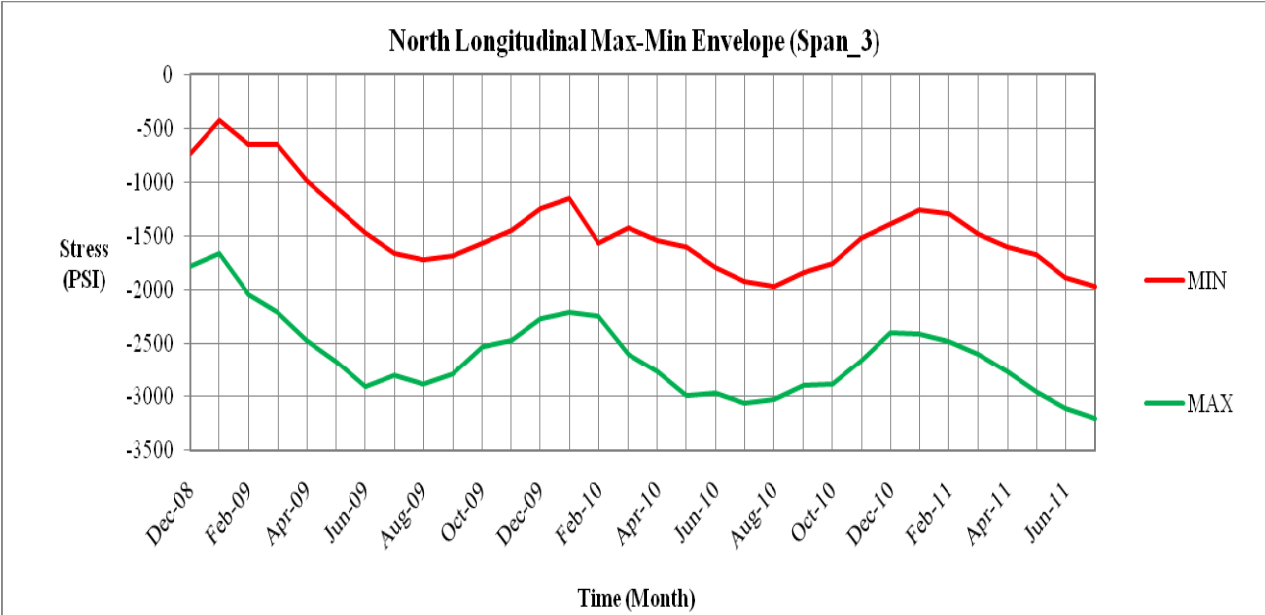
Figure C-3. Three-year envelope for north span 3 in the longitudinal direction
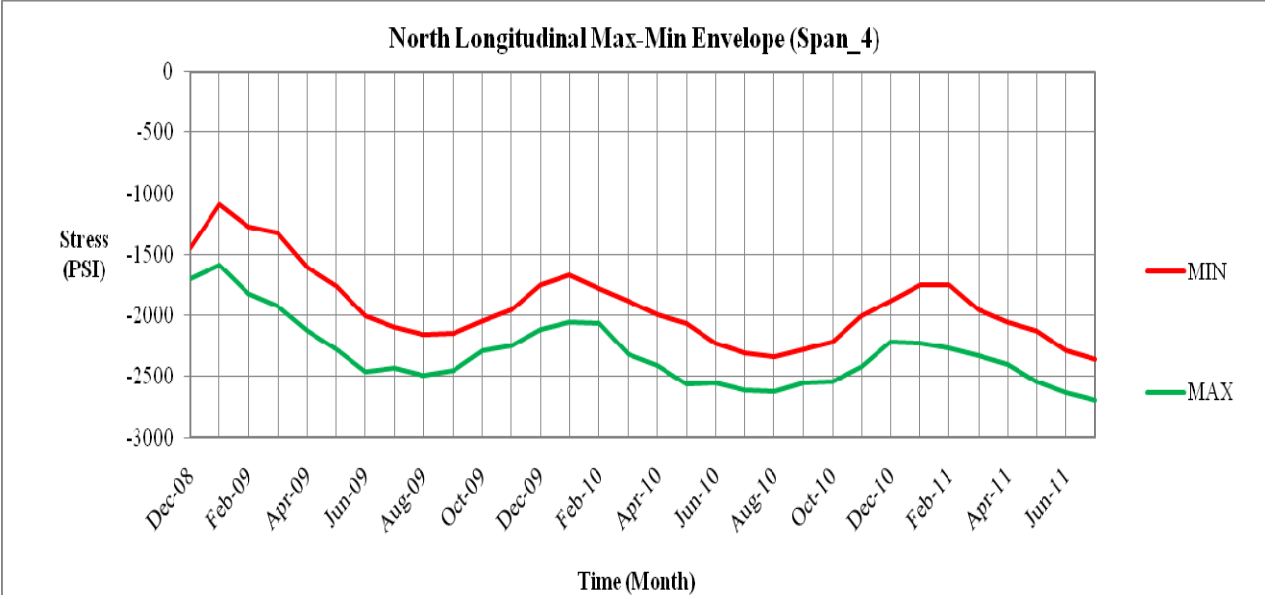
Figure C-4. Three-year envelope for north span 4 in the longitudinal direction

90
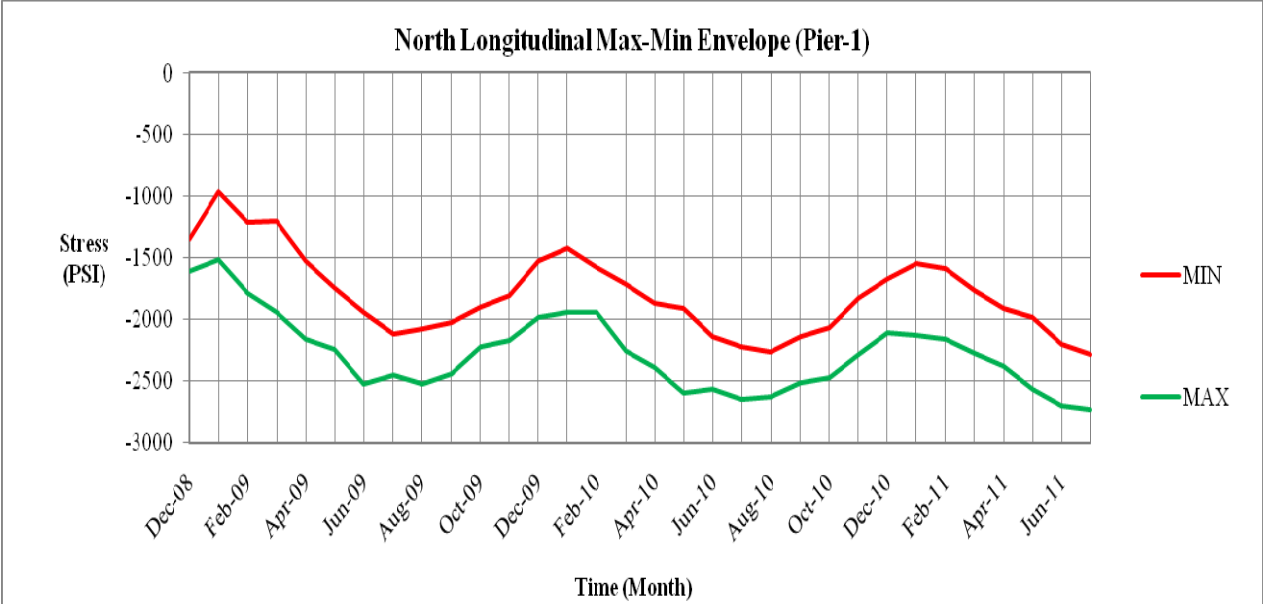
Figure C-5. Three-year envelope for north pier 1 in the longitudinal direction
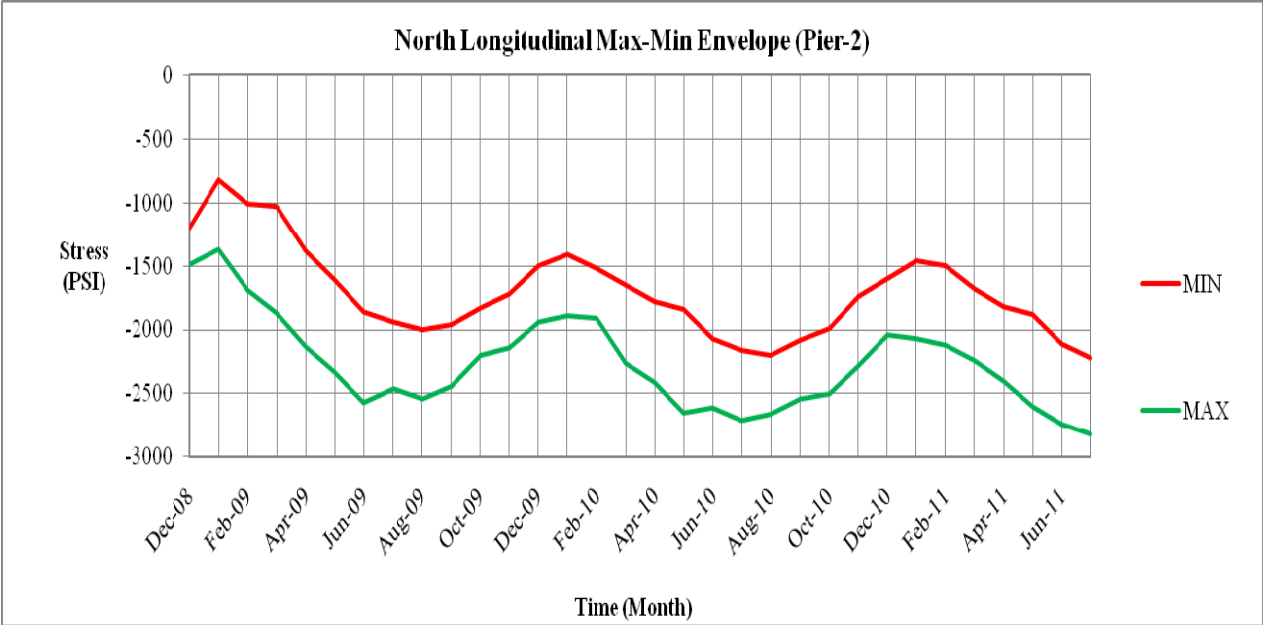
Figure C-6. Three-year envelope for north pier 2 in the longitudinal direction
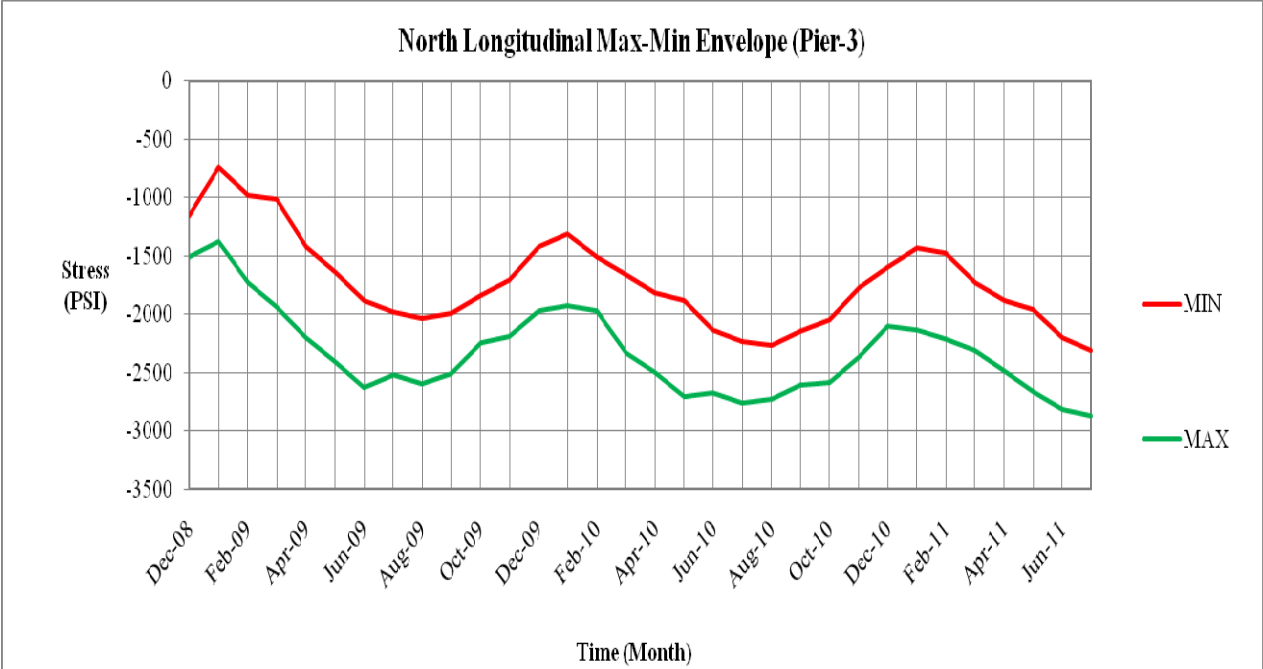
Figure C-7. Three-year envelope for north pier 3 in the longitudinal direction
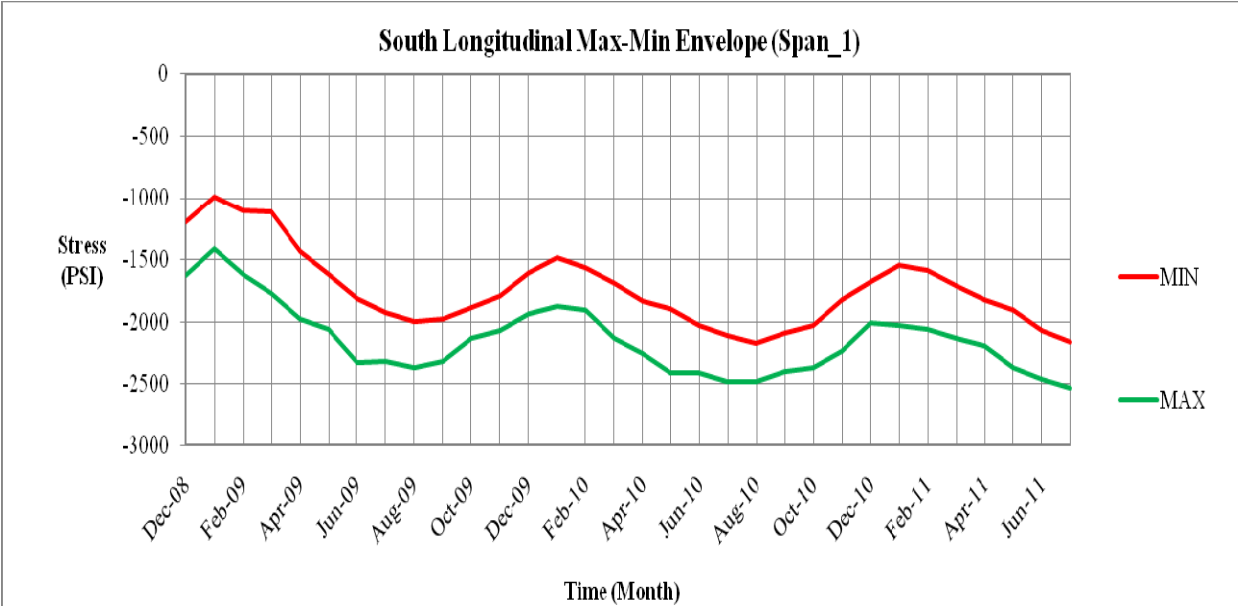
Figure C-8. Three-year envelope for south span 1 in the longitudinal direction
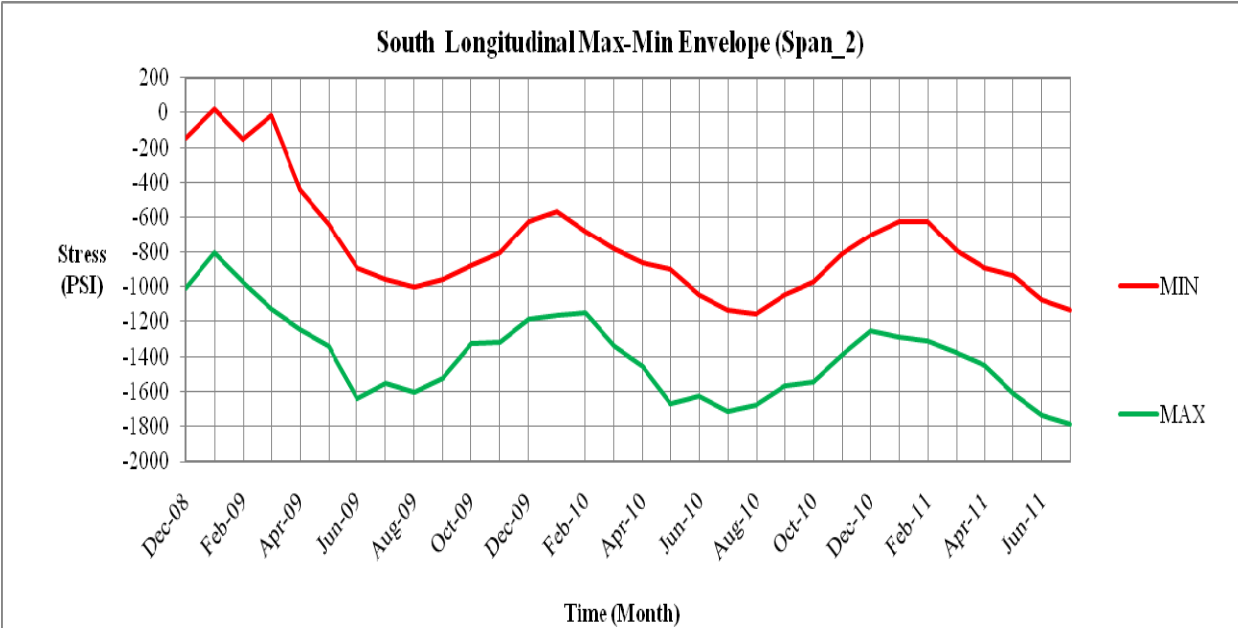
Figure C-9. Three-year envelope for south span 2 in the longitudinal direction

93
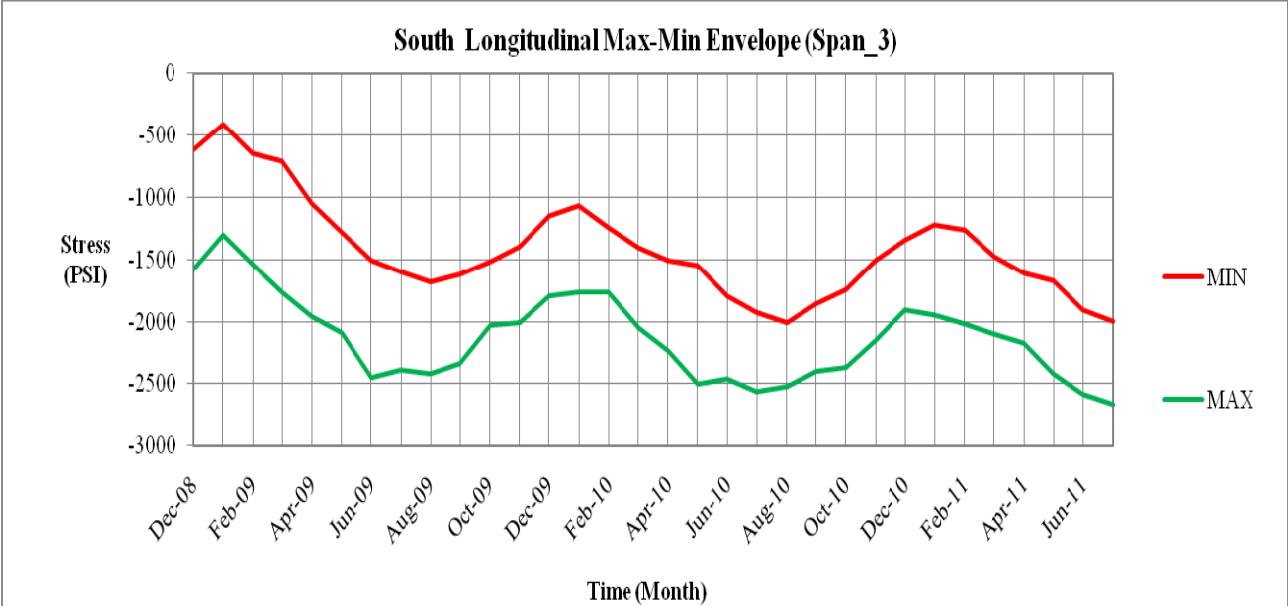
Figure C-10. Three-year envelope for south span 3 in the longitudinal direction
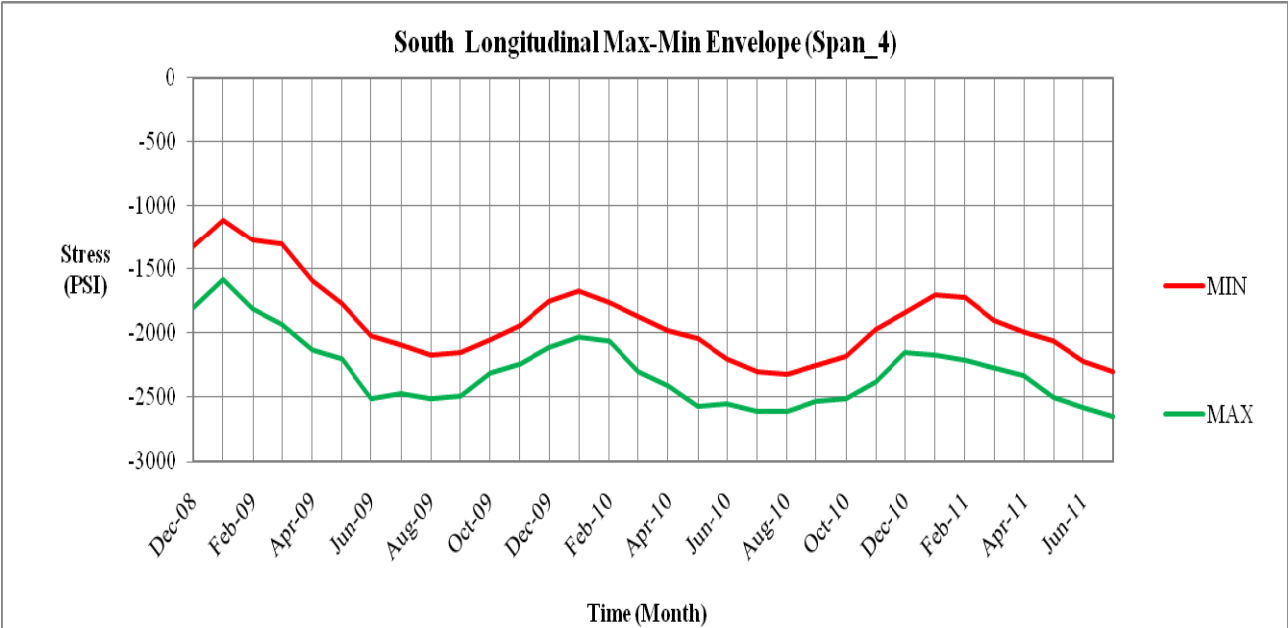
Figure C-11. Three-year envelope for south span 4 in the longitudinal direction

94
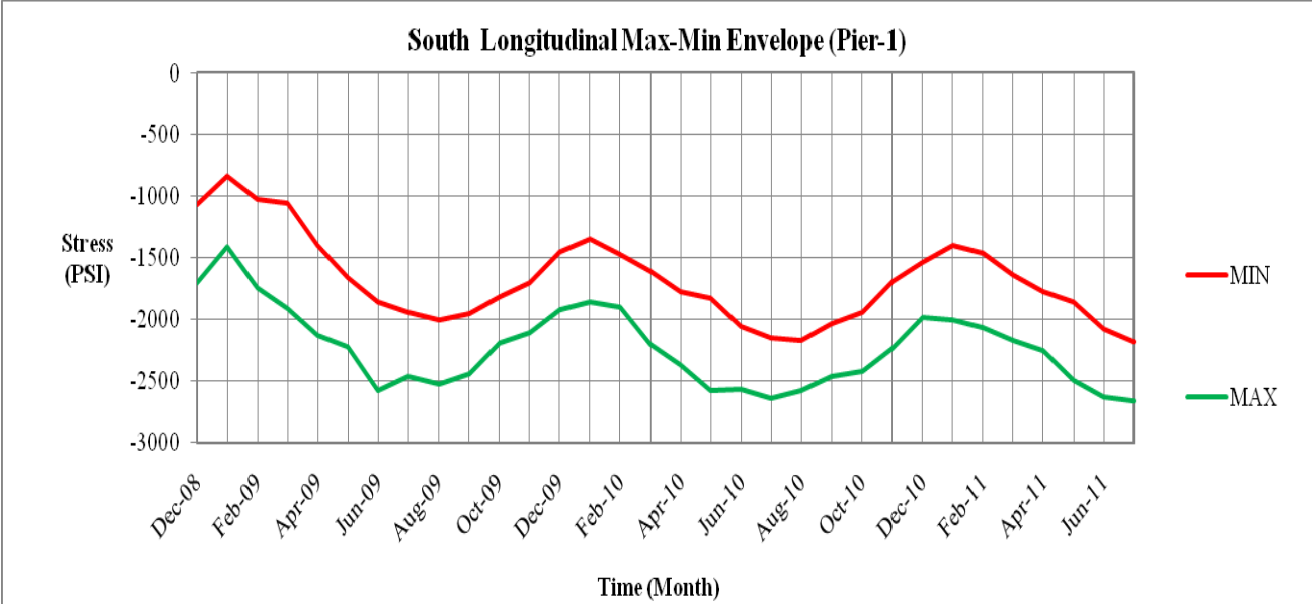
Figure C-12. Three-year envelope for pier 1 in the longitudinal direction
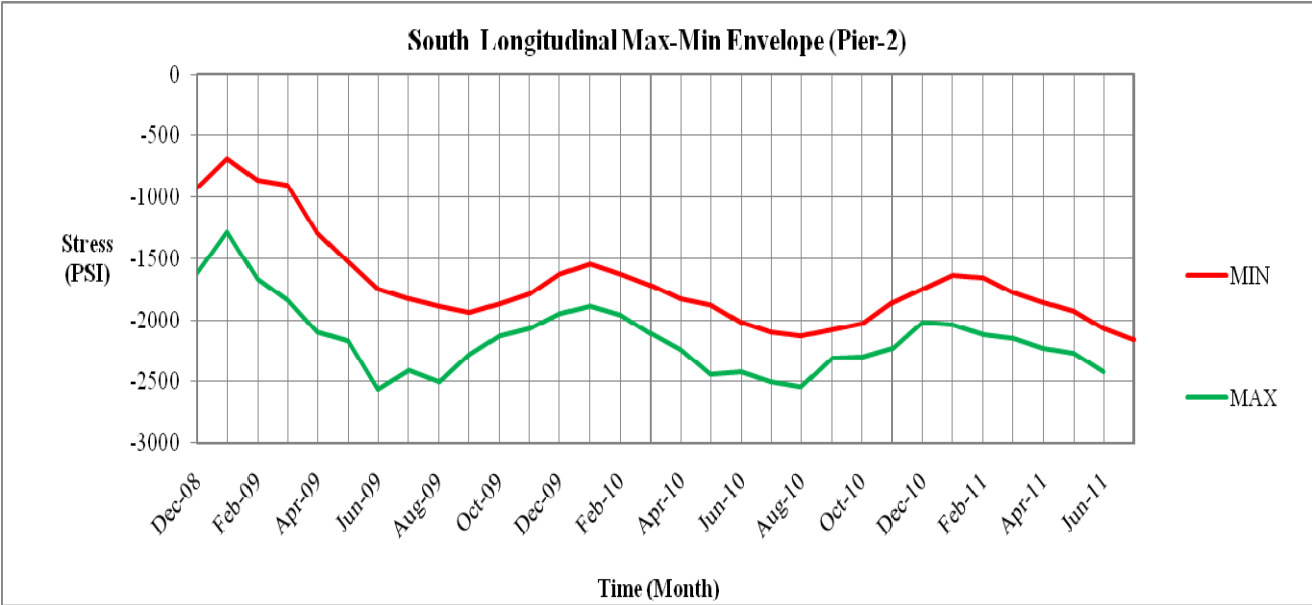
Figure C-13. Three-year envelope for pier 2 in the longitudinal direction
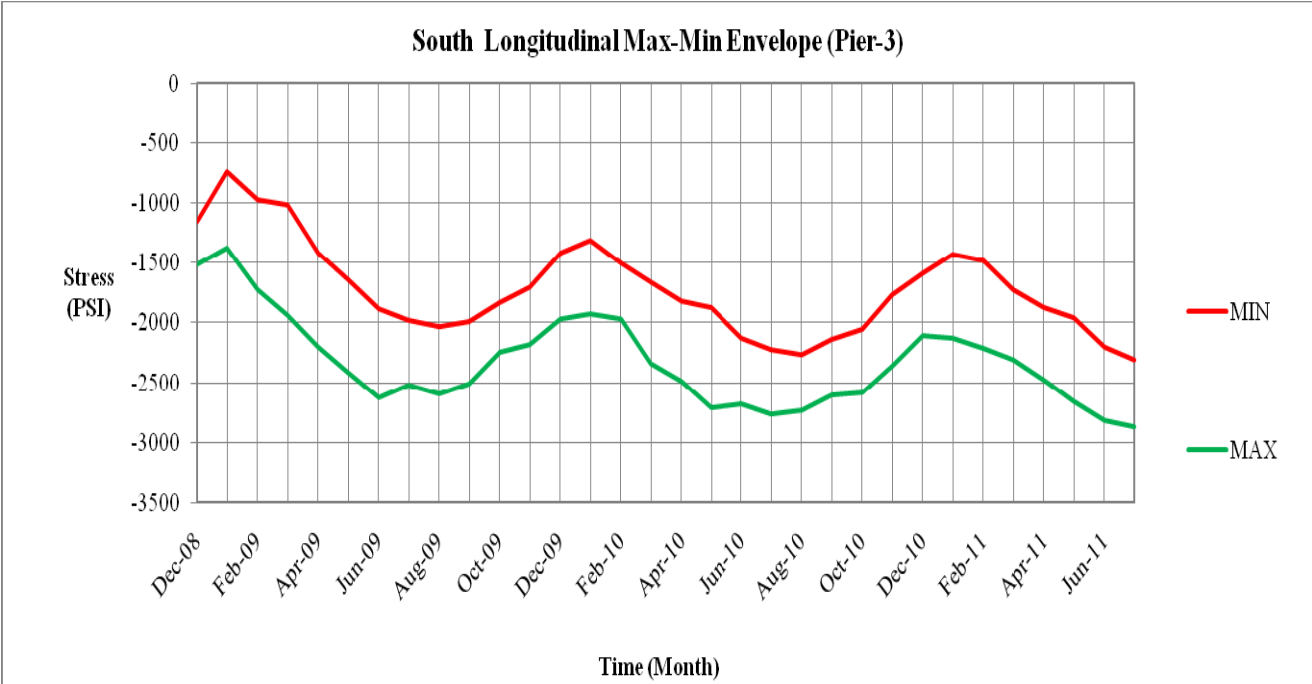
Figure C-14. Three-year envelope for pier 3 in the longitudinal direction
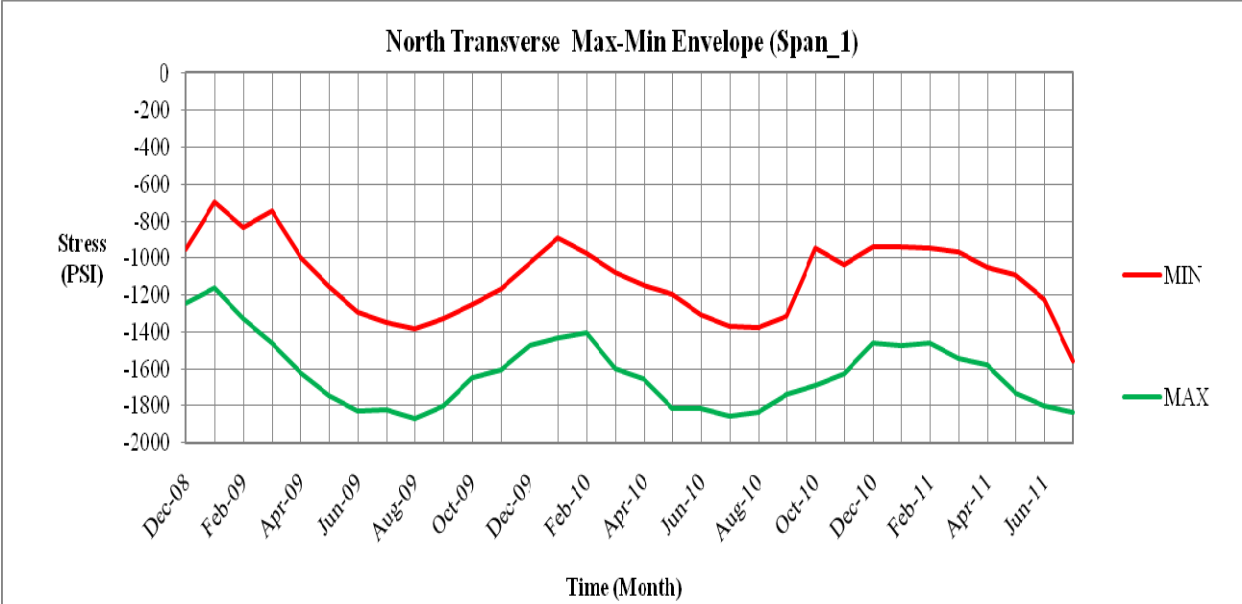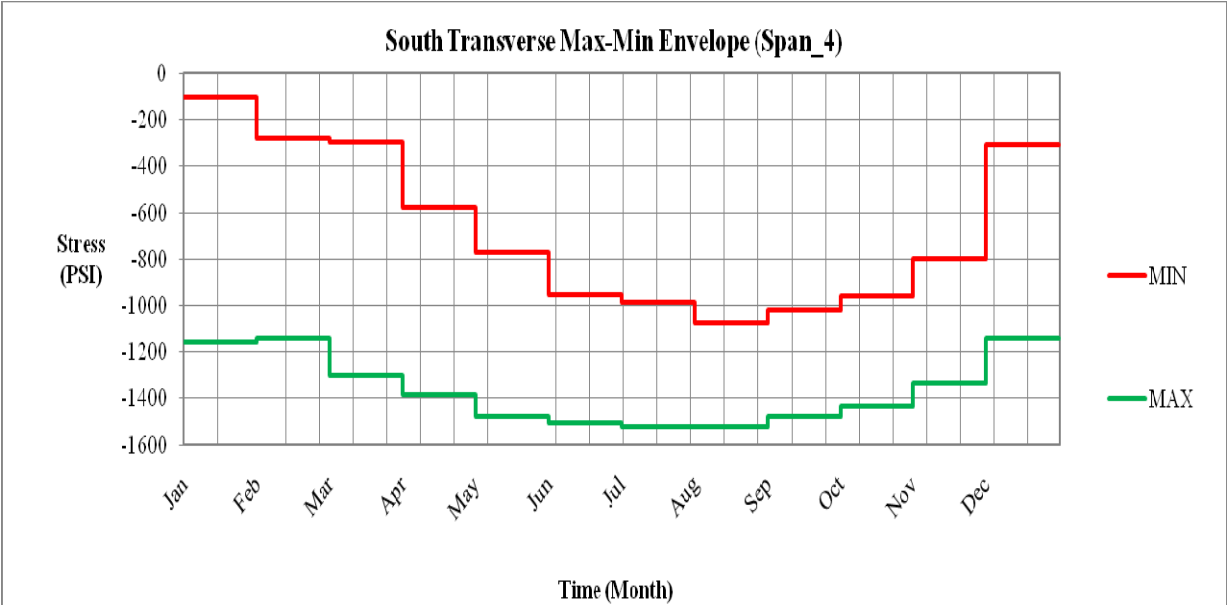
Figure C-15. Three-year envelope for north span 1 in the transverse direction
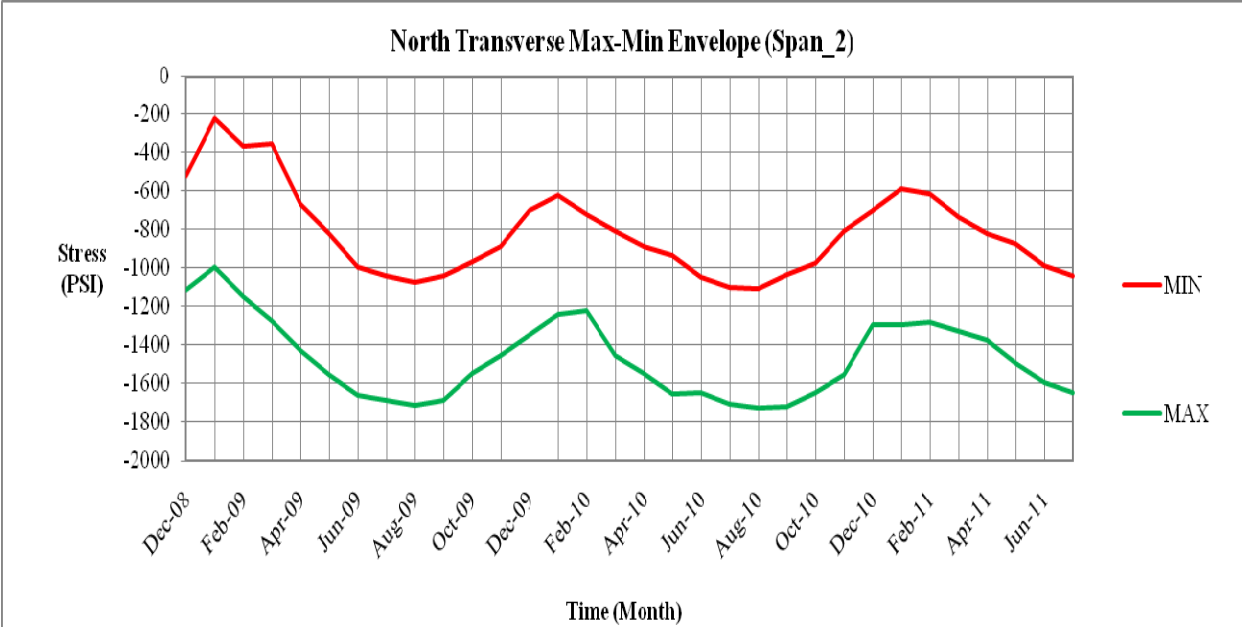
Figure C-16. Three-year envelope for north span 2 in the transverse direction
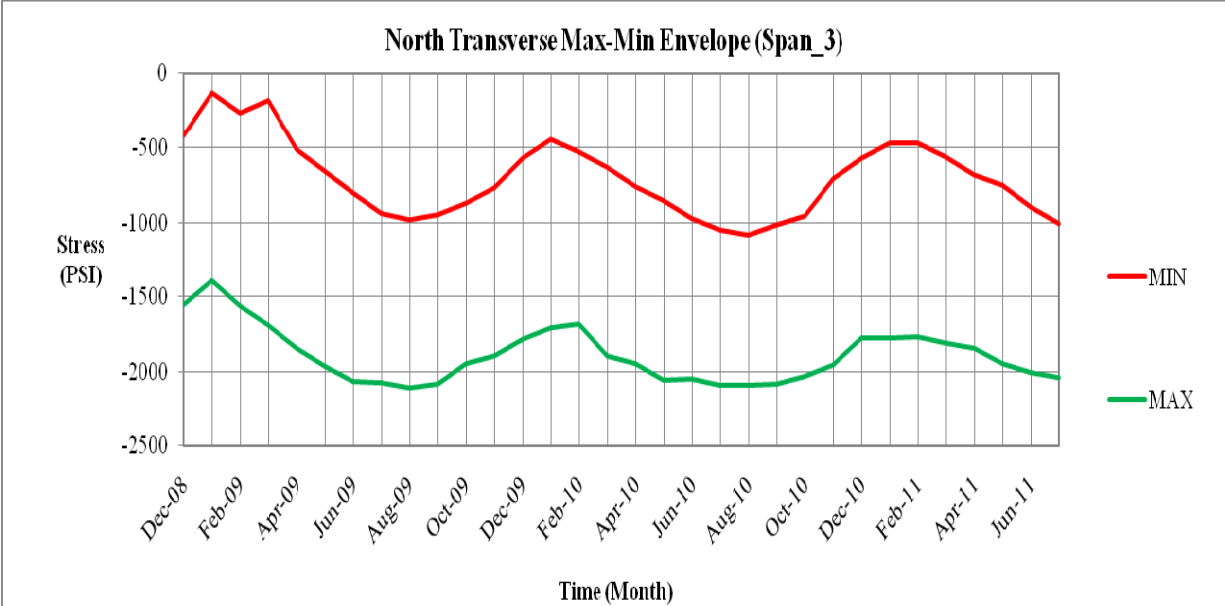
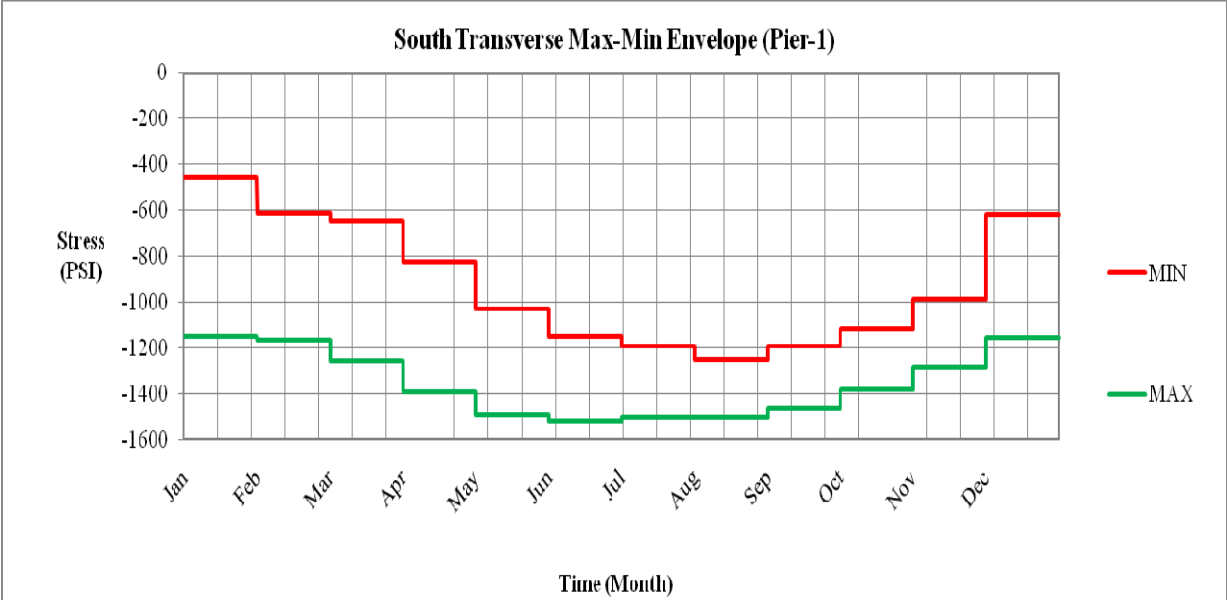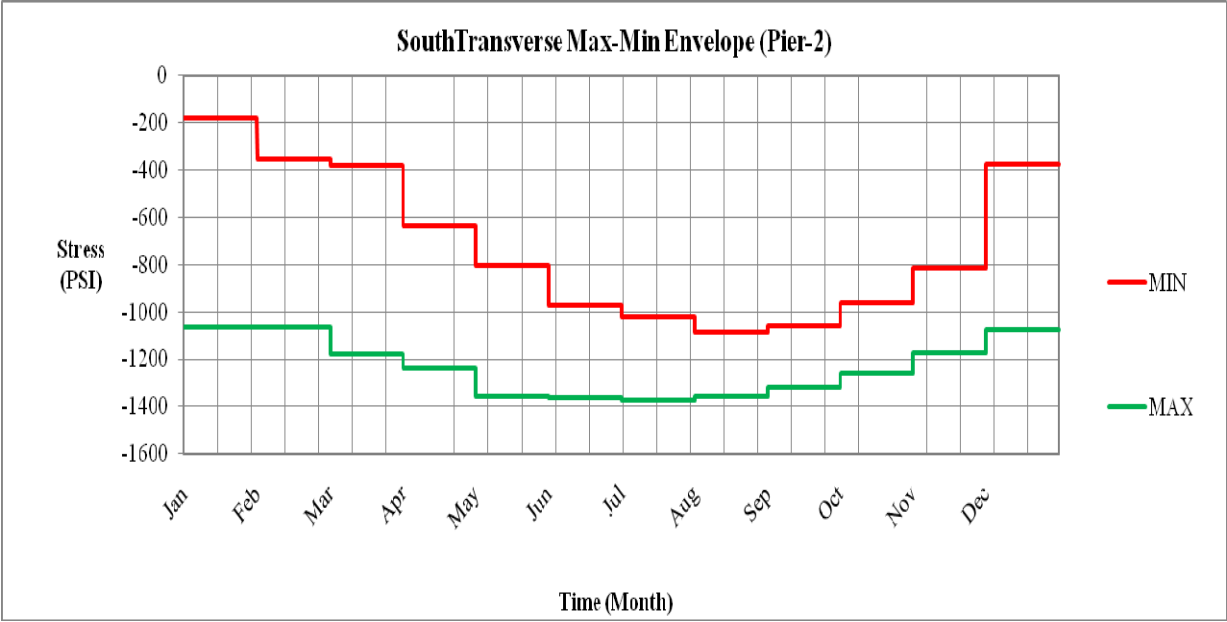**Figure C-17. Three-year envelope for north span 3 in the transverse direction**
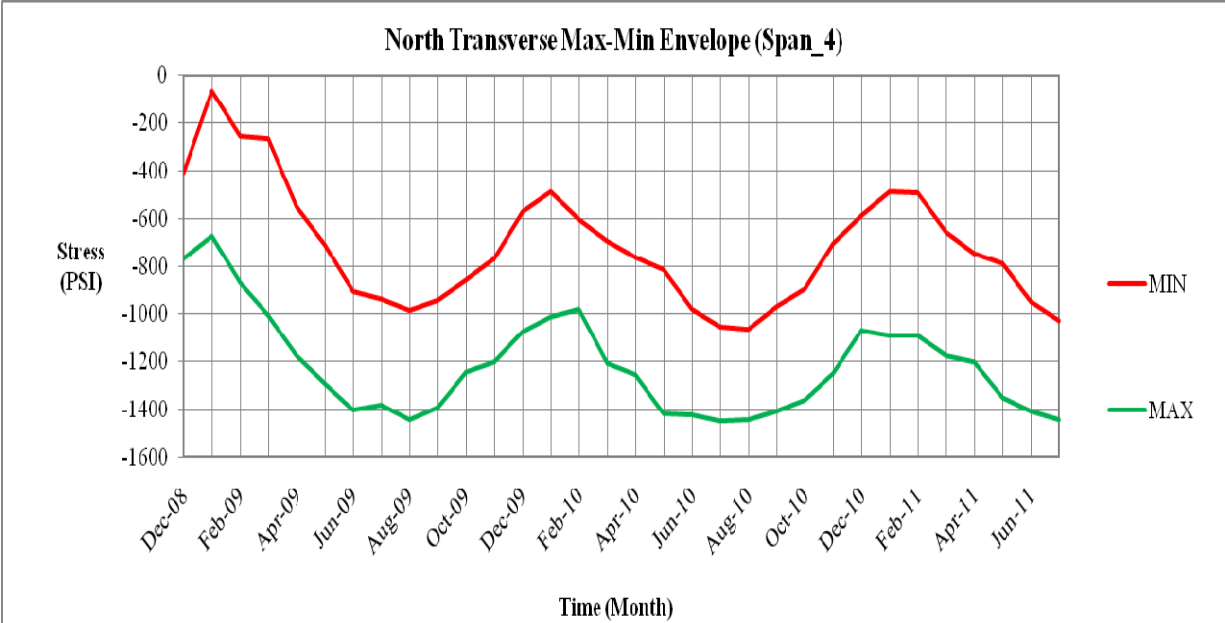
Figure C-18. Three-year envelope for north span 4 in the transverse direction
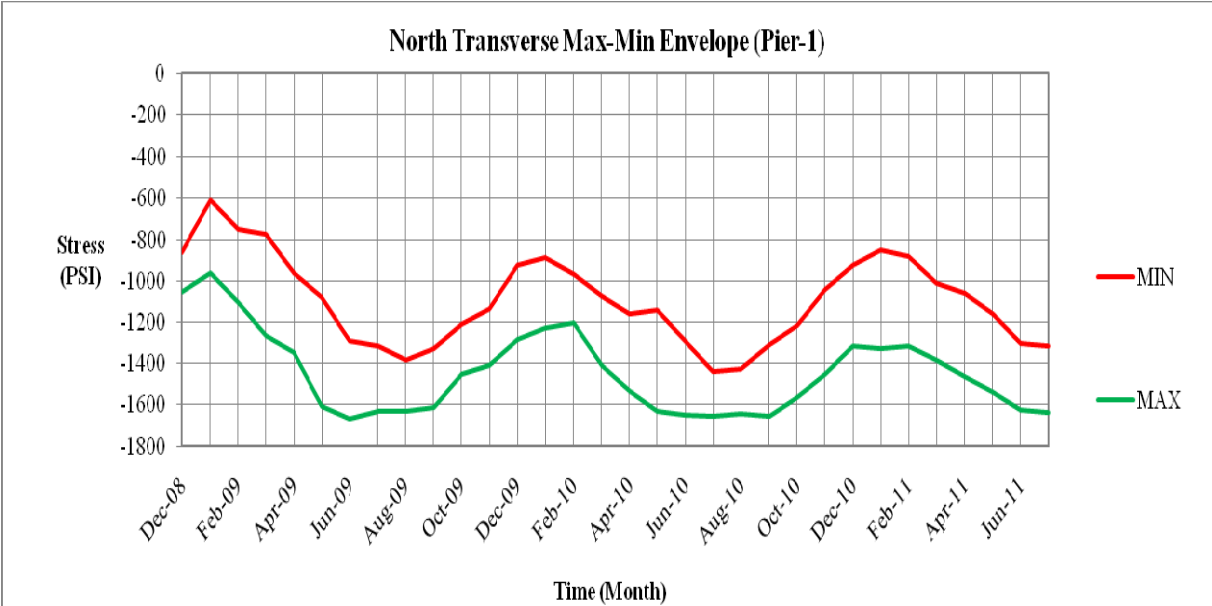
Figure C-19. Three-year envelope for north pier 1 in the transverse direction
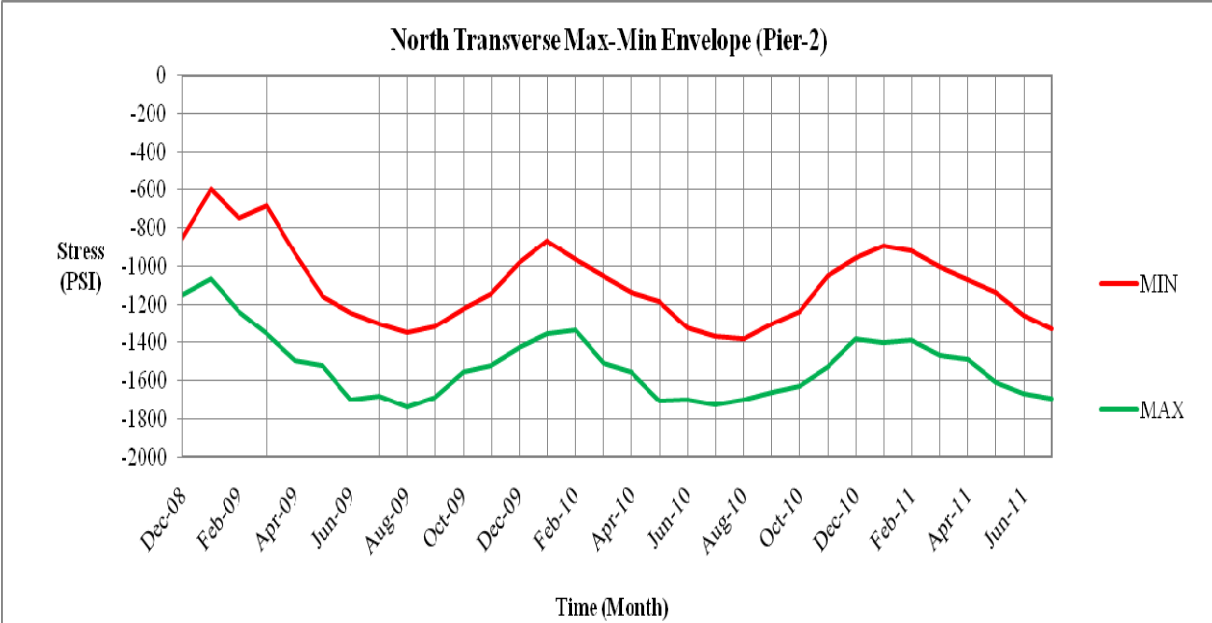
Figure C-20. Three-year envelope for north pier 2 in the transverse direction
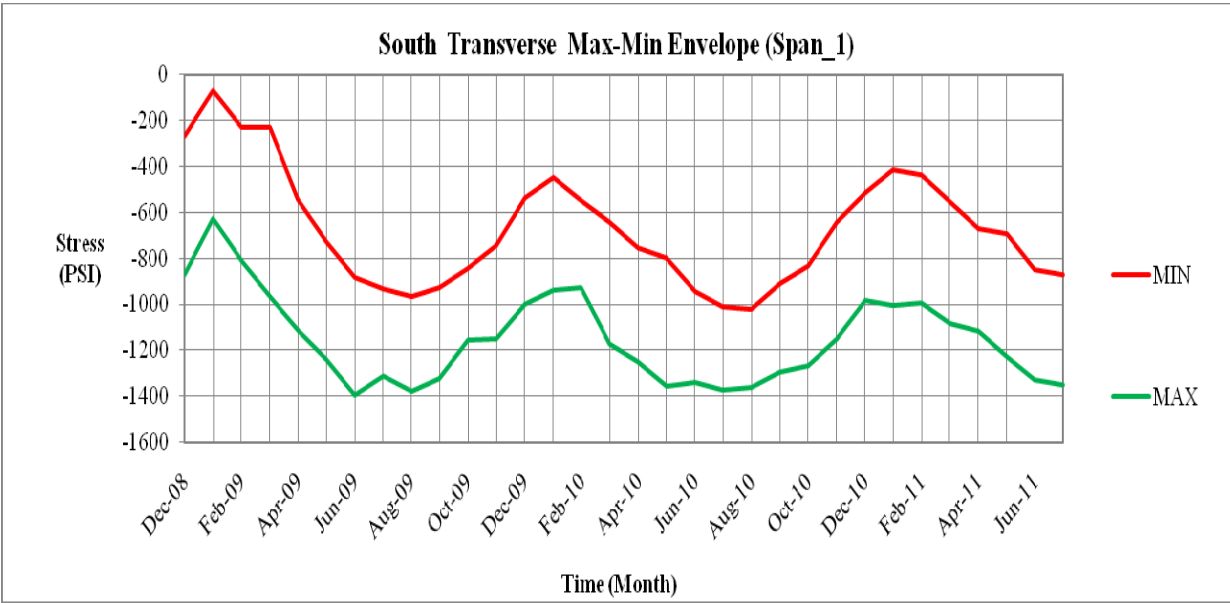
Figure C-21. Three-year envelope for south span 1 in the transverse direction
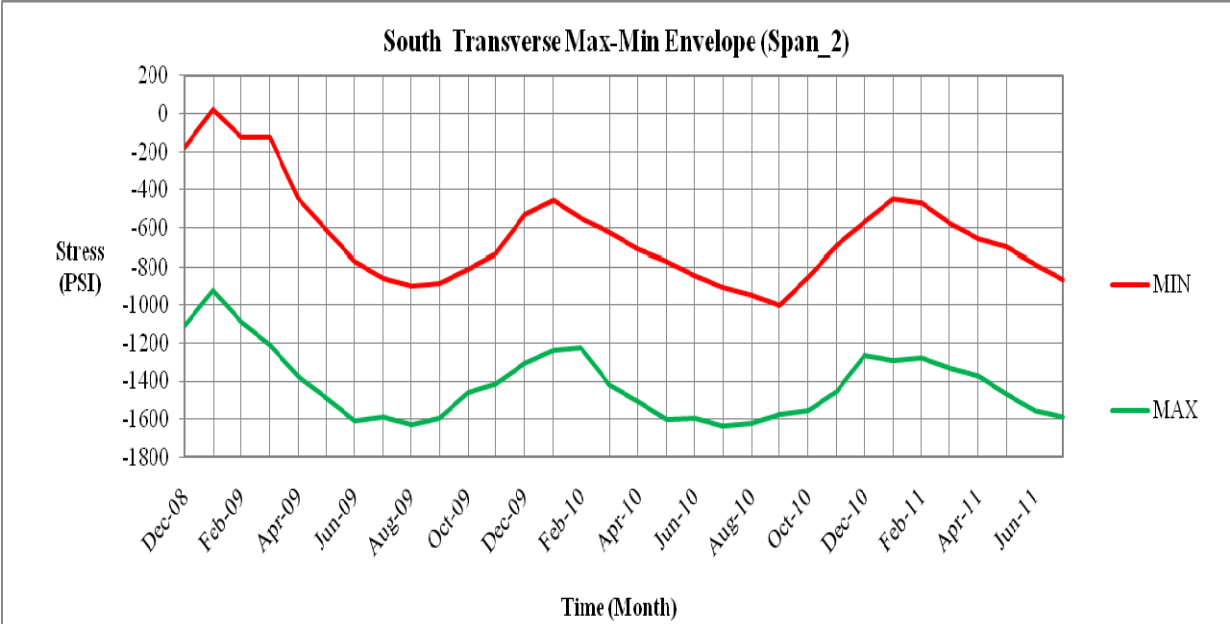
Figure C-22. Three-year envelope for south span 2 in the transverse direction
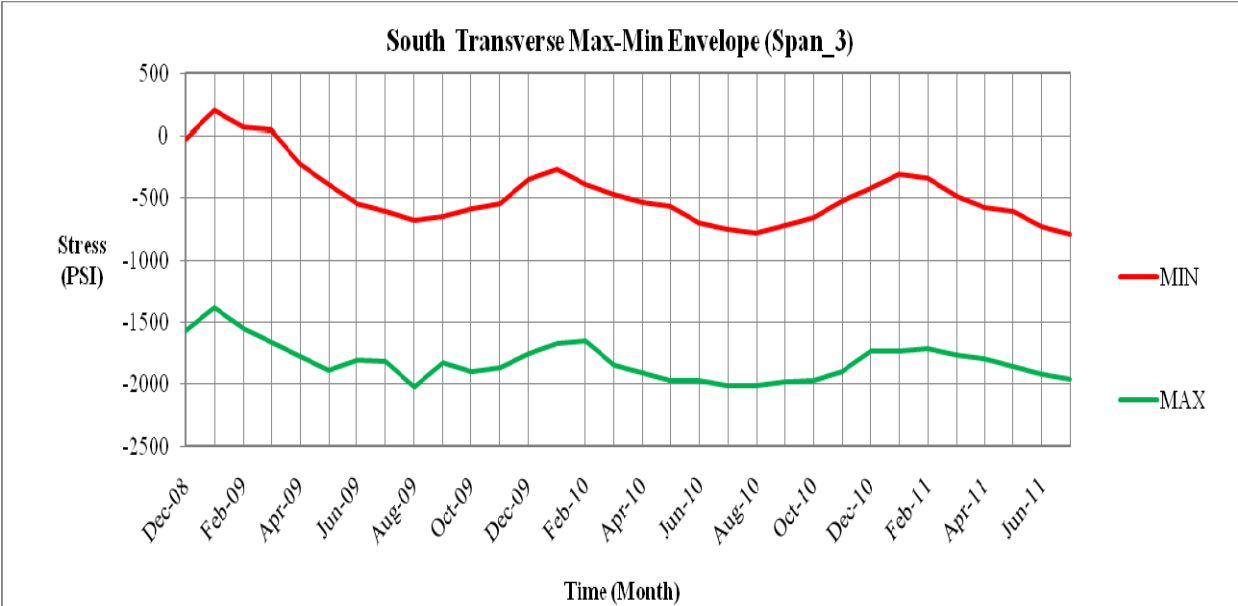
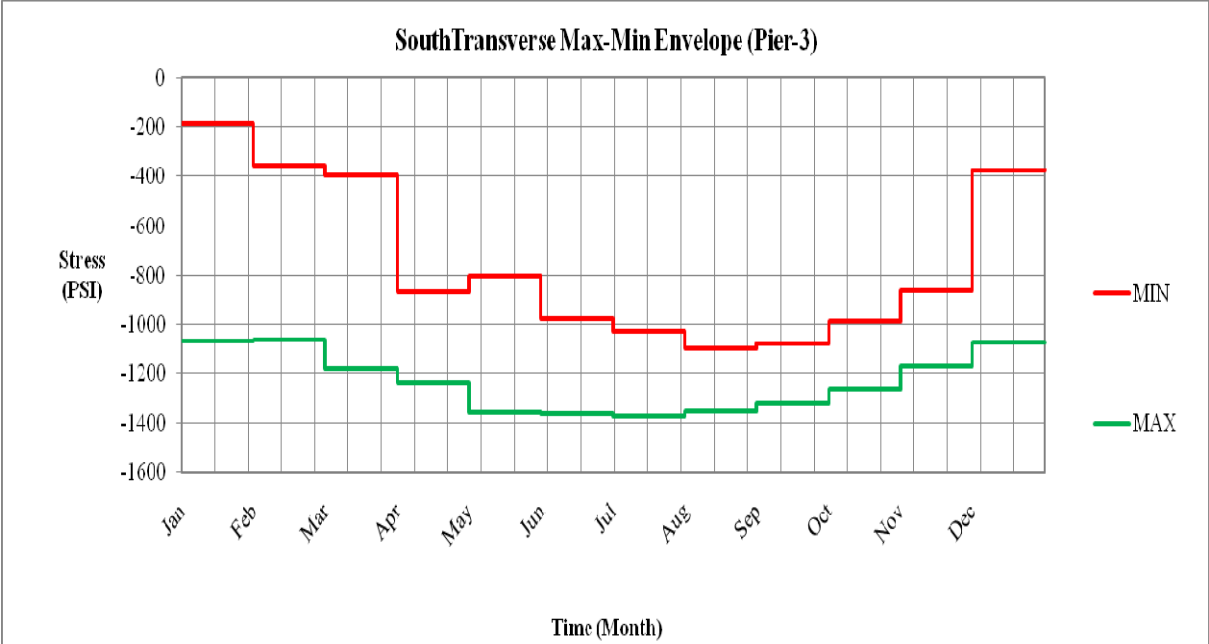**Figure C-23. Three-year envelope for south span 3 in the transverse direction**
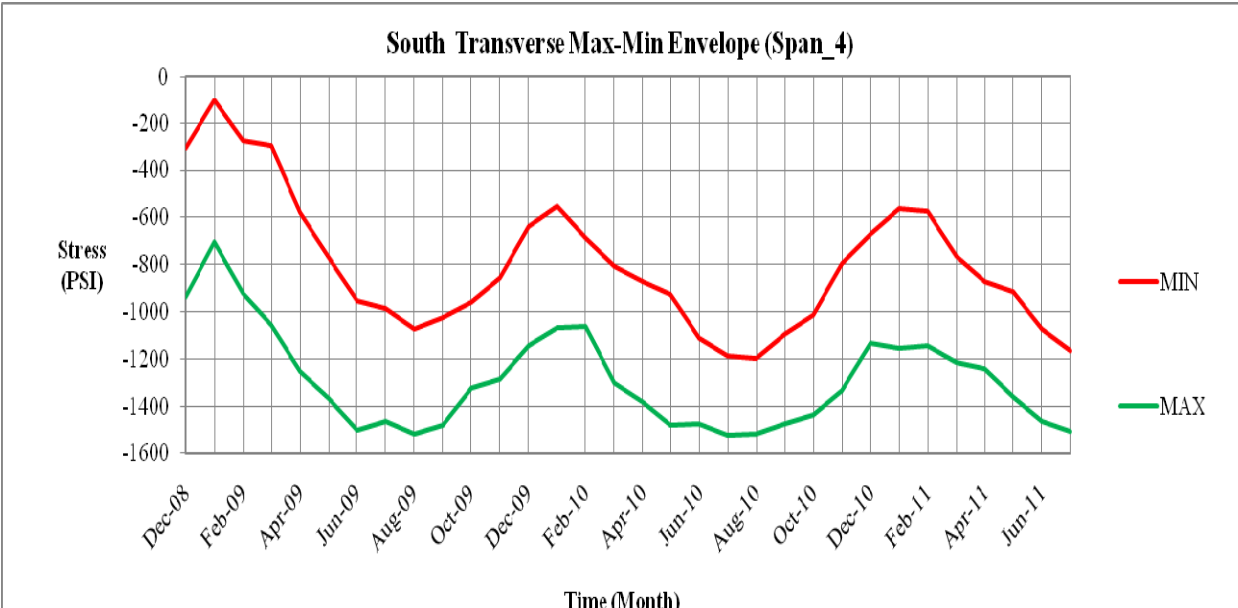
Figure C-24. Three-year envelope for south span 4 in the transverse direction
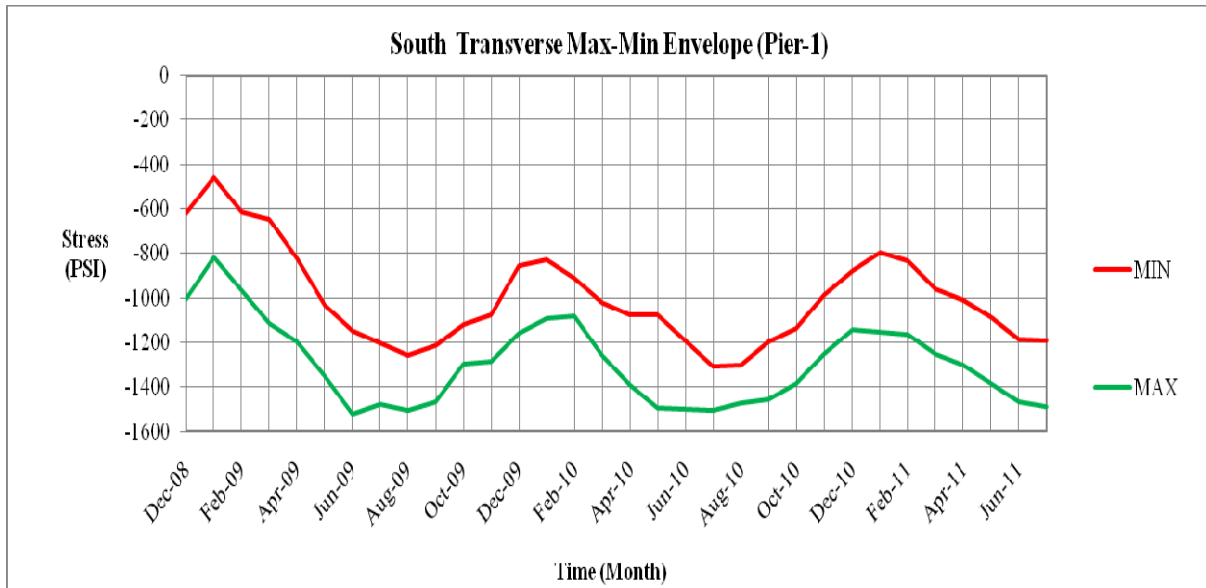
**Figure C-25. Three-year envelope for south pier 1 in the transverse direction**
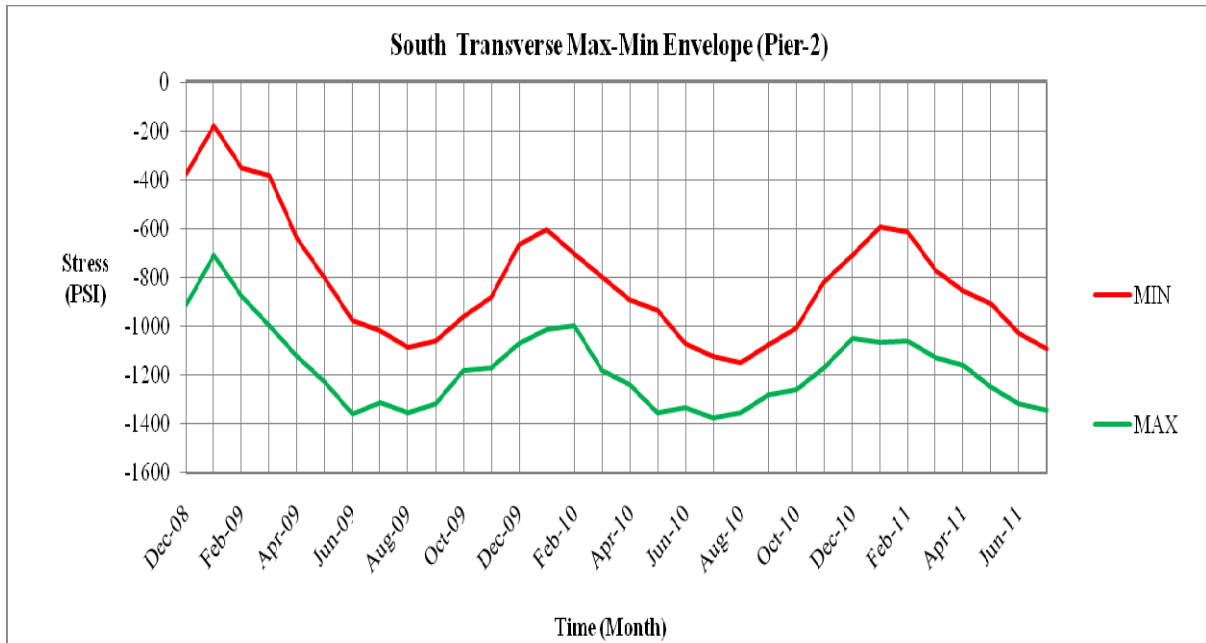
Figure C-26. Three-year envelope for south pier 2 in the transverse direction
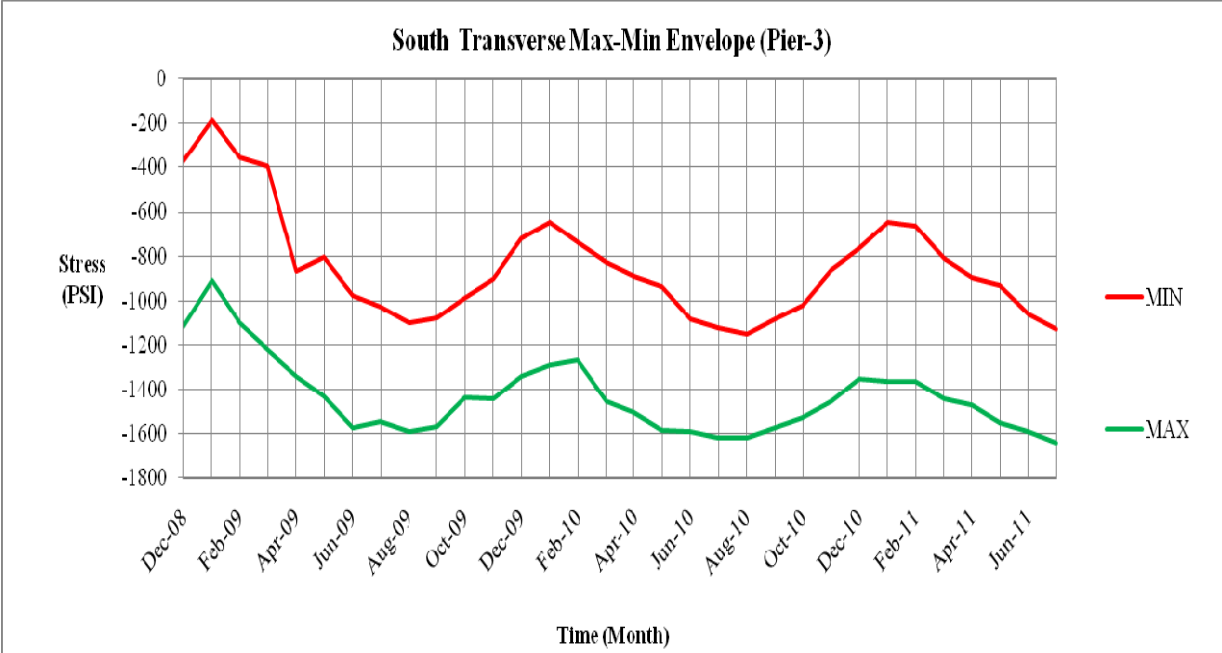
**Figure C-27. Three-year envelope for south pier 3 in the transverse direction**

APPENDIX D: ONE-YEAR STRESS ENVELOPE TEMPLATES

D.1 Longitudinal Stress Envelopes:
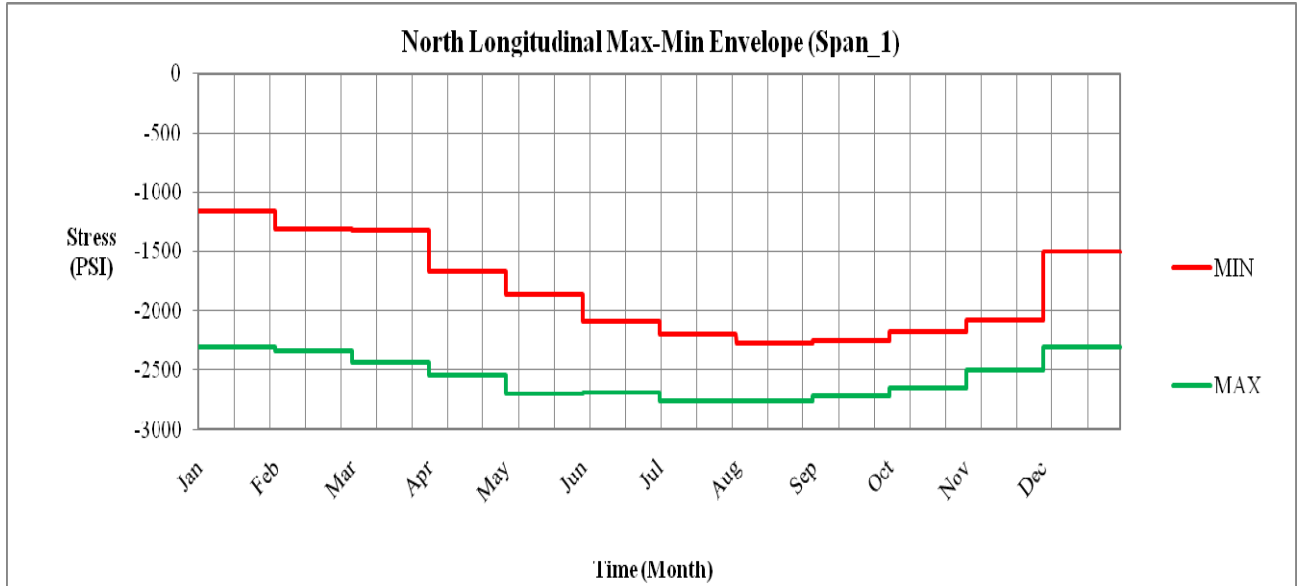
Figure D-1. One-year envelope for north span 1 in the longitudinal direction
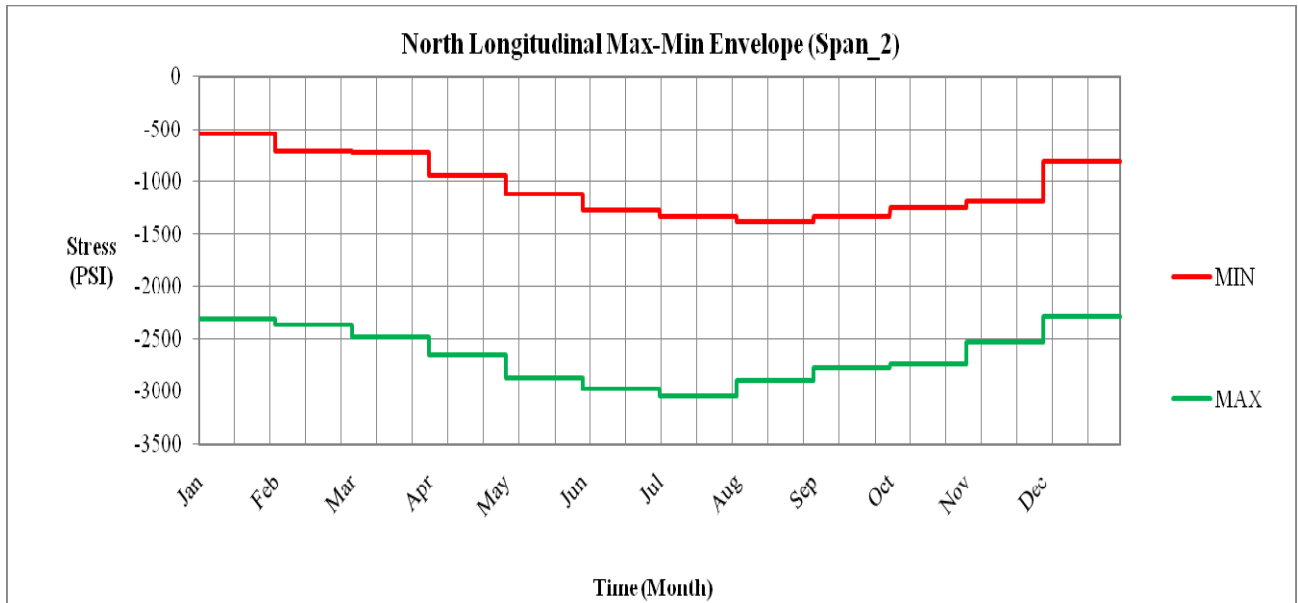
Figure D-2. One-year envelope for north span 2 in the longitudinal direction
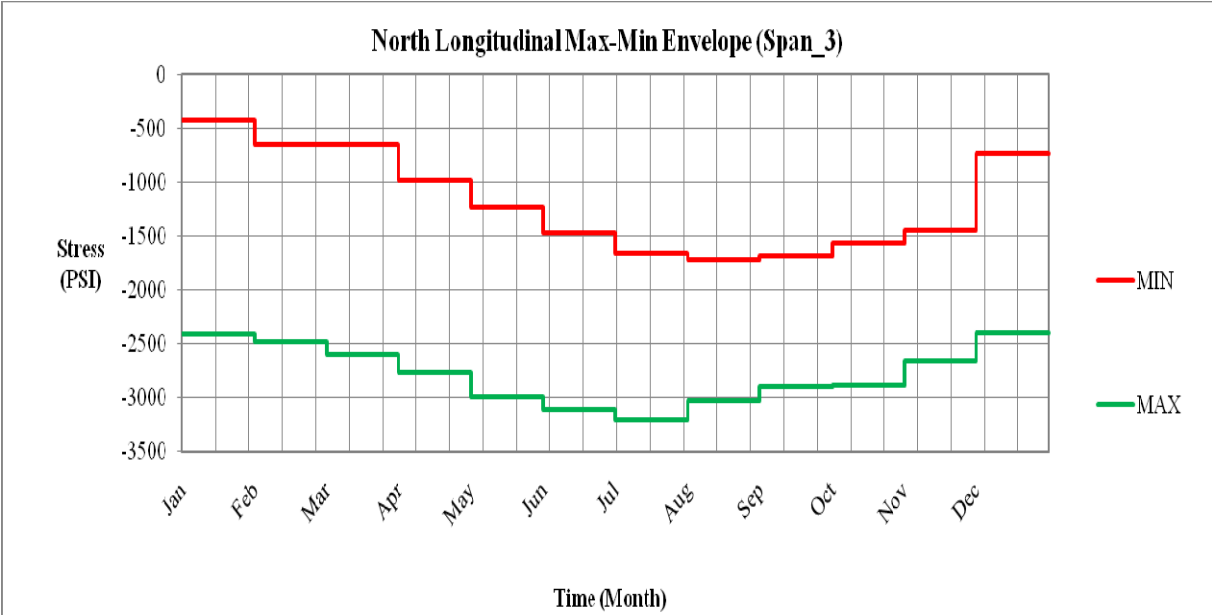
Figure D-3. One-year envelope for north span 3 in the longitudinal direction
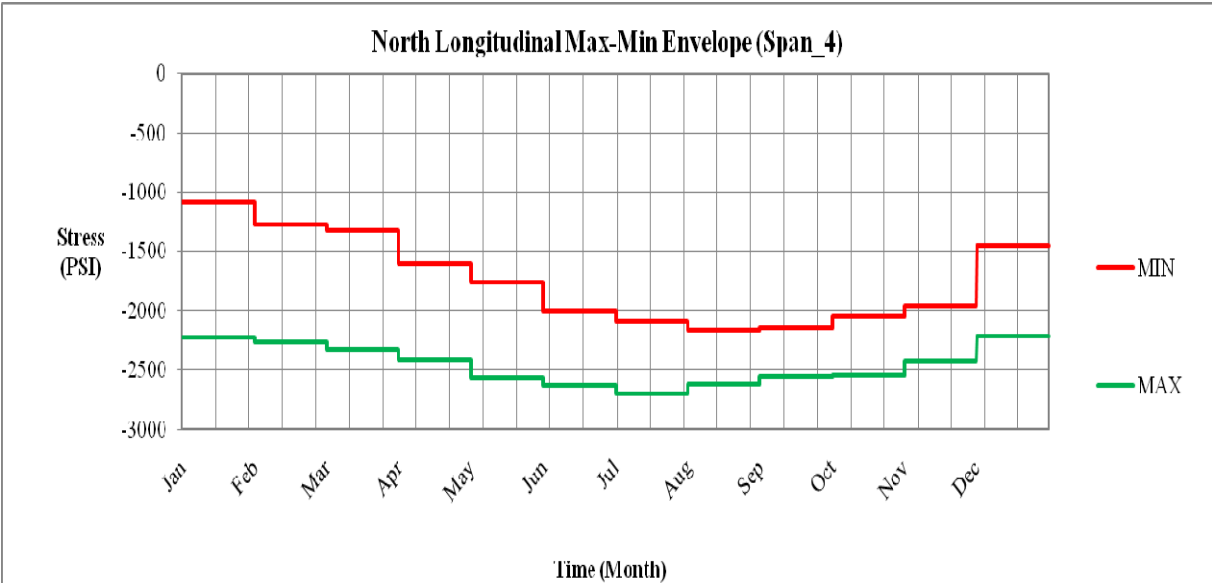
Figure D-4. One-year envelope for north span 4 in the longitudinal direction
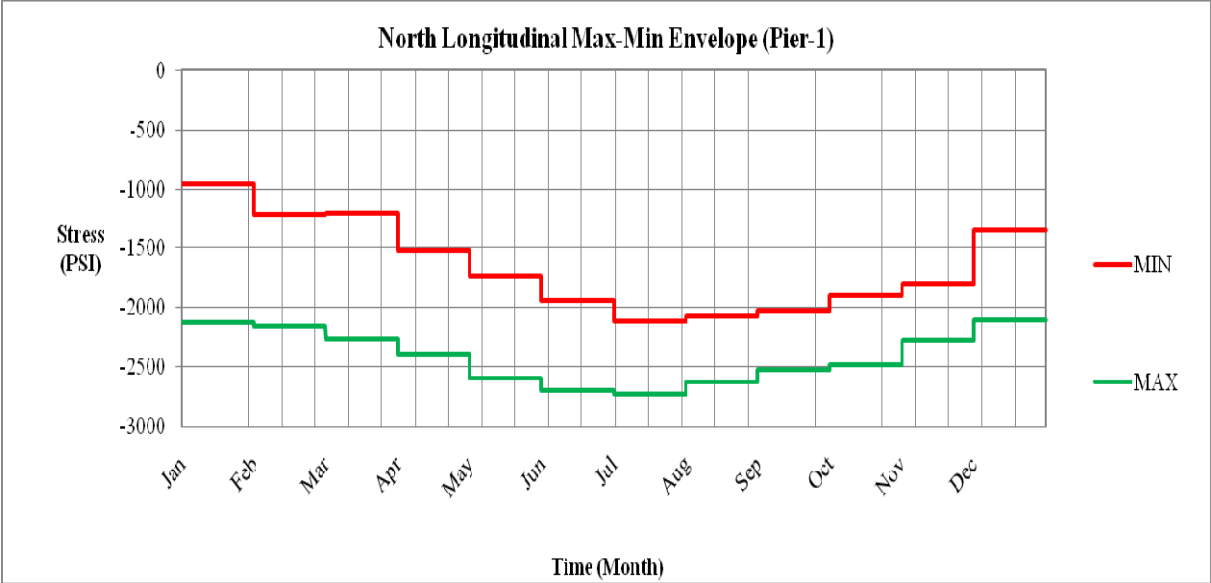
Figure D-5. One-year envelope for north pier 1 in the longitudinal direction
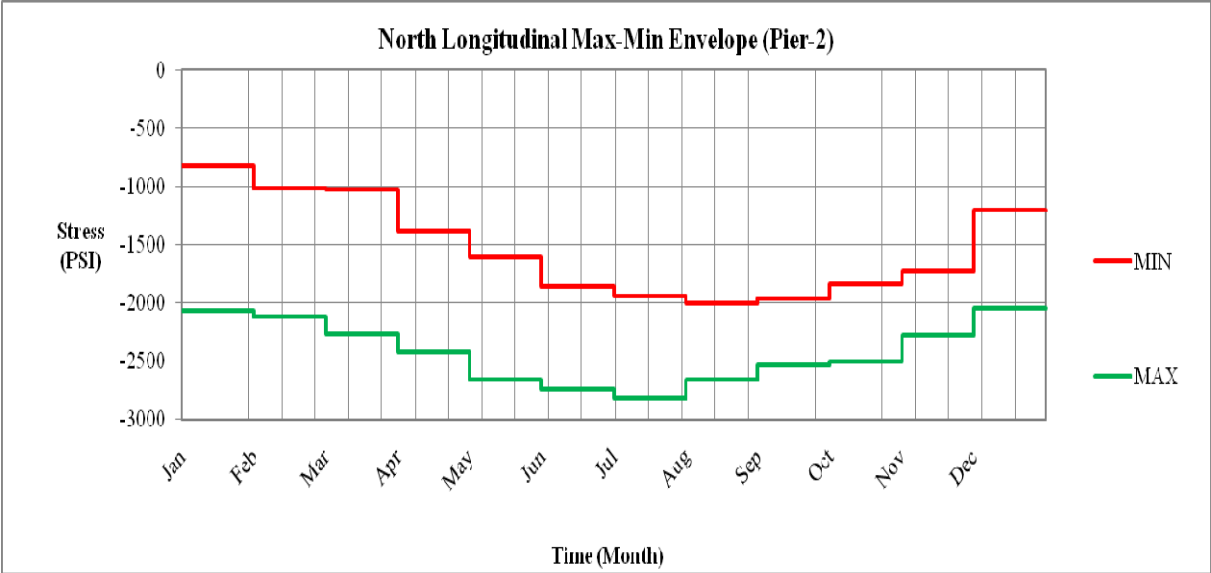
Figure D-6. One-year envelope for north pier 2 in the longitudinal direction

106
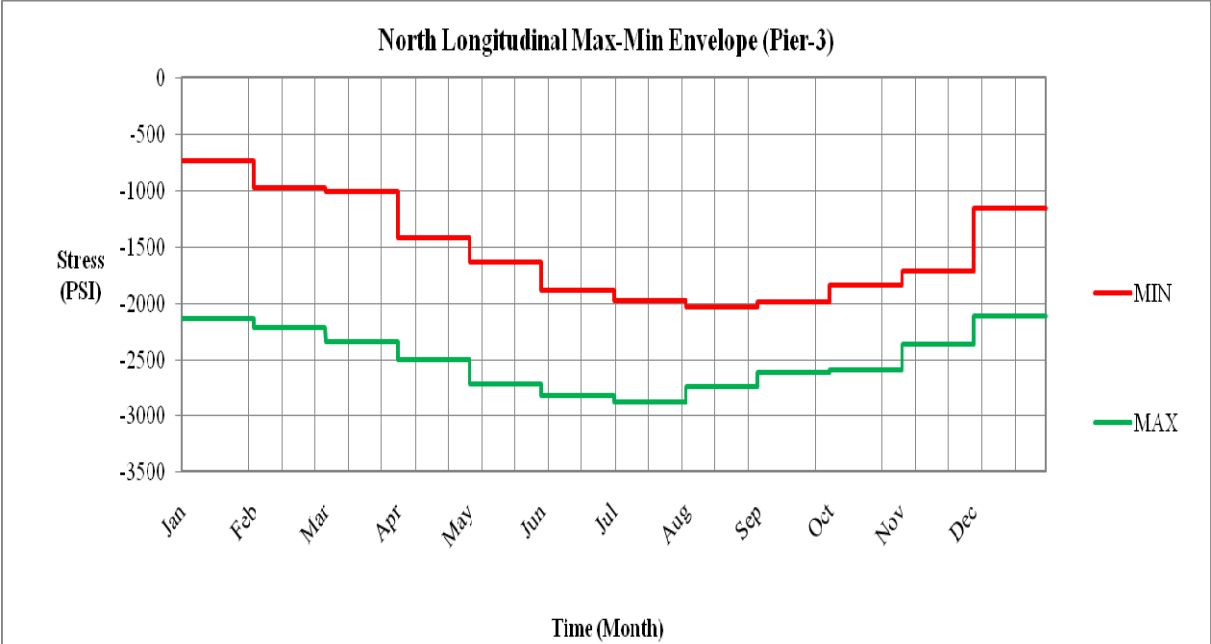
Figure D-7. One-year envelope for north pier 3 in the longitudinal direction
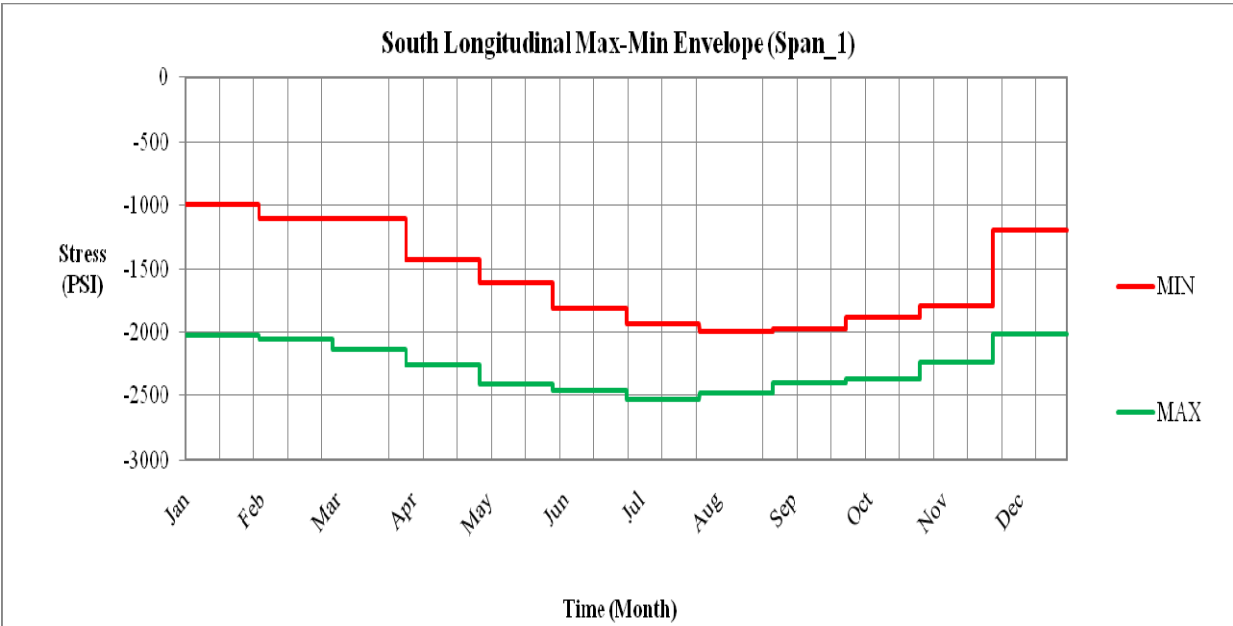
Figure D-8. One-year envelope for south span 1 in the longitudinal direction
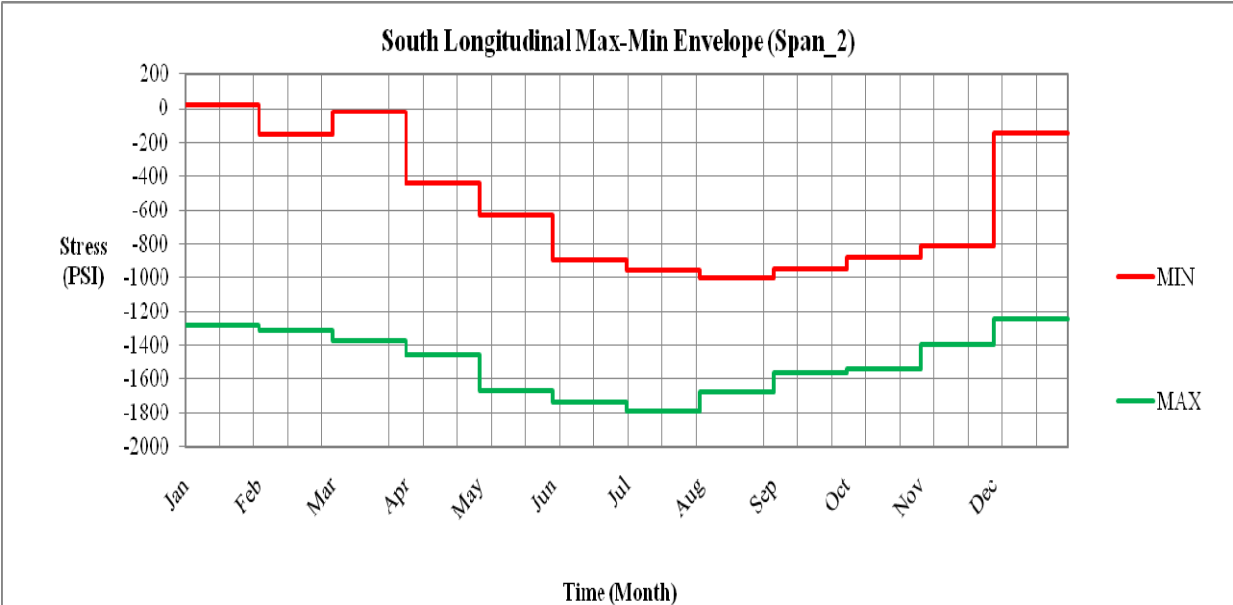
Figure D-9. One-year envelope for south span 2 in the longitudinal direction
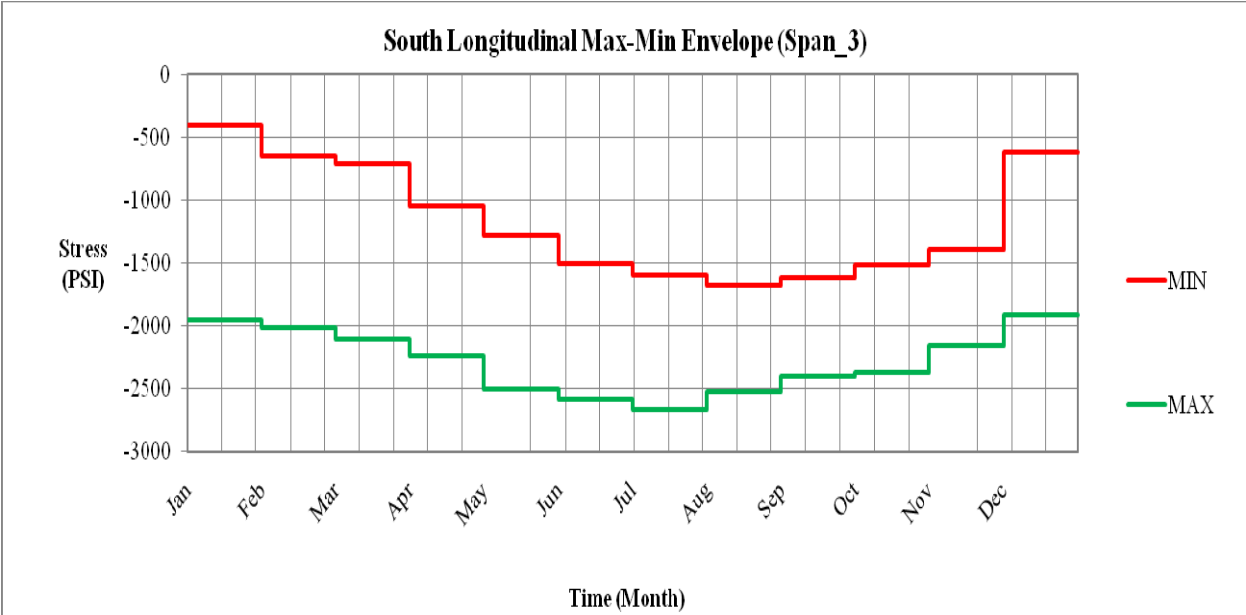
Figure D-10. One-year envelope for south span 3 in the longitudinal direction
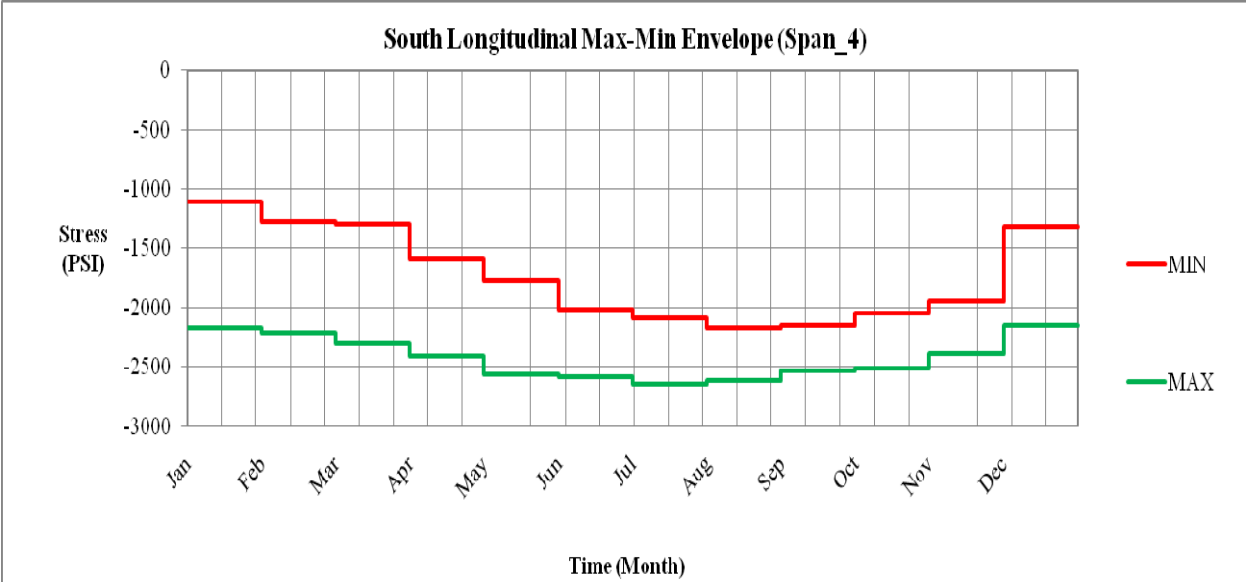
Figure D-11. One-year envelope for south span 4 in the longitudinal direction
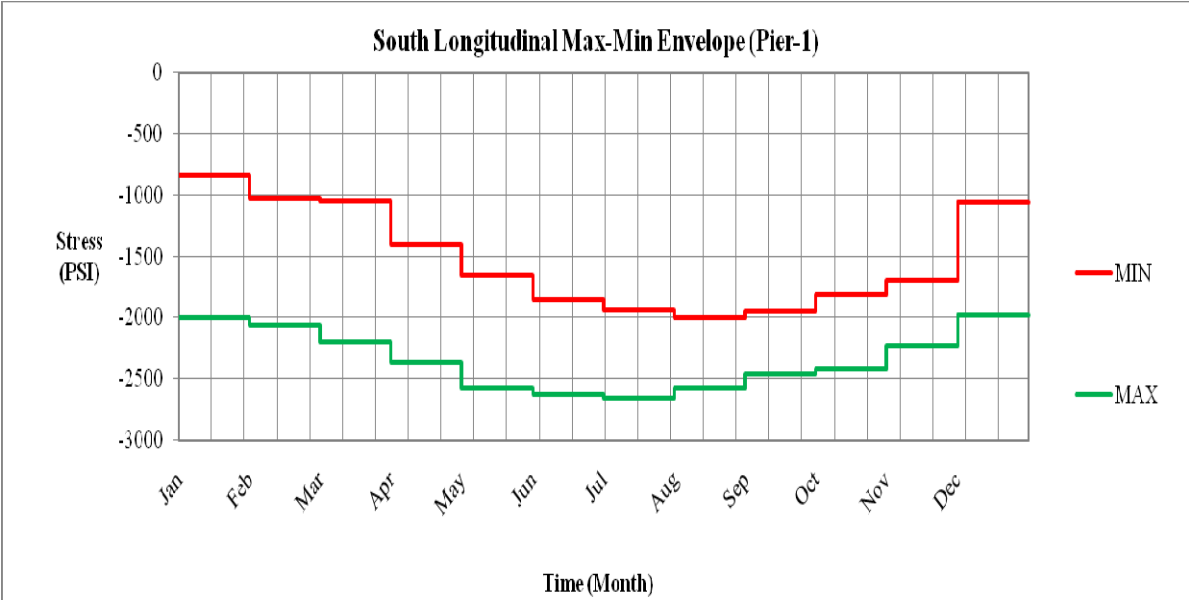
Figure D-12. One-year envelope for pier 1 in the longitudinal direction
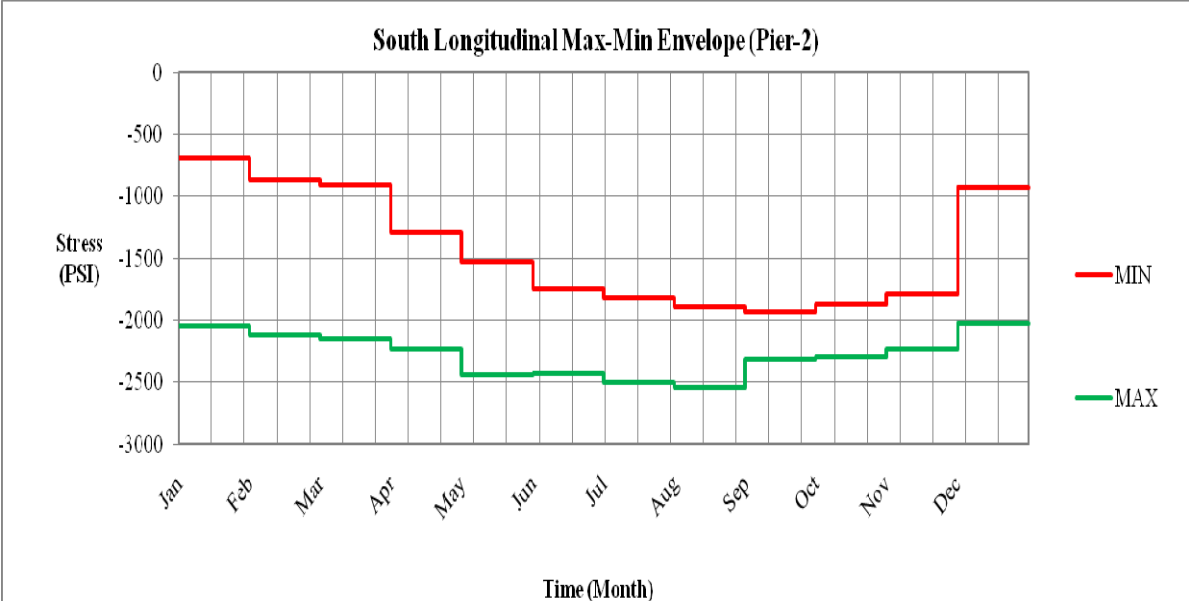
Figure D-13. One-year envelope for pier 2 in the longitudinal direction

110
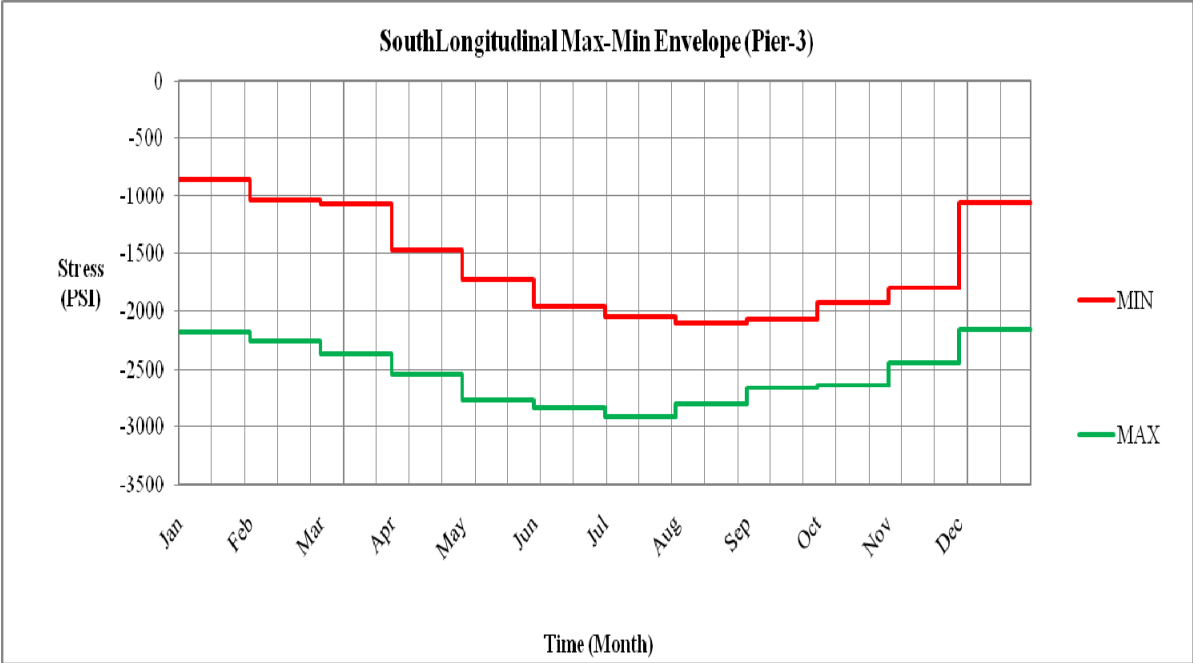
Figure D-14. One-year envelope for pier 3 in the longitudinal direction

D.2 Longitudinal Stress Envelopes:
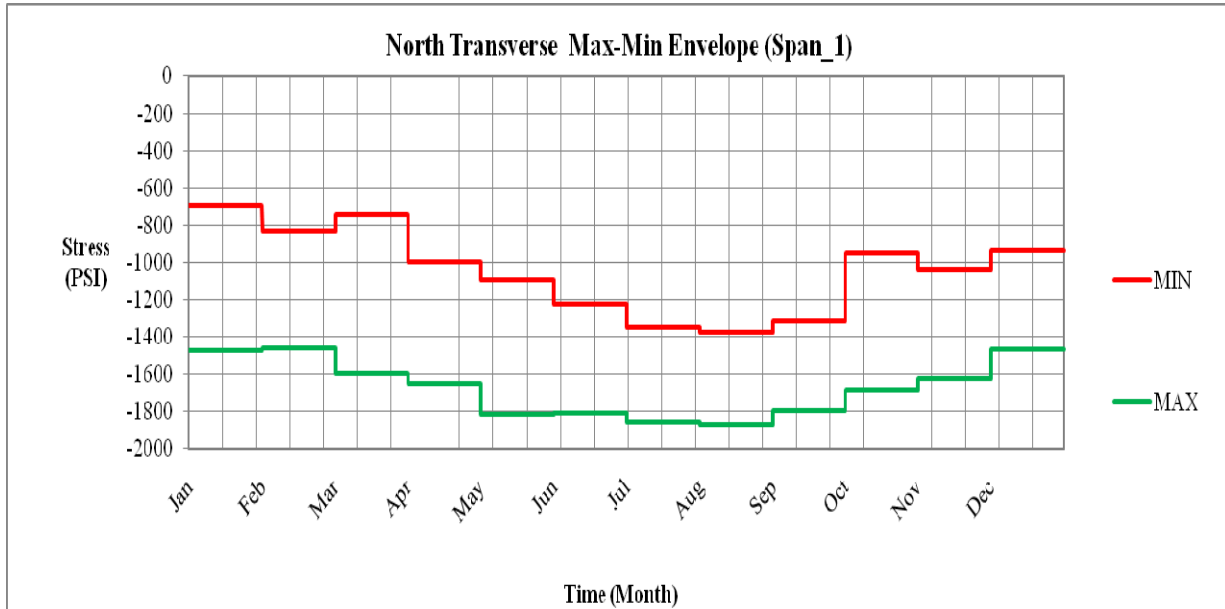
Figure D-15. One-year envelope for north span 1 in the transverse direction
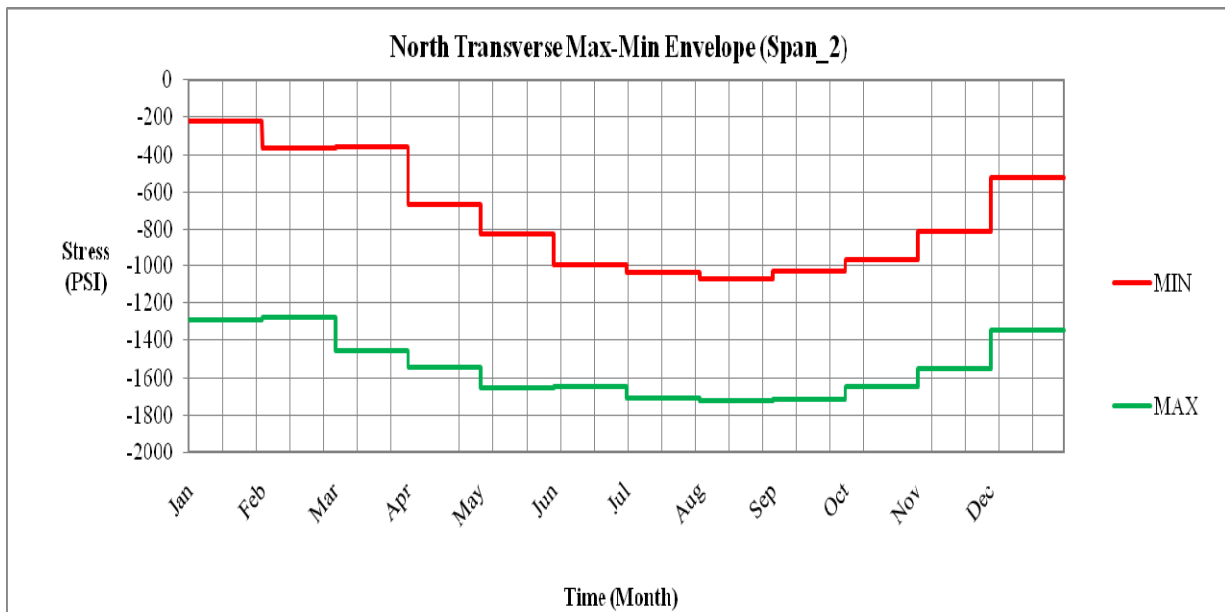
Figure D-16. One-year envelope for north span 2 in the transverse direction
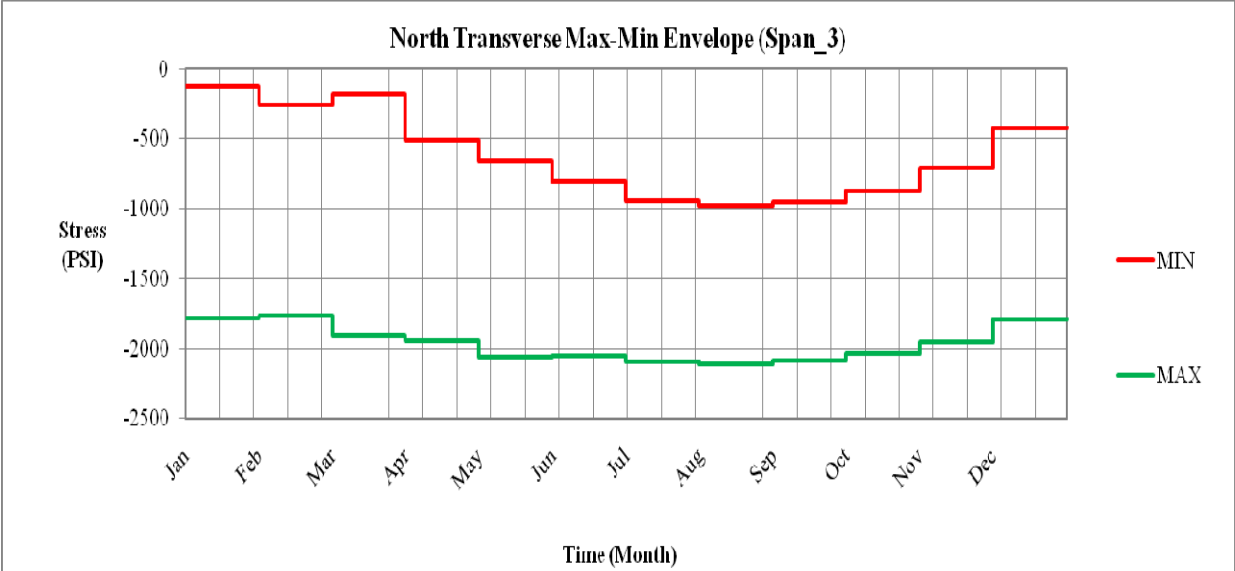
Figure D-17. One-year envelope for north span 3 in the transverse direction
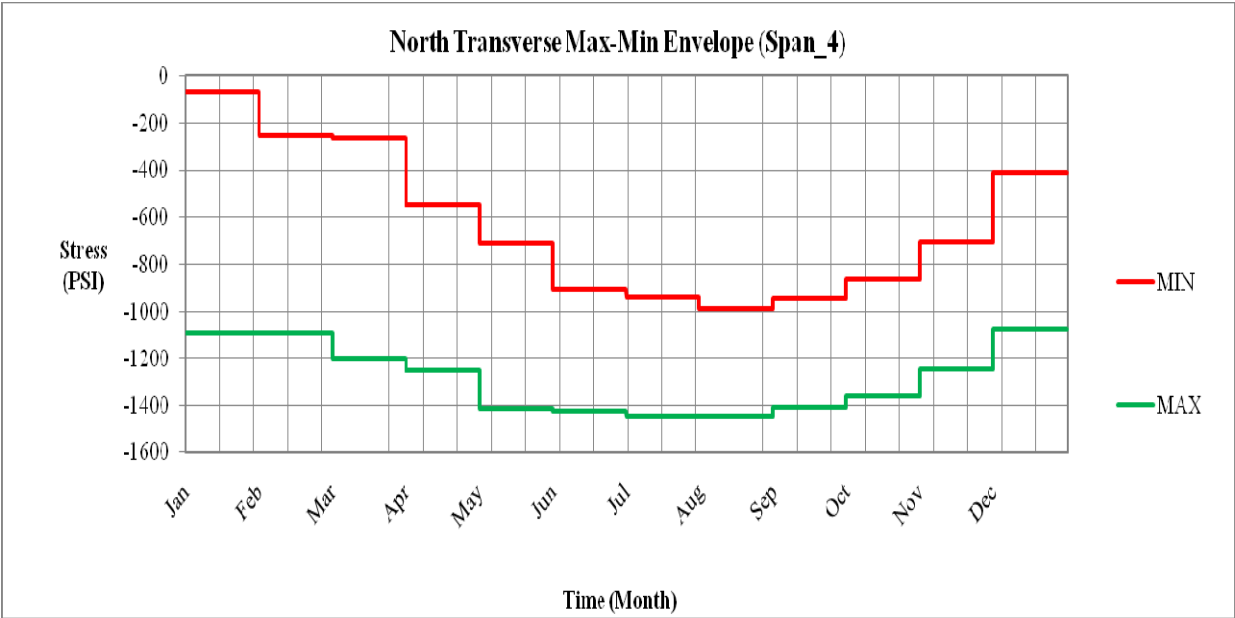
Figure D-18. One-year envelope for north span 4 in the transverse direction
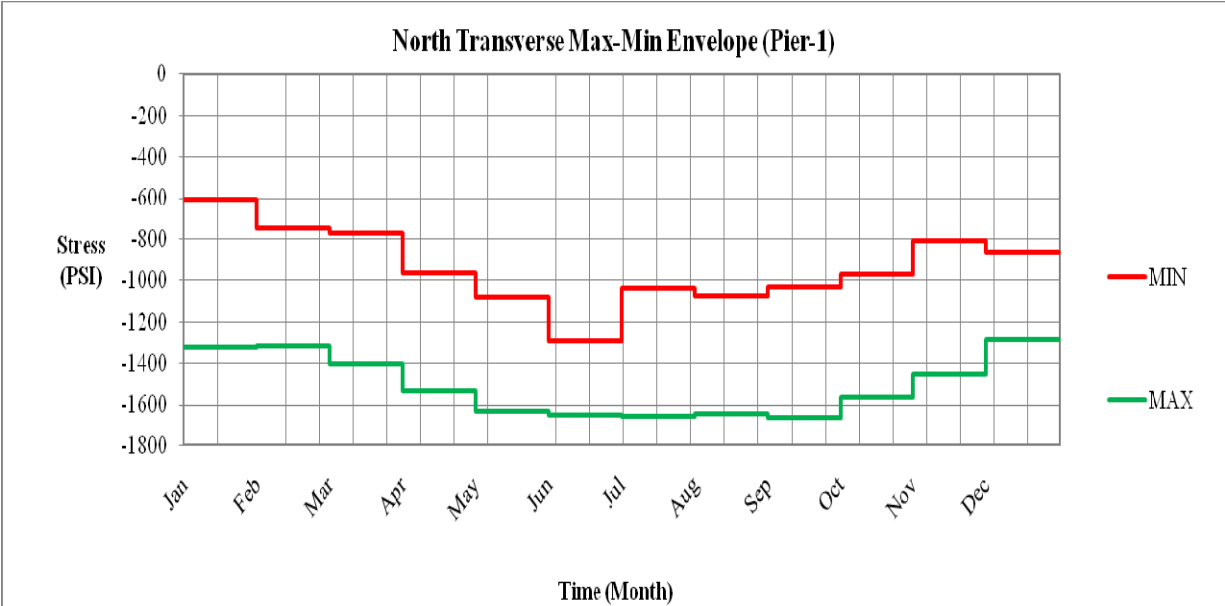
Figure D-19. One-year envelope for north pier 1 in the transverse direction
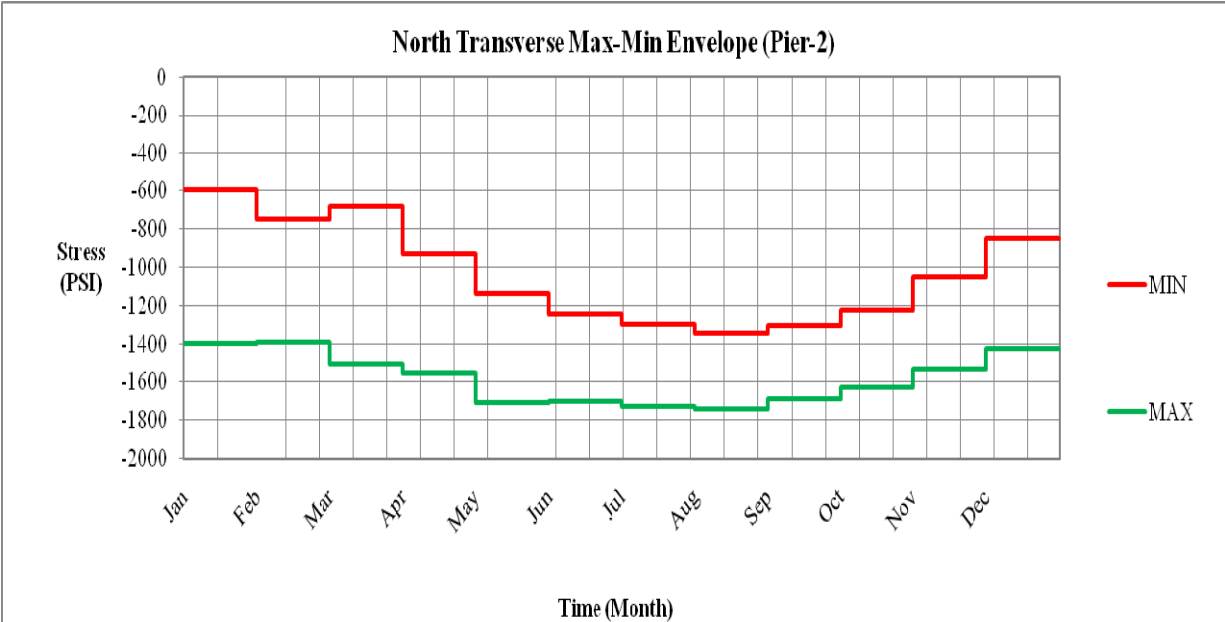
Figure D-20. One-year envelope for north pier 2 in the transverse direction
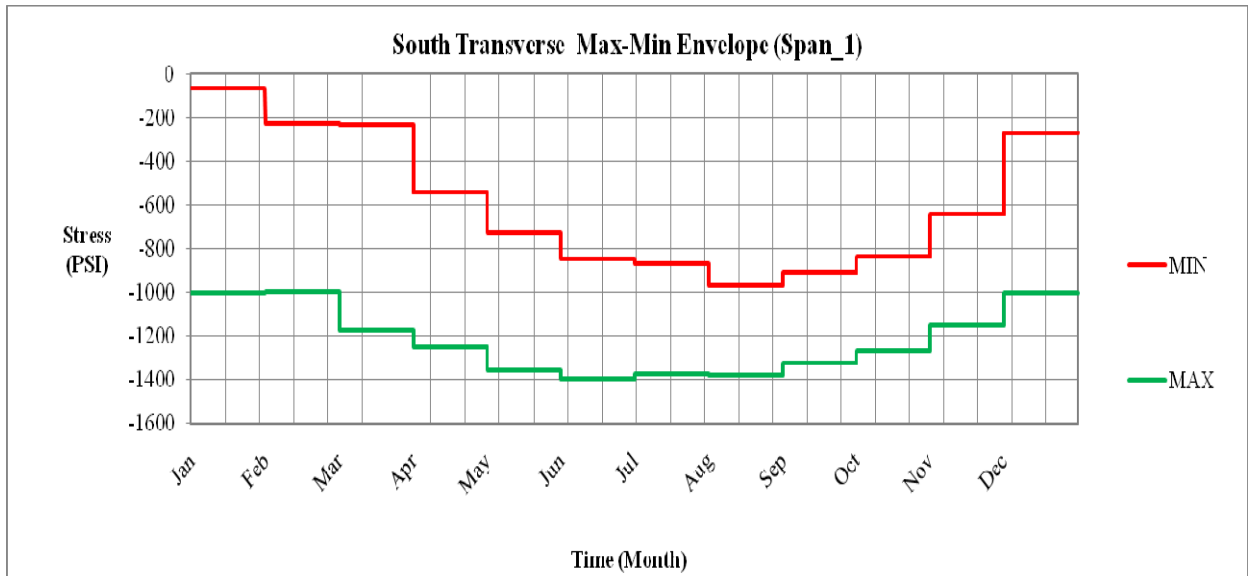
Figure D-21. One-year envelope for south span 1 in the transverse direction
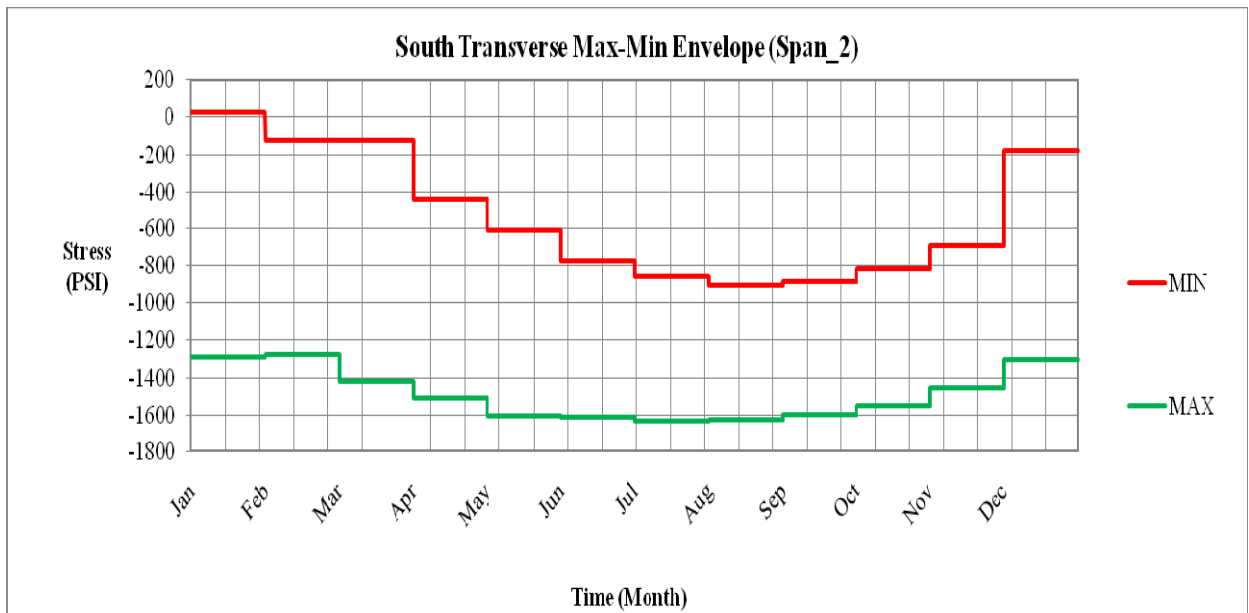
Figure D-22. One-year envelope for south span 2 in the transverse direction

116

115
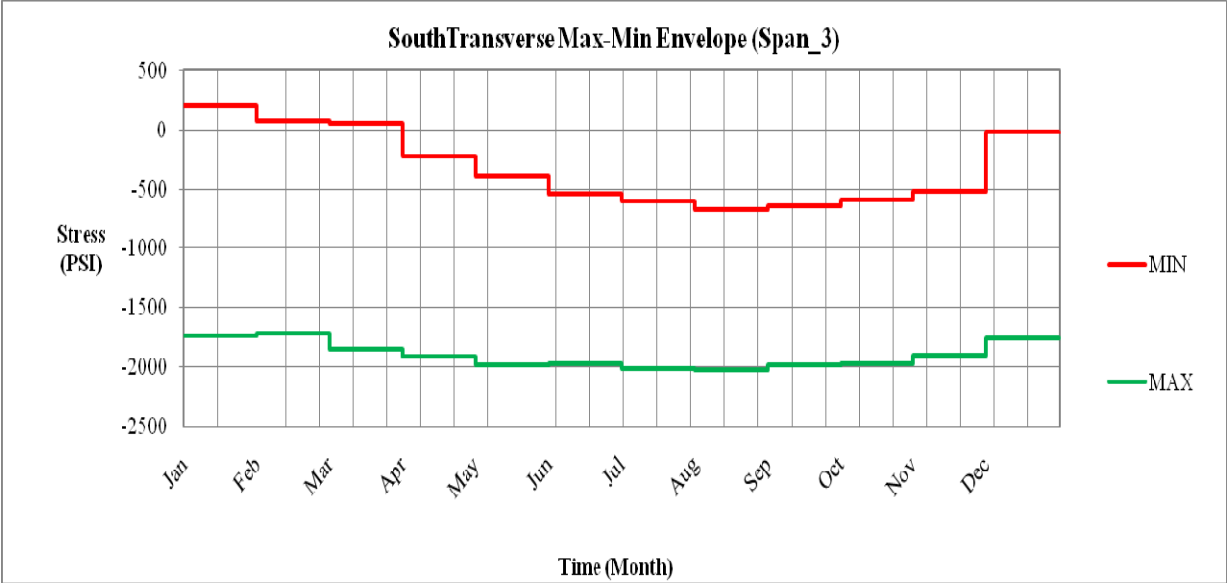
Figure D-23. One-year envelope for south span 3 in the transverse direction

Figure D-24. One-year envelope for south span 4 in the transverse direction

Figure D-25. One-year envelope for south pier 1 in the transverse direction

Figure D-26. One-year envelope for south pier 2 in the transverse direction

117

Figure D-27. One-year envelope for south pier 3 in the transverse direction

D.3 Closure Grout Stress Envelops:
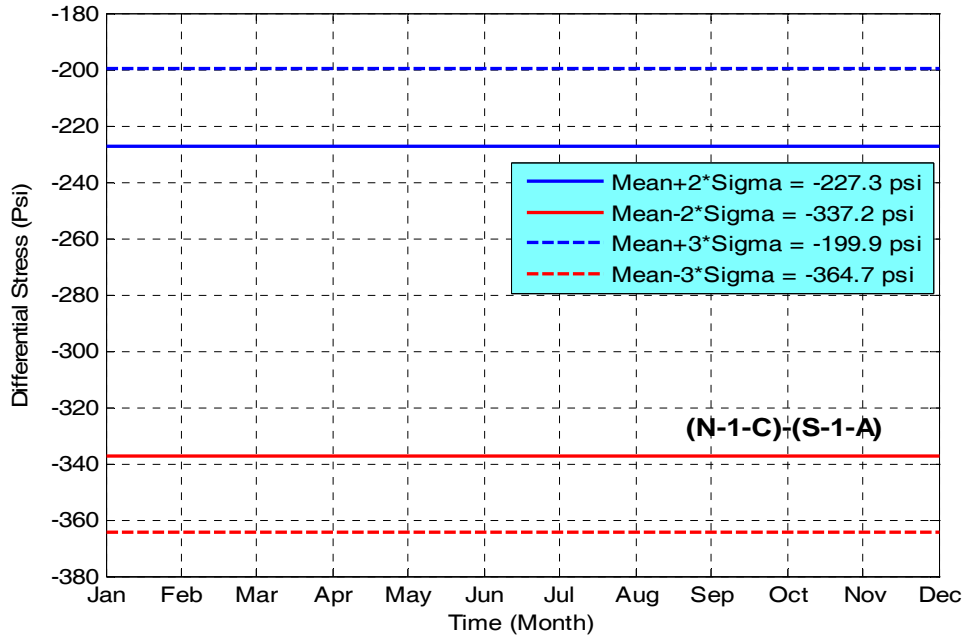
Figure D-28. One-year differential stress envelope for the closure grout sensors between north span 1 and south span 1 (span 1)
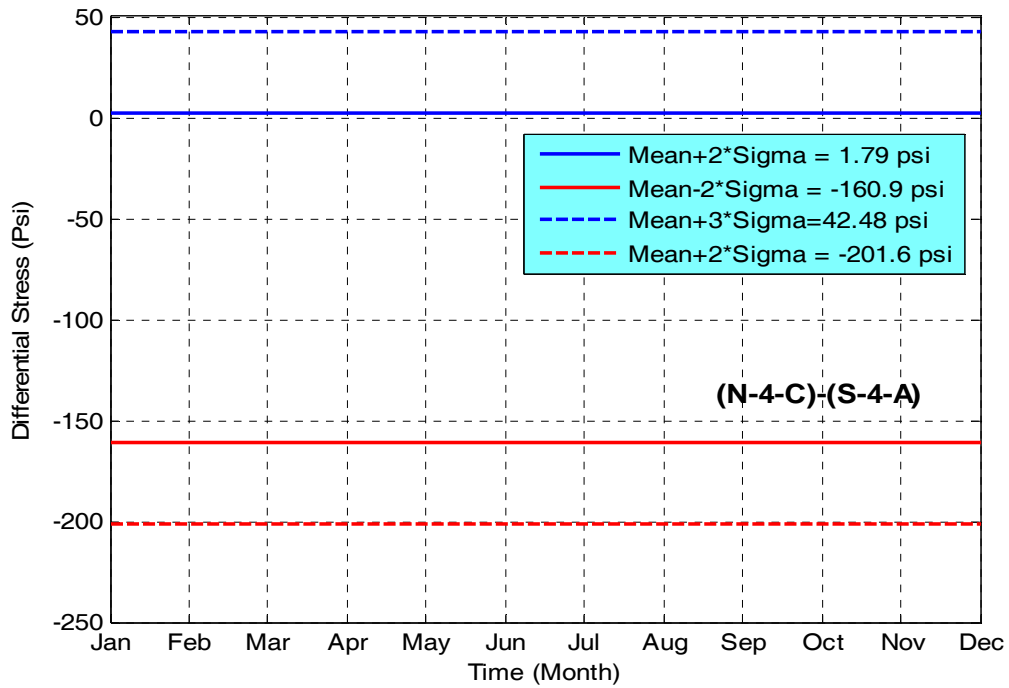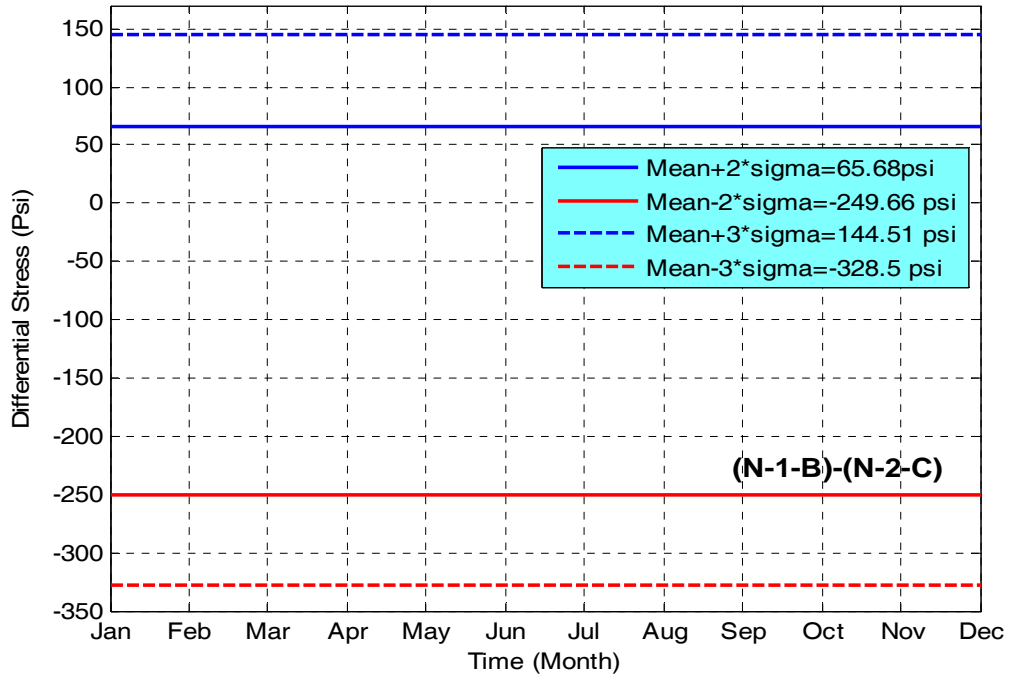

Figure D-29. One-year differential stress envelope for the closure grout sensors between north pier 1 and south pier 1 (pier 1)
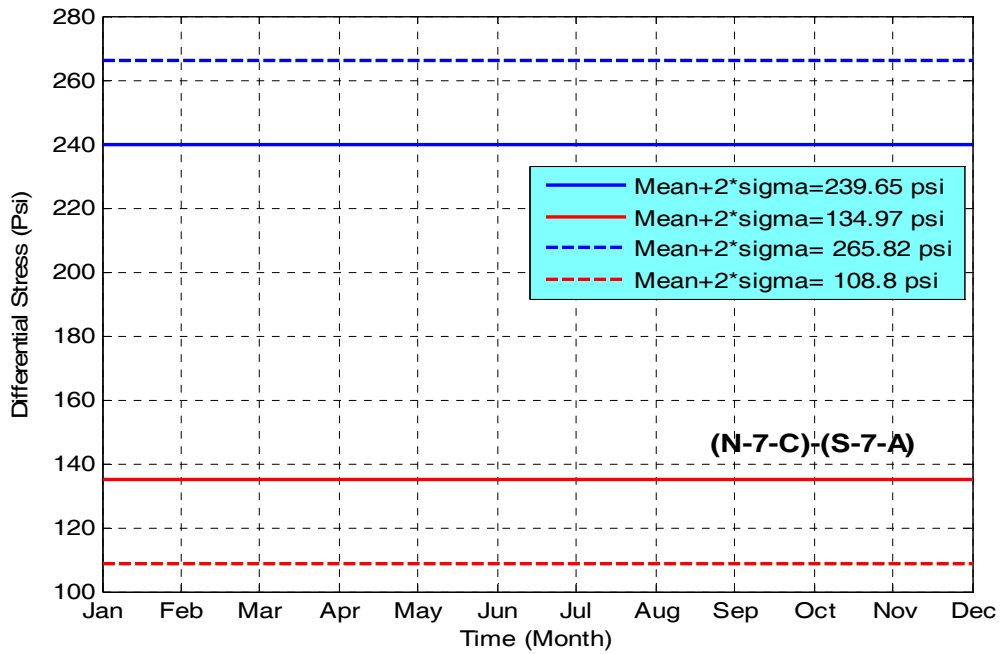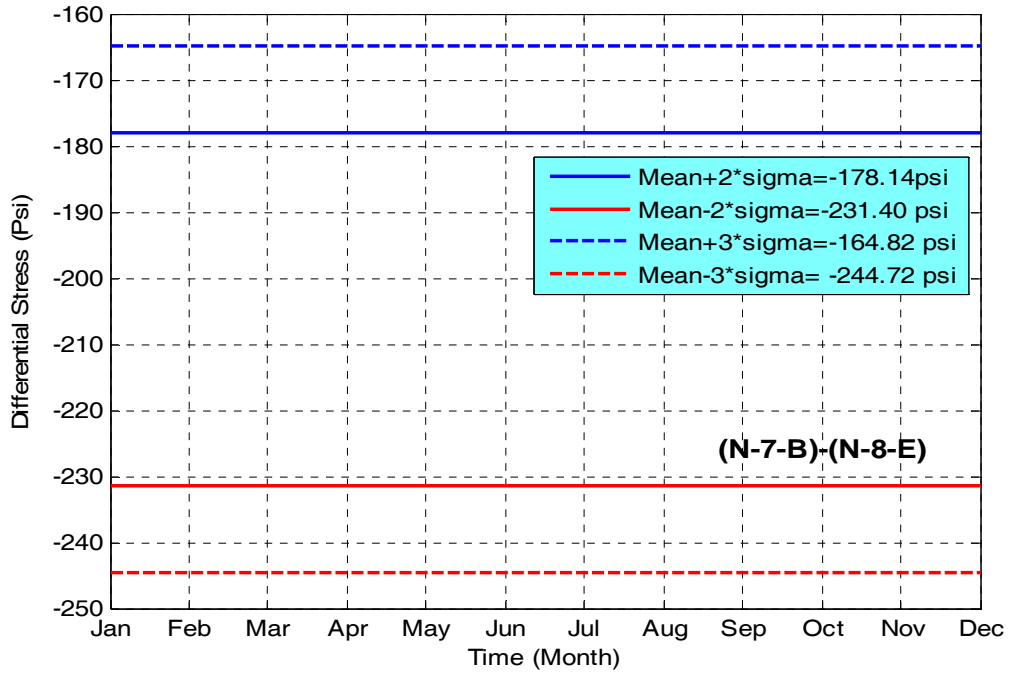
Figure D-30. One-year differential stress envelope for the closure grout sensors between north panel 7 and south panel 7 (span 2)
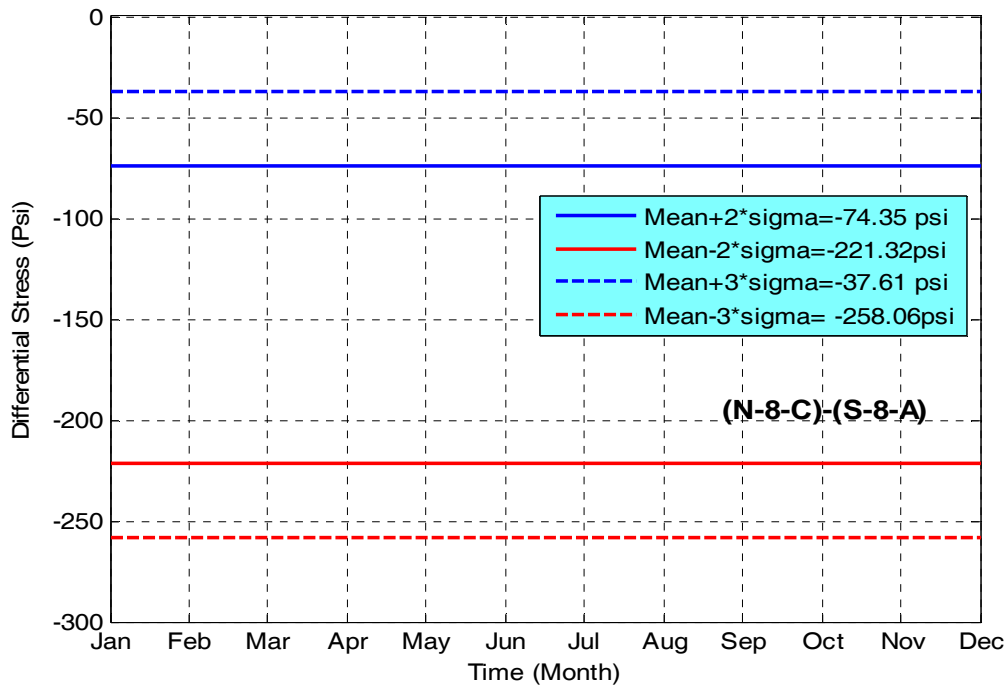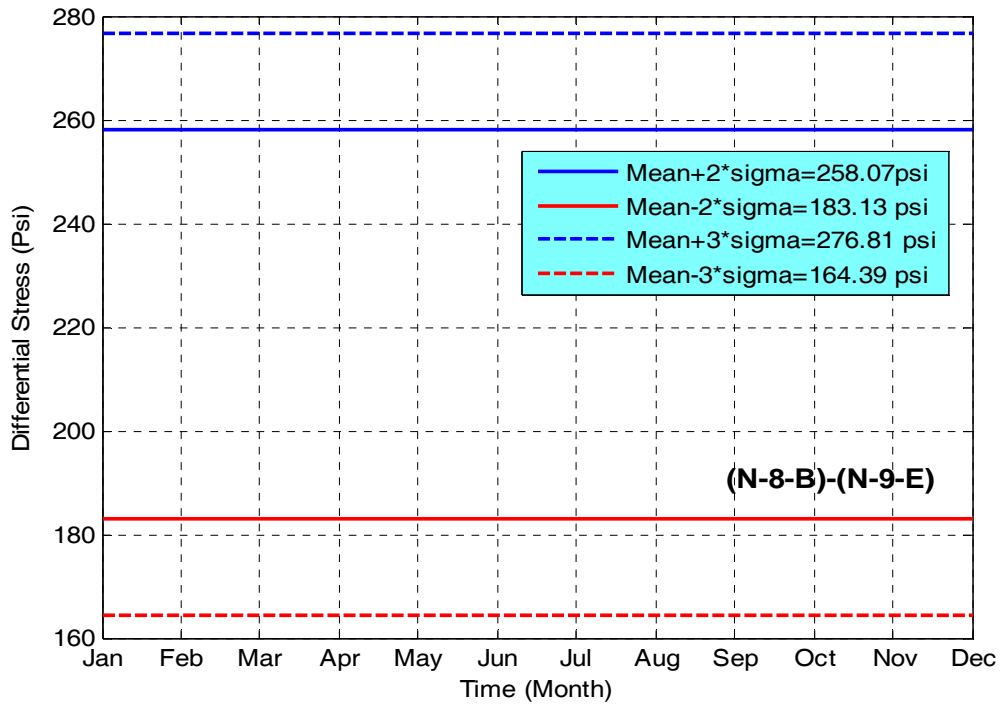

Figure D-31. One-year differential stress envelope for the closure grout sensors between north panel 8 and south panel 8 (span 2)
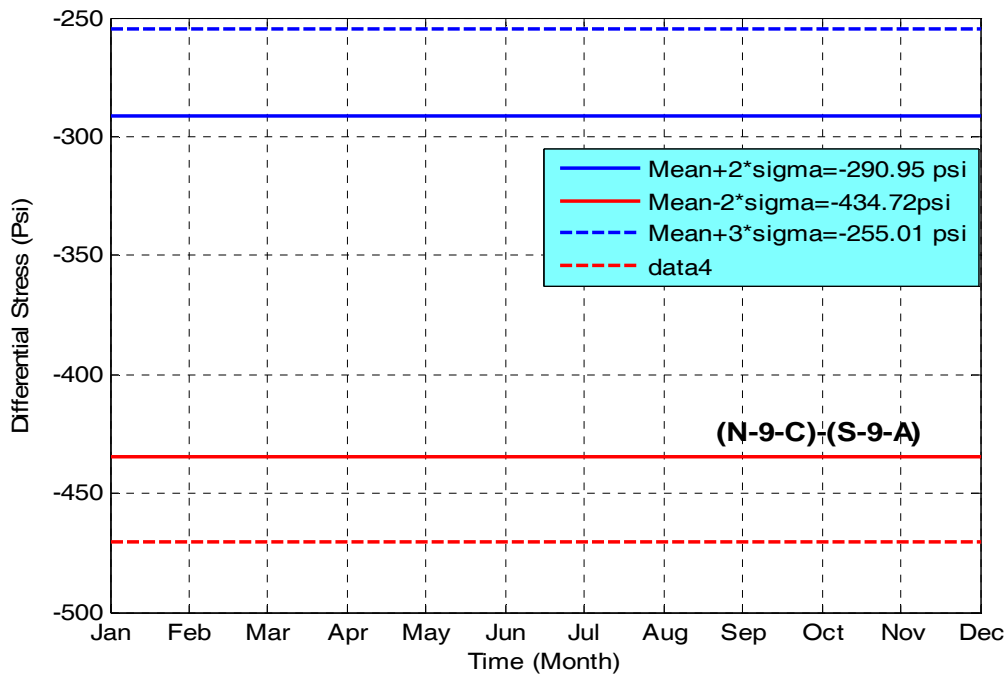
Figure D-32. One-year differential stress envelope for the closure grout sensors between north panel 9 and south panel 9 (span 2)
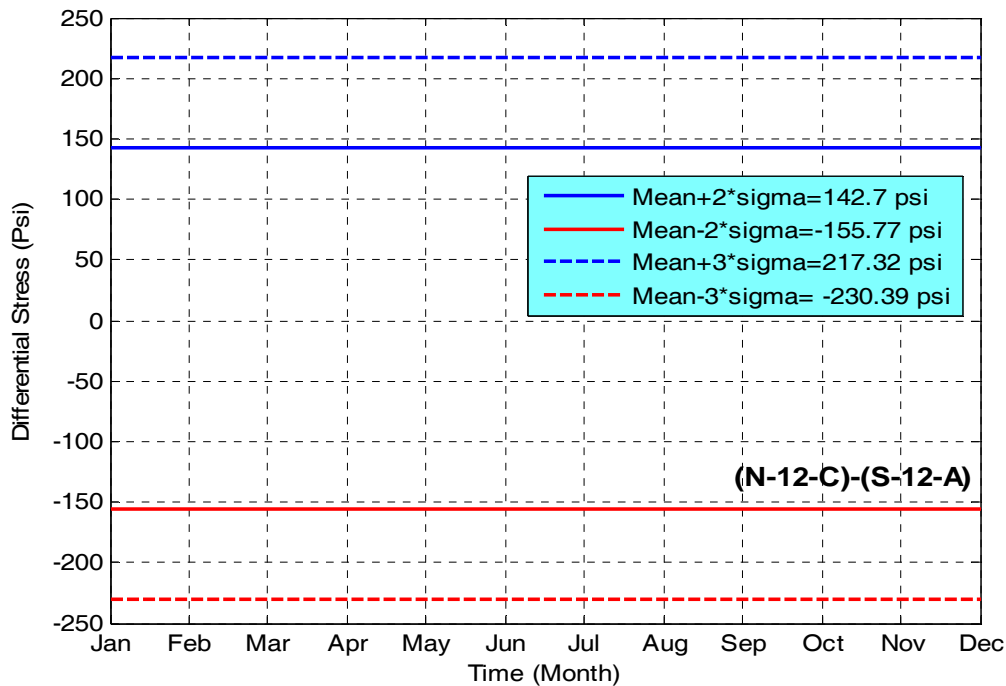
Figure D-33. One-year differential stress envelope for the closure grout sensors between north pier 2 and south pier 2 (pier 2)
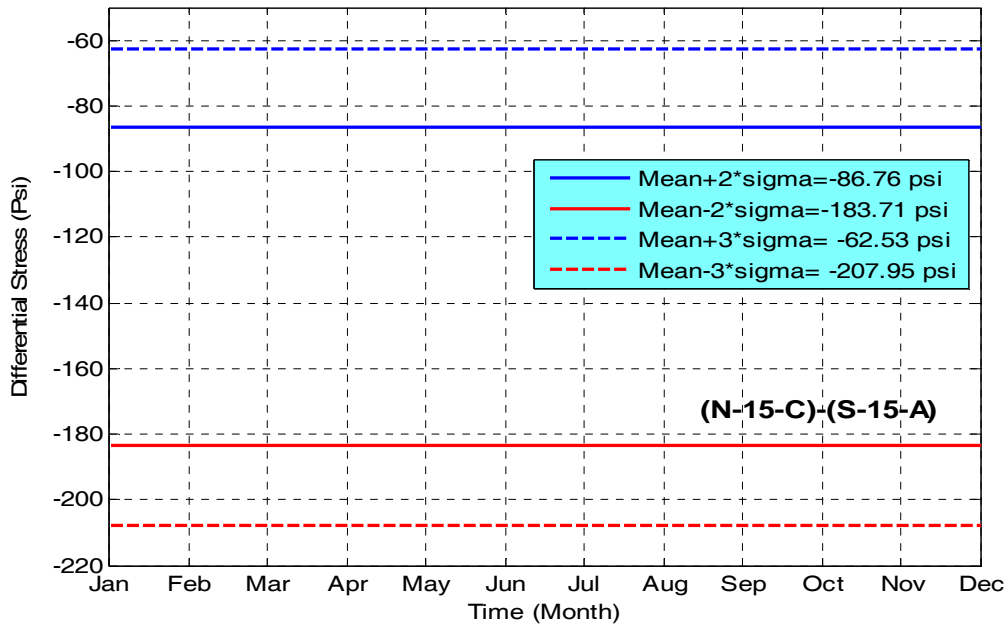
Figure D-34. One-year differential stress envelope for the closure grout sensors between north panel 15 and south panel 15 (span 3)
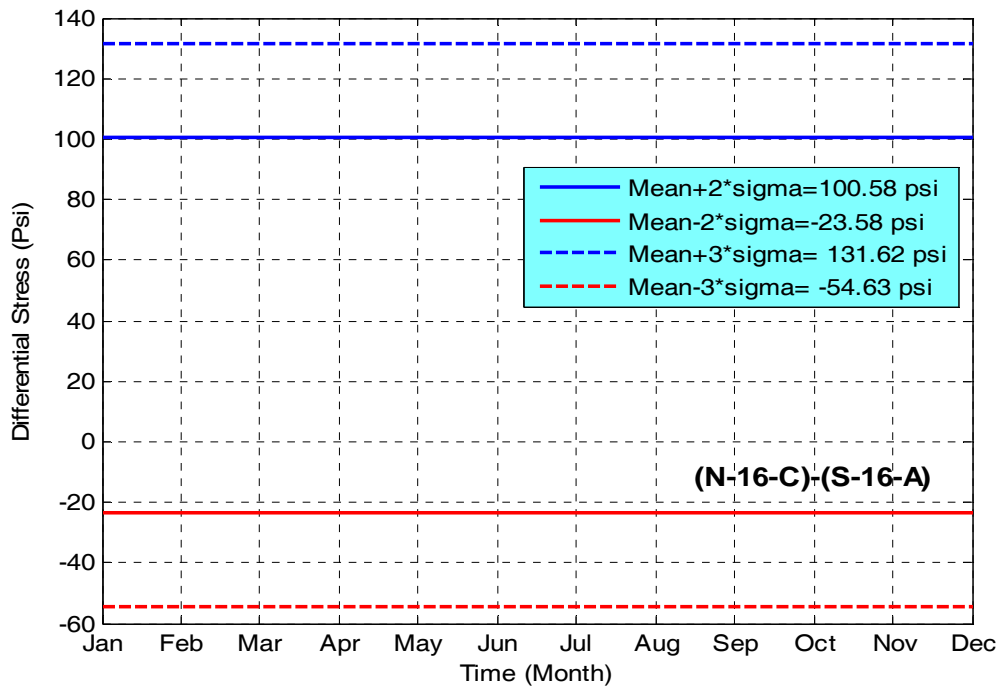
Figure D-35. One-year differential stress envelope for the closure grout sensors between north panel 16 and south panel 16 (span 3)
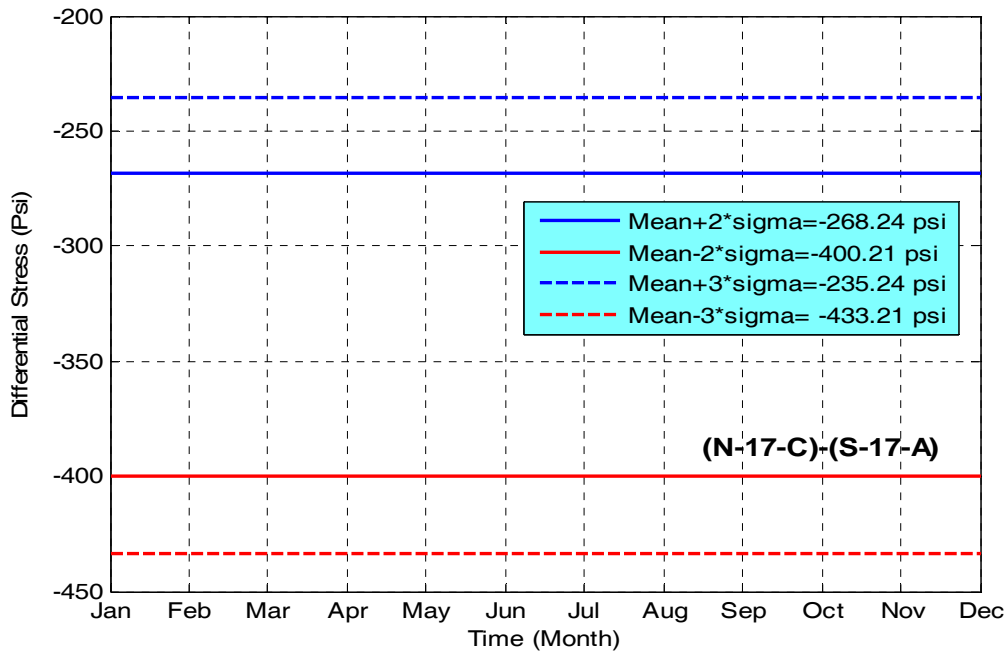
Figure D-36. One-year differential stress envelope for the closure grout sensors between north panel 17 and south panel 17 (span 3)
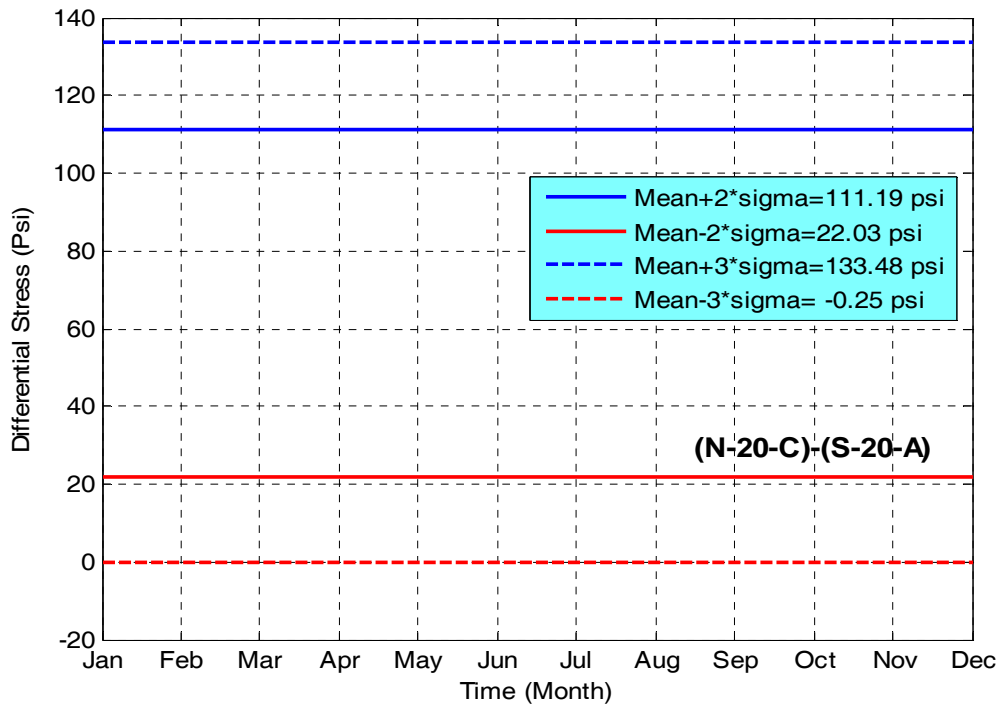
Figure D-37. One-year differential stress envelope for the closure grout sensors between north pier 3 and south pier 3 (pier 3)
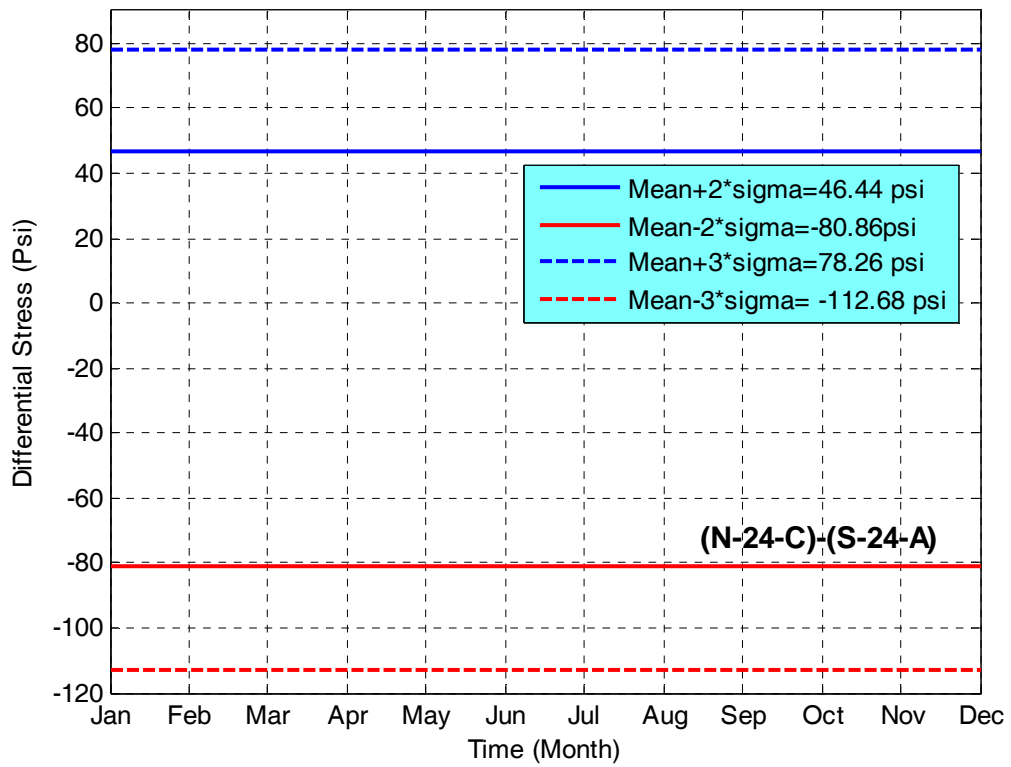
Figure D-38. One-year differential stress envelope for the closure grout sensors between north span 4 and south span 4 (span 4)

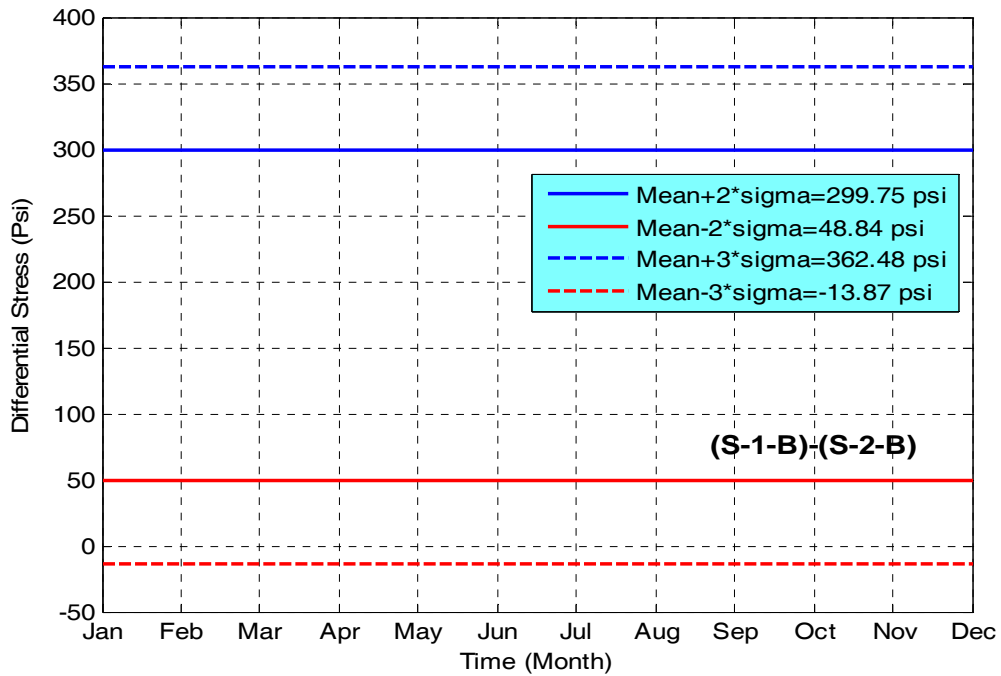## D.4 Panel Joint Stress Envelopes:

Figure D-39. One-year differential stress envelope for the joint between north panels 1 and 2 (span 1)

Figure D-40. One-year differential stress envelope the joint between north panels 7 and 8 (Span 2)

Figure D-41. One-year differential stress envelope for joint between north panels 8 and 9 (span 2)
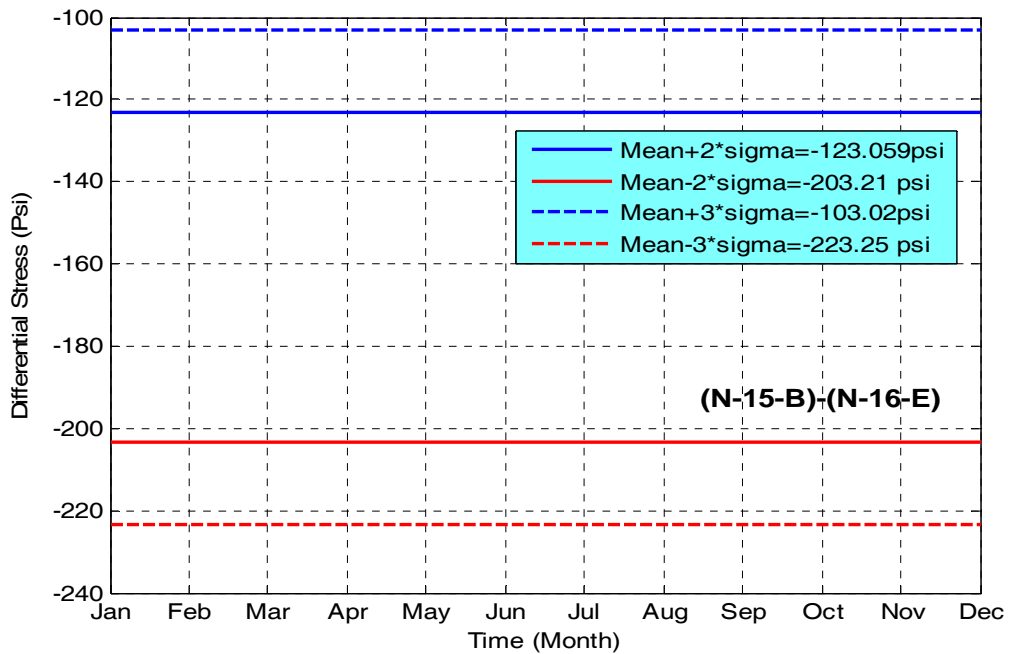
Figure D-42. One-year differential stress envelope for joint between north panels 15 and 16 (span 3)
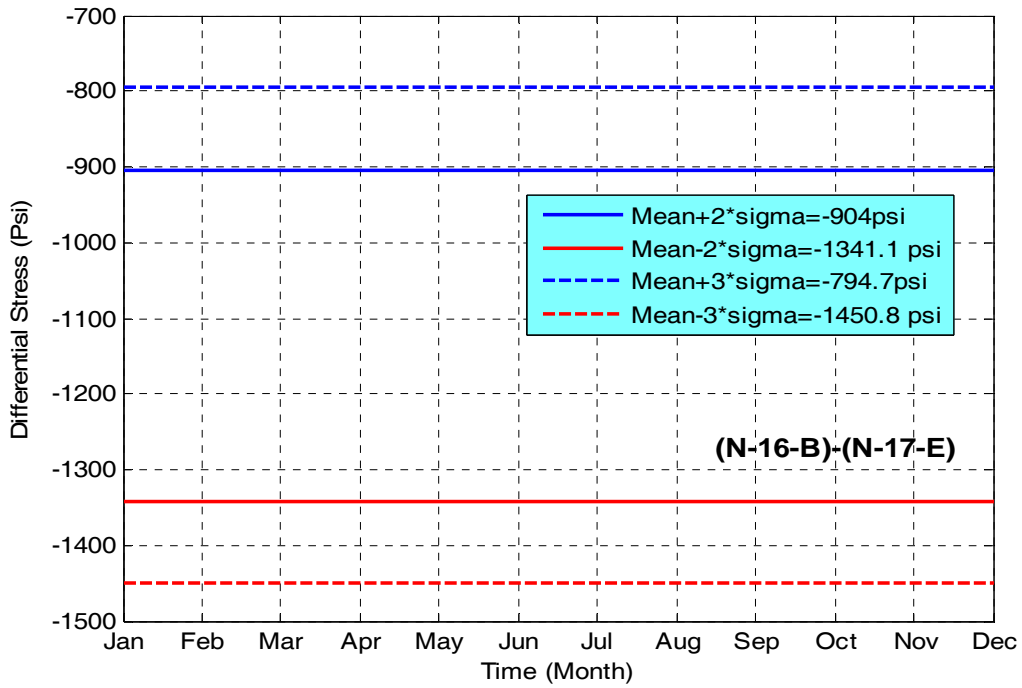
Figure D-43. One-year differential stress envelope for joint between north panels 16 and 17 (span 3)
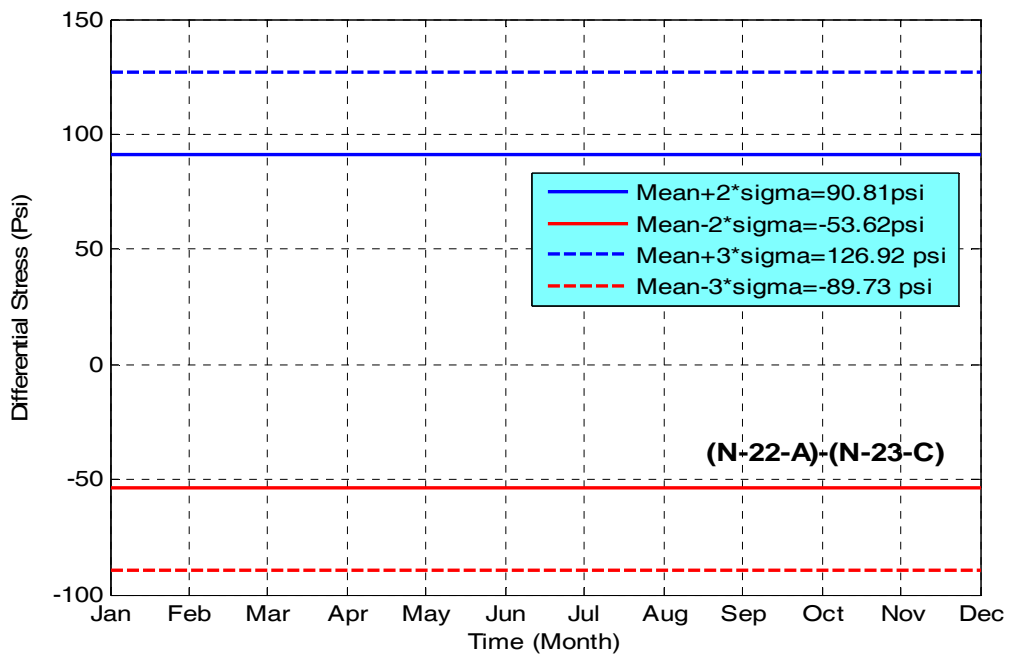
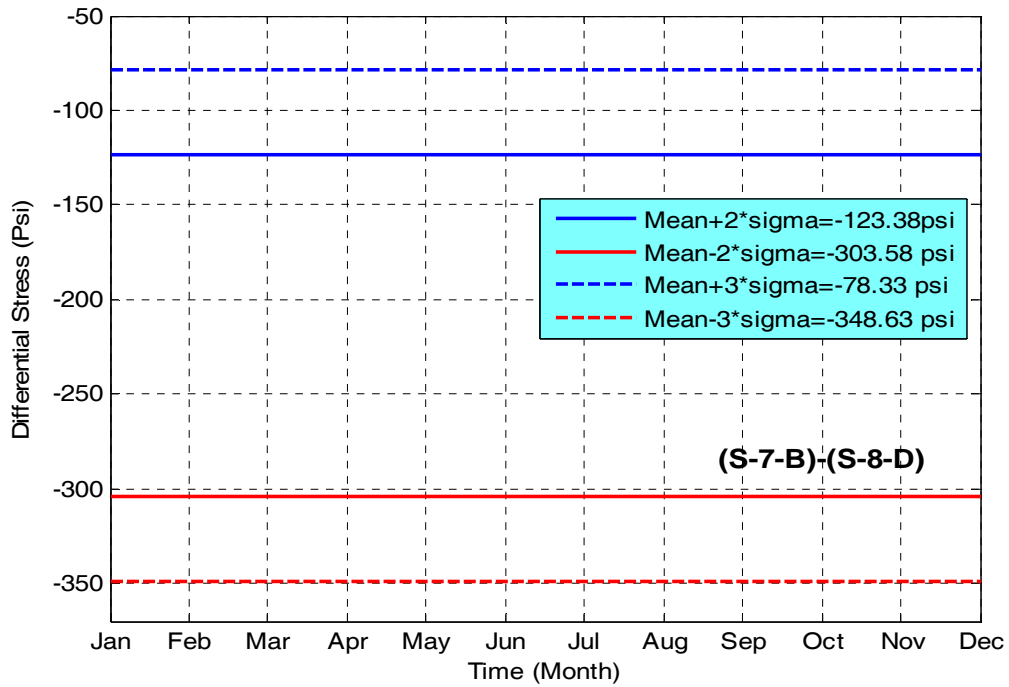**Figure D-44. One-year differential stress envelope for joint between north panels 22 and 23 (span 4)**
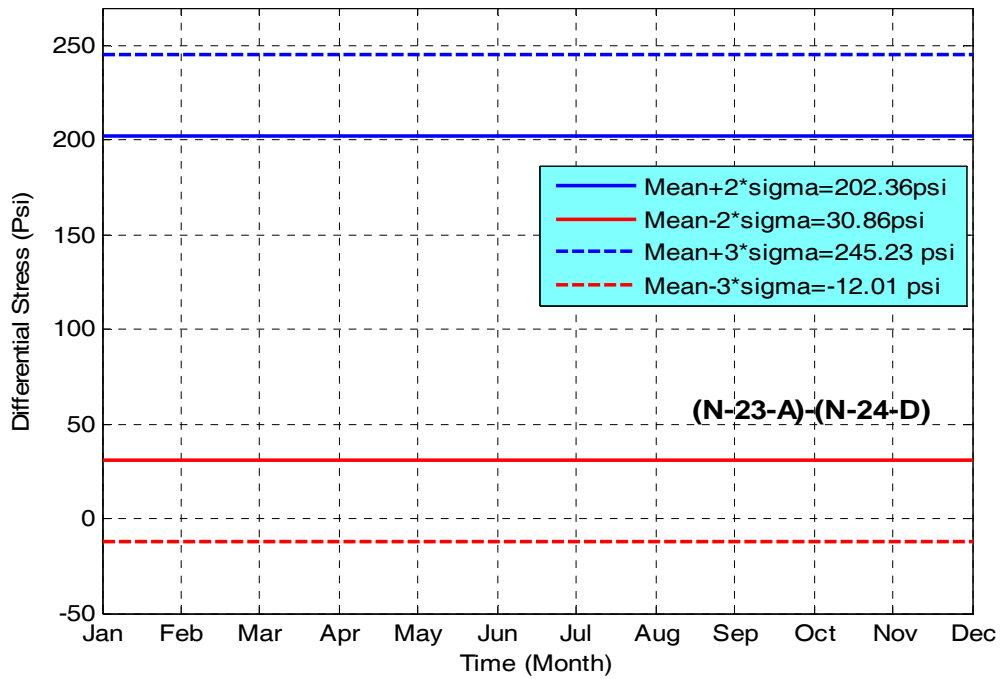
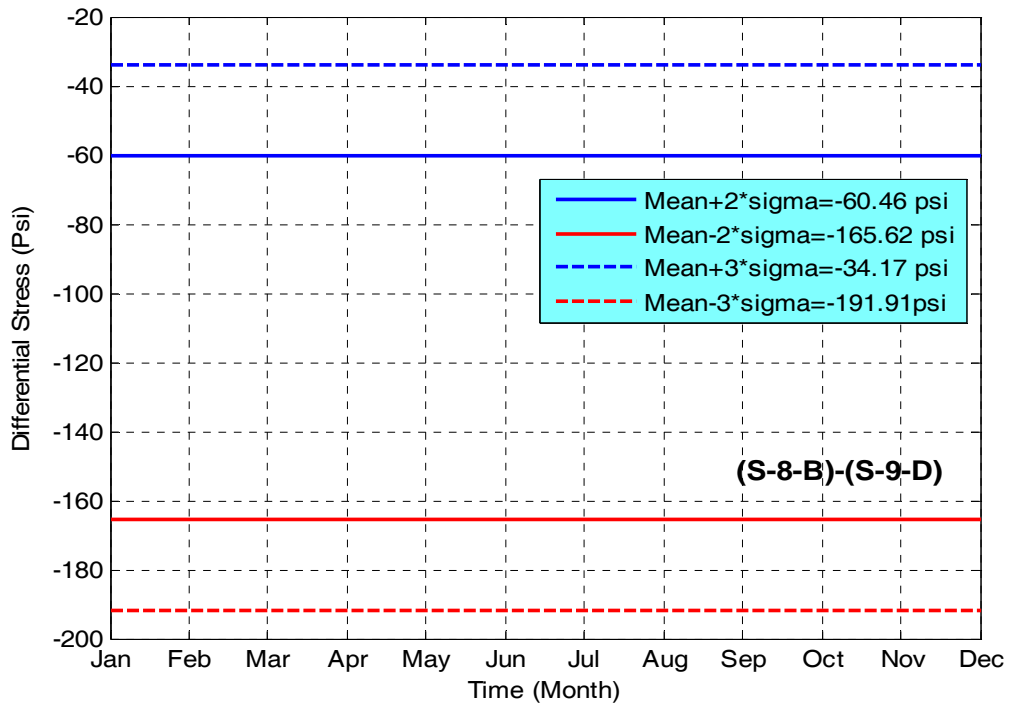**Figure D-45. One-year differential stress envelope for joint between north panels 23 and 24 (span 4)**

Figure D-46. One-year differential stress envelope for joint between south panels 1 and 2 (span 1)
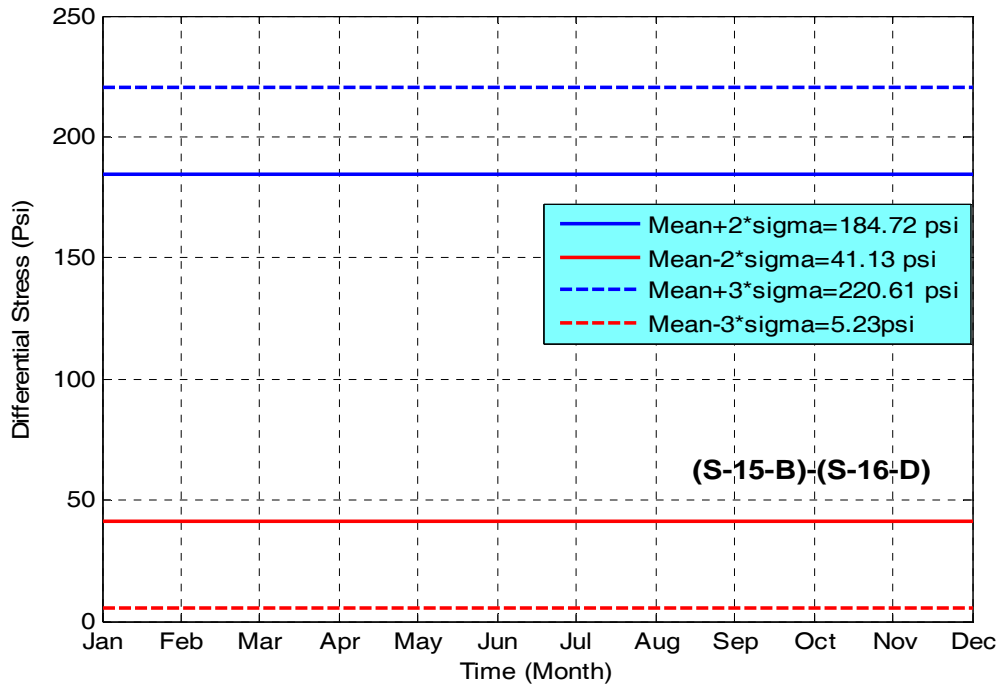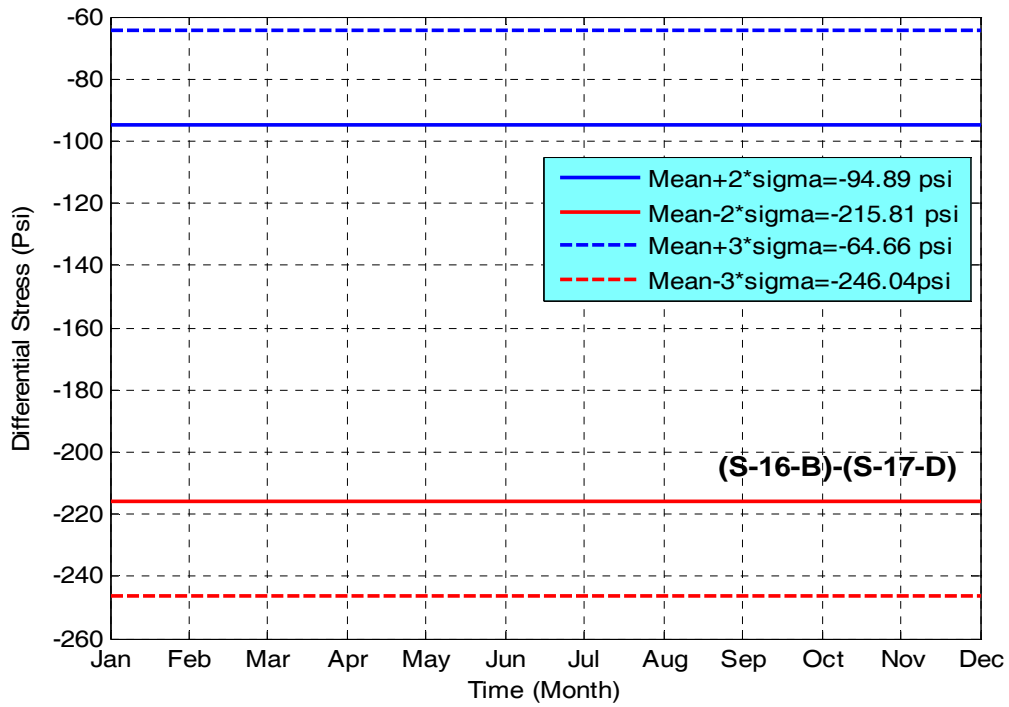
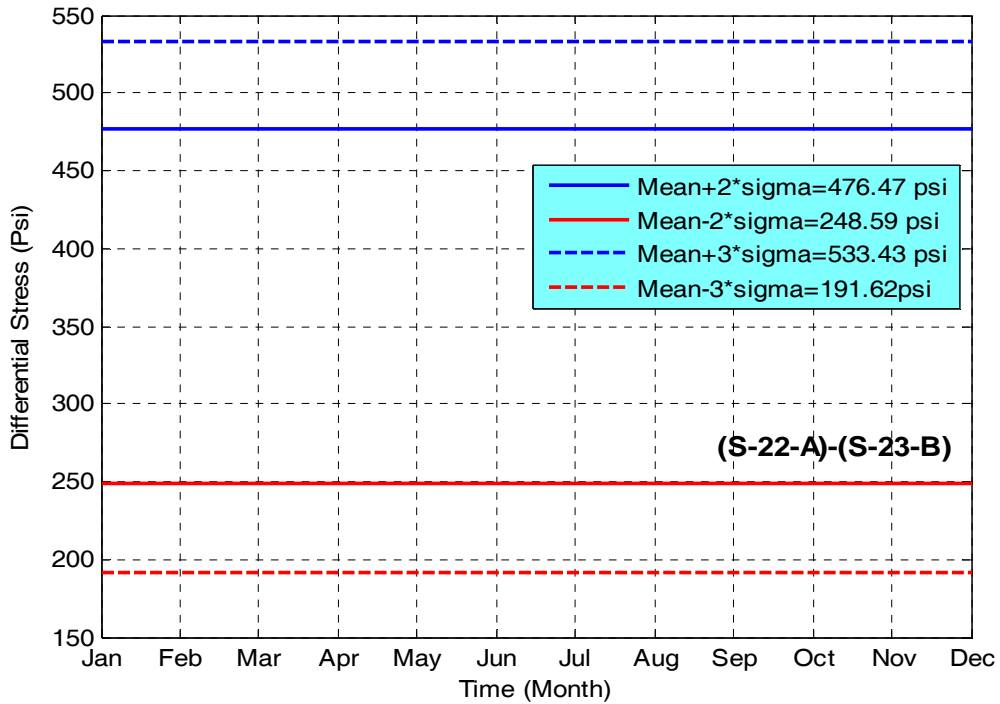**Figure D-47. One-year differential stress envelope for joint between south panels 7 and 8 (span 2)**

Figure D-48. One-year differential stress envelope for joint between south panels 8 and 9 (span 2)
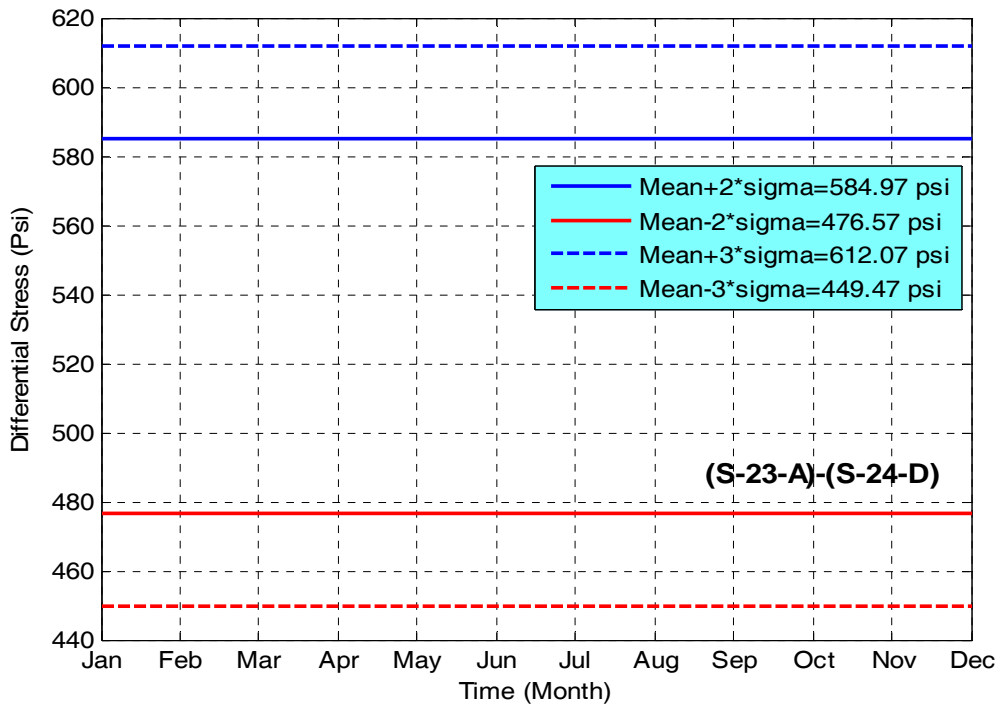
129

Figure D-49. One-year differential stress envelope for joint between south panels 15 and 16 (span 3)

Figure D-50. One-year differential stress envelope for joint between south panels 16 and 17 (span 3)

Figure D-51. One-year differential stress envelope for joint between south panels 22 and 23 (span 4)

Figure D-52. One-year differential stress envelope for joint between south panels 23 and 24 (span 4)

APPENDIX E: SENSOR STRESS CHARTS AND DATA (CD-ROM)

Three years worth of sensor stress charts and data are provided on the attached CD organized in two separate folders:

- Stress Charts
- Raw Data Spreadsheets

The organization of the stress charts and the raw data folders are shown in the following two illustrations.